2003

An experimental investigation of whirl instability including effects of lubricant temperature in plain circular journal bearings

Darryl, Jr. Chauvin
Louisiana State University and Agricultural and Mechanical College, djchauvin@yahoo.com

AN EXPERIMENTAL INVESTIGATION OF WHIRL INSTABILITY INCLUDING EFFECTS OF LUBRICANT TEMPERATURE IN PLAIN CIRCULAR JOURNAL BEARINGS

A Thesis

Submitted to the Graduate Faculty of the
Louisiana State University and
Agricultural and Mechanical College
in partial fulfillment of the
requirements for the degree of
Master of Science in Mechanical Engineering

in

The Department of Mechanical Engineering

By
Darryl Chauvin, Jr.
B.S. , Nicholls State University, 1998
May 2003

Acknowledgments

The work that was done on this thesis lies in the hands of many others than myself. Academically, Dr. Khonsari, Dr. Ram, and Dr. Pang have given invaluable assistance in completing this thesis. The fellow graduate students in the CeRoM laboratory have provided support through ideas and discussions. I thank Zoog for the donations of his time and his thoughts during the early stages of this project. Ultimately, my parents have structured the foundation and opportunity for this advanced study. I thank them for their belief in my abilities and their unaltered support from the beginning of my decision to take on this challenge. I thank Jason, Justin, and my wife, Shelly, for standing by me through the duration of this study; without them, this thesis would not have been completed.

This work was partially sponsored by an Industrial Ties Research grant sponsored by the Louisiana Board of Regents (LEQSF (2000-03)RD-B-02) and Gulf South Compression-Rotating Machinery Symposium (GSCC). Also, the contribution of the Baton Rouge branch of Bently Nevada through generous donation of equipment is greatly appreciated.

Table of Contents

List of Tables

List of Figures

Nomenclature

C	=	radial clearance, inch
$c_{ij}(I,j=x,y)$	=	damping coefficients of fluid film,
$\bar{c}_{ij}(I,j=x,y)$	=	dimensionless damping coefficients of fluid film,
D	=	journal diameter, inch
E	=	eccentricity of journal center to the bearing center, inch
$F_x(x=a\ldots g)$	=	variable in threshold derivation
f_x, f_y	=	forces developed in the lubricating film
$G_x(x=a\ldots g)$	=	variable in threshold derivation
G	=	gravitational constant, 386.4 in/s^2
H	=	fluid film thickness
K	=	stiffness of rotor
$\bar{K}$		dimensionless stiffness of rotor, k*C/W
$k_{ij}(I,j=x,y)$	=	stiffness coefficients of fluid film,
$\bar{k}_{ij}(I,j=x,y)$	=	dimensionless stiffness coefficients of fluid film,
L	=	bearing length,inch
L	=	length of rotor, inch
M	=	mass of rotor
$\bar{m}$	=	dimensionless mass of rotor
R	=	journal radius, inch
U	=	partial fluid velocity in the circumferential direction
V	=	partial fluid velocity in the radial direction
W	=	partial fluid velocity in the axial direction
P	=	local values of pressure
s	=	imaginary part of eigenvalue
S	=	(imaginary part of eigenvalue)$^{0.5}$
S	=	Sommerfeld #
W	=	bearing load, lb
x	=	coordinates defining the journals motion laterally
x_r	=	position of rotor in lateral direction
x_j	=	position of journal in lateral direction
y	=	coordinates defining the journals motion vertically
y_r	=	position of rotor in vertical direction
y_j	=	position of journal in vertical direction
μ	=	lubricant film viscosity, reyns
ω	=	rotational speed, radians/s
$\bar{\omega}$		dimensionless speed, *instability threshold*
ϕ	=	attitude angle
θ	=	cicumferentail coordinate

λ	=	eigenvalue
ε	=	eccentricity ratio
r		real part of eigenvalue

Abstract

The purpose of this thesis is to experimentally investigate the effect of lubricant temperature on the presence of whirl instability in journal bearings. The first set of conditions that are studied is an extremely low eccentricity rotor and the occurrence of oil whirl at the start-up of the experiment. Lubricant temperature, bearing temperature, frequency and amplitude of vibration, and rotational speed are monitored and analyzed in relation to presence of whirl instability. Additionally, another rotor with a slightly higher eccentricity is tested with respect to the presence of such instability. Particularly with this rotor, the system is brought just below the threshold of instability. Thermal equilibrium is achieved and then the lubricant temperature is increased. This effectively increased the Sommerfeld number and reductions in the threshold of instability were detected. A brief discussion on the findings of rotor unbalance is presented. Also, the experimental transition into whirl instability is discussed

1. Introduction

Hydrodynamic bearings are common components of rotating machinery. They are frequently used in applications involving high loads and/or high speeds between two surfaces that have relative motion. Journal bearings are specific to surfaces that mate cylindrically with the applied load in the radial direction. In the study of journal bearings many aspects of engineering are present. Stress analysis, fluid dynamics, instrumentation, vibration, material properties, thermodynamics, and heat transfer are some of the common subjects encountered in understanding hydrodynamic bearings. Particular to this research, heat transfer plays a significant role in the properties of the solids (the journal and the bearing) as well as the properties of the lubricant. In hydrodynamic lubrication small clearances between the journal and the bearing are present, and the smallest change in bearing or journal dimensions has an effect on the whirl instability threshold of the system. Likewise, the lubricant within a journal bearing is affected by the thermal conditions. Commonly, a rise in the temperature directly causes a decrease in the viscosity and thickness of the lubricant film. Thus, a greater eccentricity of the journal is present, and less power is needed to rotate the journal. However, attention must be given to the possibility of surface-to-surface contact at high eccentricity ratios.

Temperature also affects the dynamic properties of the lubricant. The stiffness and the damping effect that the lubricant has on the journal action changes as the viscosity changes. Since the stiffness and damping properties have been documented to be the destabilizing cause of oil whirl, the lubricant temperature plays a major role in whirl stability.

The behavior of the lubricant between the journal and the bearing is quite complex. There is a significant temperature variation around the circumference, and, although often neglected, there is a temperature variation along the film thickness. Therefore, the lubricant becomes a complex spring and damping system that, ultimately, must provide support to a dynamic journal. Undertaking these effects along with many other complexities would be necessary to realistically model the behavior of hydrodynamic stability. This thesis aims at development of an experimental rig to firmly establish some insight on the relationship between thermal effects and hydrodynamic stability. The experimental system was designed by the author to provide a framework for the theoretical predictions made in this thesis. Another motivation for the current research is the peculiar results produced by Maki and Ezzat[1]. Their experimental work indicates that the temperature of the oil relative to the temperature of the bearing surface has a stabilizing/destabilizing effect. Through the construction and experimentation with our experimental test rig, this thesis reproduces conditions similar to those used by Maki and Ezzat. It also investigates the region of a slight decrease in the instability threshold, seen as the slight dip in Figure 2.5. Basic geometries and design concepts were used so that simple theoretical prediction of the onset of oil whirl may be possible, and conclusions may be drawn on the occurrence of any thermal phenomena.

In achieving such an understanding, the first portion of the thesis explains the theoretical methods used to predict the onset of oil whirl. Following, a thorough description of the experimental set-up is given along with the method used to experimentally verify the onset of oil whirl. The experimental results of each rotor are

explained. Finally, the results of all work are accompanied by the conclusions and discussions of this thesis.

2. Literature Review

The first reported discovery of self-excited vibration referred to as oil whirl was published in 1925 by Newkirk and Lewis entitled "Shaft Whipping due to Oil Action in Journal Bearings"[2]. In studying vibration in a cylindrical journal bearing, the experimenters noticed that oil flow to the bearing had an effect on the vibration of the rotor bearing system. Under the given conditions, the rotor would cease vibration when they stopped the supply of oil to the bearing. This prompted further investigation into the phenomenon. The experimenters then tried different journal bearing systems and found that the presence of lubricant played a significant role in the measured vibration. This discovery prompted the immense volume of ongoing research.

After some time scientists discovered that the lubricant, like all other components of the rotor bearing system, has stiffness and damping effects on the system. In most

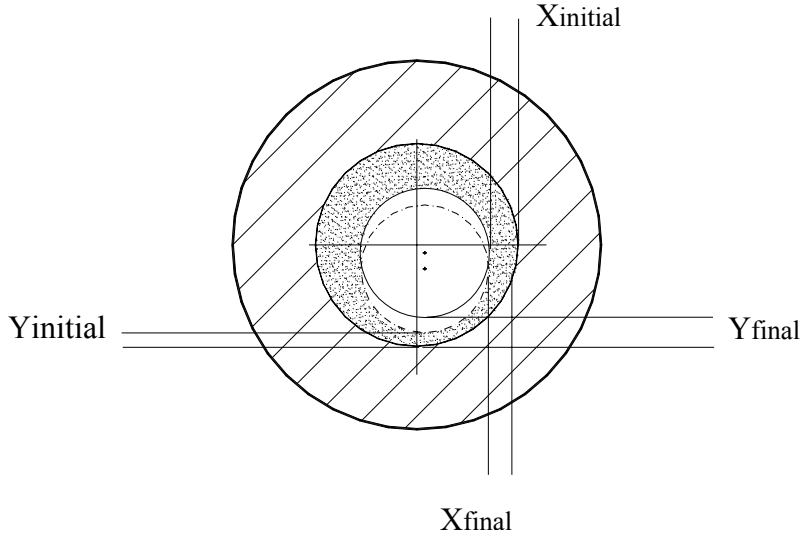

Figure 2.1 Effect of shaft movement in purely the y-direction with the resulting change in film thickness in the x-direction

solid materials stiffness and damping is only significant in the direction in which the force is applied. However, in the study of journal bearing stability, a movement in the x-

direction produces a change in oil film thickness in the y-direction, as shown in figure 2.1. The stiffness and the damping properties of the lubricant are directly dependent on the thickness of the lubricant film. Thus, the stiffness in the y-direction changes from just a direct motion in the x-direction since the journal becomes closer to the bearing in both directions. This is due to the curvature of the bearing and journal surfaces. Therefore, there exist two direct stiffness (k_{xx}, k_{yy}) and two direct damping (c_{xx}, c_{yy}) terms, along with the so-called cross-coupling components (k_{xy}, $k_{yx,}$ c_{xy}, and c_{yx}). An illustration of the stiffness and damping components are shown in figure 2.2.

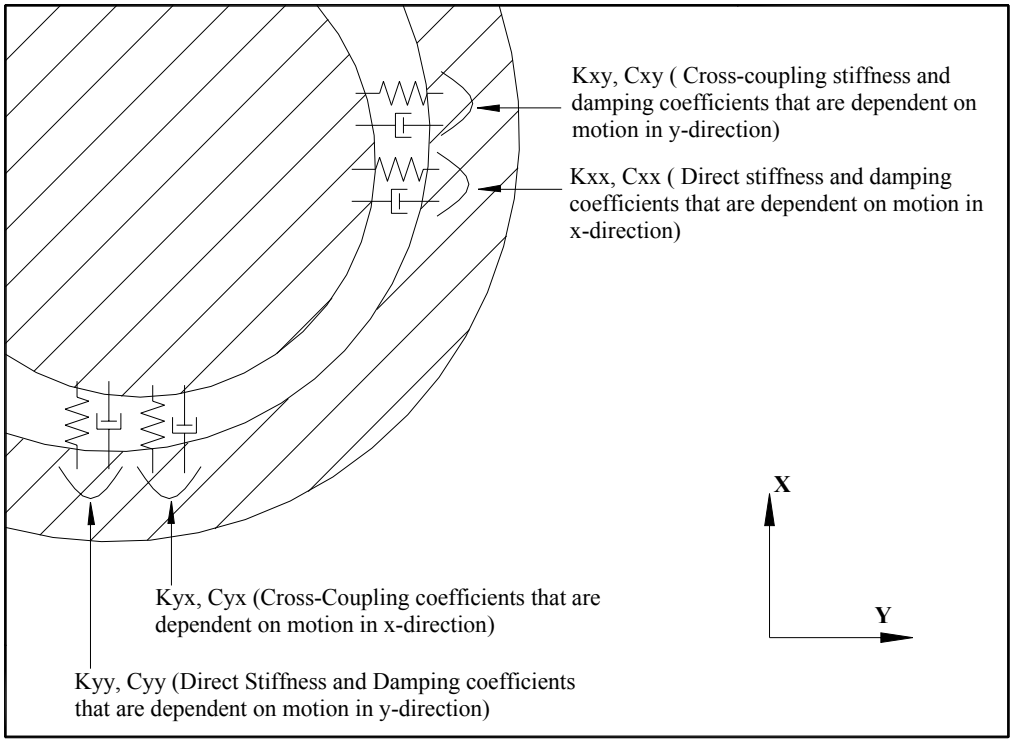

Figure 2.2 Illustration of the eight dynamic coefficients of stiffness and damping

Newkirk and Lewis published another experimental study entitled "Oil-Film Whirl-An Investigation of Disturbances Due to Oil Films in Journal Bearings."[3] They performed experiments with a combination of three rotors, five bearings, and various oil viscosities in an attempt to find regions of stable operation. In doing this they noted two

distinguishable vibrations, namely whirl and whip. Whirl was categorized by a non-violent, self-excited vibration that rotated the journal's center about some point at one-half the running speed of the journal. The second type --whip-- was also a self-exited vibration; however, the whirling frequency locked onto the natural frequency of the rotor system and the amplitude of vibration becomes very large and violent. Both of the disturbances are due to the presence of the oil film within the clearance space of the bearing.

Bently Nevada Corporation[4] offers insight into the difference between whirl and whip in their article archives. Whirl and whip are both self-excited vibrations that occur when the fluid forces generated in the lubricant tend to rotate the rotor within the bearing. The key to distinguishing the difference between the two lies in the understanding of the stiffness of the rotor bearing system. The stiffness of the rotor and the stiffness of the bearing, or fluid, act in series (figure 2.3). The weaker stiffness controls the overall stiffness of the rotor bearing system. During whirl, the bearing's stiffness is weaker than the shaft's stiffness. As the rotor begins to whirl, the orbit diameter grows in size. Since the bearing stiffness is a direct function of eccentricity, the bearing stiffness increases slightly with this movement. When the bearing stiffness makes this slight increase, the system remains unstable, but does not continue to grow in amplitude. Because the increased stiffness raises the natural frequency of the rotor bearing system, the rotor remains in a constant orbital motion. It is the bearing stiffness that keeps increasing the rotor bearing system's natural frequency during whirl; thus, a resonance condition is not met. The system remains at this point until the speed is increased again. Then the cycle

repeats itself. This continues to happen until the system reaches a point where the bearing

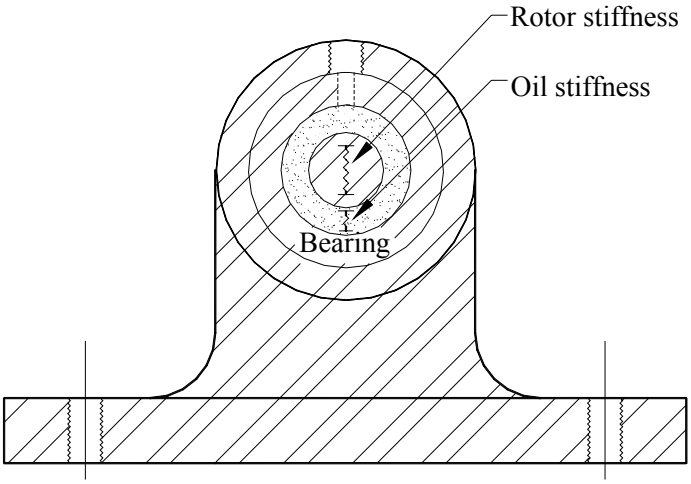

Figure 2.3 Illustration of uni-direction stiffness in the rotor bearing system

stiffness equals the rotor stiffness. When the rotor stiffness becomes the weakest component of the system, the rotor begins to whip. Since the rotor's stiffness cannot increase, the natural frequency does not increase anymore. The rotor begins to resonate and the amplitude of vibration grows. This condition is referred to as oil whip and usually correlates to the "nameplate critical speed" on most rotating machinery.

In a brief article on oil whip, A. C. Hagg[5] explained his understanding of the mechanism of oil whip. He states that oil whip is characterized by the journal motion in an area enclosed path and a forward whirl (shaft's center rotates in the same direction as that of the shaft's rotation about its own axis). The energy source causing oil whip is proclaimed to be the component of the fluid film force acting tangent to the path of the journal whirl. If a journal is running stable, then there is no whirling motion. When this is true, the external load applied to the journal -usually the weight of the rotor- is equal and opposite to the summation of the pressure developed by the fluid film. In the case of

oil whip, the pressure of the fluid film overcomes the external load, and a resultant force is acted onto the journal. Since the journal is enclosed in a cylinder, the

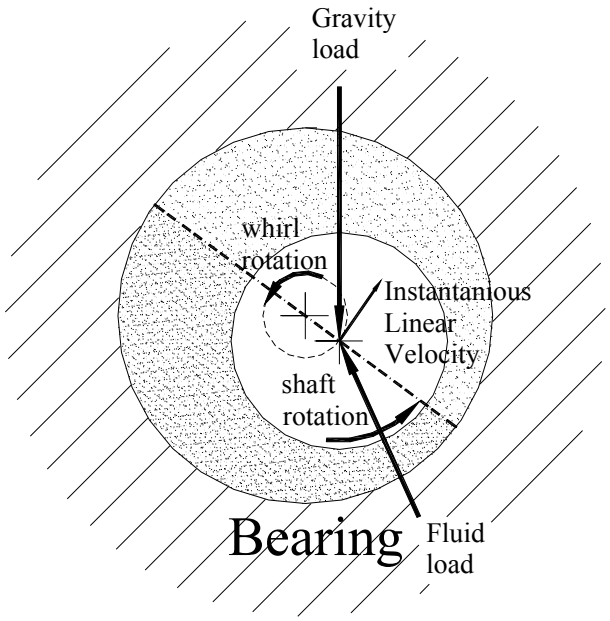

Figure 2.4 A. C. Hagg's explanation of oil whip

resultant fluid force is always tangent to the path of the whirl, as illustrated in figure 2.4. The typical ratio of oil whip frequency to the shaft rotational frequency is 0.40 - 0.49. A method for calculating oil whip frequency for a given set of parameters is briefly stated in his journal publication. However, Hagg notes that," the possibility of oil whip as indicated above (through his calculation) does not mean that it will actually materialize. For any given rotor system this question must be resolved by tests or by a stability analysis." This statement is yet another implication of the many uncertainties present in the study of oil whip. He concludes by insisting that the lubricating film force must do work on the journal for oil whip to occur.

In regards to general rotor stability versus system geometry, Hagg agrees that sleeve bearings are more susceptible to whirl than modified types of geometry. He

proclaims that a narrow bearing gives a higher stable speed than that of a wider bearing. Also, he has noted that a circumferential groove is "often effective in eliminating oil whip."

In 1960, Holmes published an article entitled "The Vibration of a Rigid Shaft on Short Sleeve Bearings"[6] where he illustrated that one could predict when a journal bearing system would begin to oil whirl. He used the short bearing application of the Reynolds equation to equate the fluid forces exerted on the bearing. He then determined the fluid forces as functions of the linearized stiffness and damping coefficients and applied them to stability criteria. This resulted in a border that gave the threshold of a stable to an unstable system in terms of oil whirl.

Adding to the experimental/theoretical compliance, Hagg and Warner[7] concluded that rotor flexibility would decrease the speed at which the theoretical oil whip would occur. Oil whip is directly related to the natural resonant frequency of the rotor. As the flexibility of the rotor decreases, so does the natural resonant frequency. Thus, the threshold for oil whip decreases and the system results in a smaller range of stable operation. In similar work, Hahn[8] reported that a flexible rotor also decreases the whirl threshold of instability. He compared the linearized instability prediction of a rigid rotor to several cases of flexible rotors and found that the instability threshold border simply dropped down as the flexibility increased. There was no significant lateral shifting on the stability chart. The resulting effect may be seen in figure 2.5.

Maki and Ezzat published an article entitled "Thermally Induced Whirl of a Rigid Rotor on Hydrodynamic Journal Bearings,"[1] which took a different look into oil whirl. Due to the many contradictions and inaccuracies in the published reports of

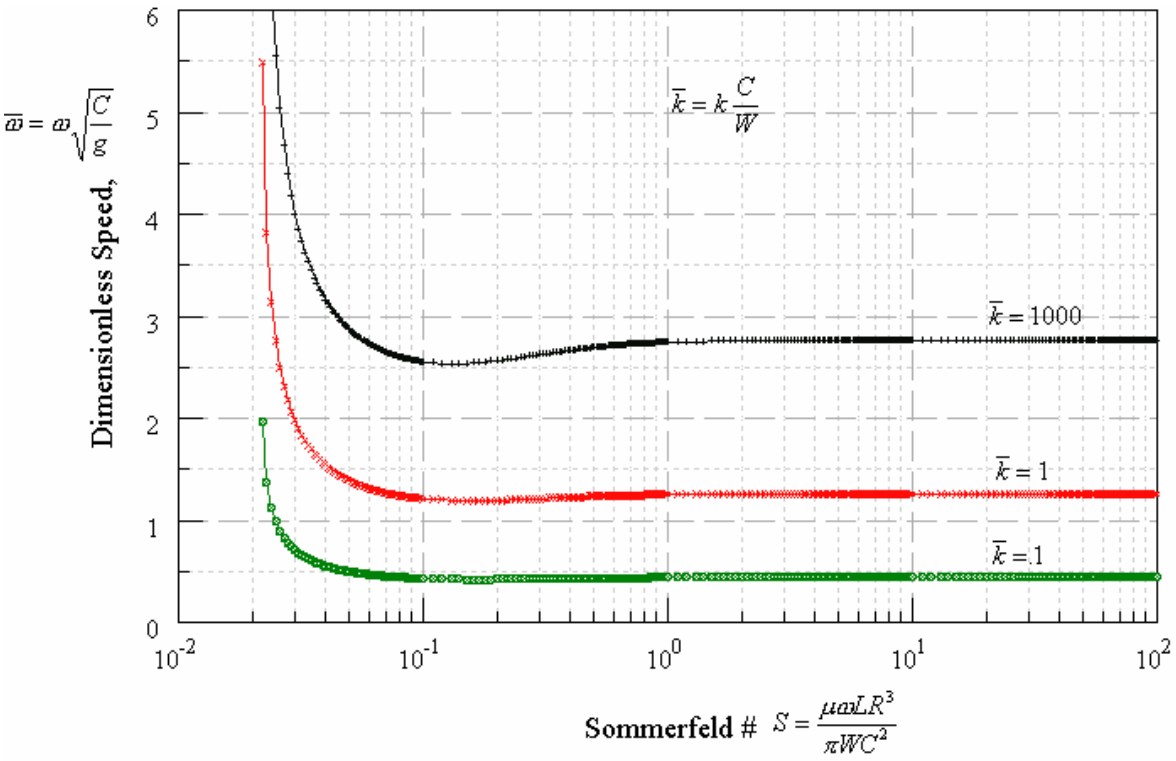

Figure 2.5 Effect of rotor stiffness on oil whirl stability

whirl instability, Maki and Ezzat performed a comprehensive study of experiments involving the thermal effects on the stability of a hydrodynamic bearing. In doing these tests, they encountered a phenomenon of oil whirl being induced by thermal conditions. It was first reported by Newkirk and Lewis that the lubricant temperature, along with other variables, has an effect on the onset of oil whirl. Although Newkirk and Lewis did not experience the phenomenon that Maki and Ezzat encountered, it seems as though it was their research that may have instigated these experiments.

The details of the physical elements of Maki and Ezzat's experiment are as follows. A solid, 51 mm journal rotates in two identical journal bearings (L/D=1). The journal was then connected to a drive quill, which was connected to an intermediate drive shaft. The intermediate drive shaft was then coupled to a planetary speed system that

allowed a variety of speeds for the rotor. With the use of a belt, the planetary unit was driven by an electric motor. Since, alignment of the rotor within the journal bearings is extremely important, a small diameter drive quill was used, allowing a great deal of flexibility in the drive system before the supplied torque reached the investigated journal bearing. Also, since the system is driven by a belt and a motor that is not inline with the driven components, an intermediate drive shaft was used to prevent any cocking of the rotor. The experimenters took care to balance the rotor to 0.7 g mm, which would more likely comply with the linearized prediction of oil whirl. Linearized prediction assumes negligible amplitude in vibration prior to the onset of oil whirl; thus, a significant unbalance in the rotor would include a negated term in the Reynolds' equation. For all sets of experiments the axially adjustable bearings were set at their maximum distance, 222 mm. Having the bearings set closer with a long shaft may amplify any existence of a conical motion.

The actual bearings were cylindrical in shape and circumferentially grooved. The groove's dimensions measured 6.34mm wide by 3.05mm deep located around the mid-plane. The width of the groove is on the order of 12% of the bearings entire length. Notably, four equally spaced, 6.34 mm diameter oil inlet holes were positioned in the bottom of the circumferential groove. Hence, the supply of an adequate amount of lubricant is possible to all parts of the bearing.

Thermocouples, pressure taps and proximity probes were instrumented in an attempt to monitor the bearing and rotor's reaction to the various conditions presented. Eight thermocouples were located 14.2 mm from one end of the bearing or 11.3 mm from its mid-plane. Also, the thermocouples were attached 1.52 mm from the inner surface of

the bearing. In addition to the circumferential thermocouples, four bearing surface temperatures were measured on the top of one bearing in the axial direction. This gives a total of 12 bearing surface temperatures on one of the bearings and eight circumferential on the other. The oil temperature was taken 50 mm from the oil inlet along with the test cavity ambient oil temperature and oil sump temperature. Six pressure taps were put in the circumferential groove to monitor the change of pressure as the system changed from a whirl state to that which was not whirling. Finally, proximity probes were positioned just outside of the bearings and on the drive quill to monitor the vibration of the journal.

Maki and Ezzat followed a basic guideline when performing most of the experiments. Before the rotor was started, heated oil circulated through all components of the system, except for the bearings. This helped to maintain a constant inlet oil temperature throughout each test by bringing most components, except the bearings, to the temperature of the heated oil. Proximity and pressure detectors were calibrated to ensure accurate results. At the instant the oil was supplied to the bearing, the motor was started and rotated at 52 radians/second. After this point, the speed was increased to 104 radians/second and stepped up by 104 radians/second from then on. The maximum speed reached in these experiments was 1571 radians/second. The duration at which any one speed was maintained was not reported and assumed to vary throughout all tests. However, it is understood that thermal equilibrium was not reached for each rotational speed. At the end of each experimental run, the pressure and proximity detectors were recalibrated.

In total ninety-five separate experiments were performed. In these tests the system presented oil whirl at start-up (52 rad/s). After different periods of time, the oil

whirl diminished. Recall, the inlet oil was heated prior to operation and the temperature of the inlet oil was greater than the bearing surface at the start-up. They reported that the system whirled until the bearing surface temperature equaled the inlet oil temperature. Notably, the "bearing surface temperature" was taken by the experimenters to be the average of all circumferential thermocouple measurements for each bearing. As Maki and Ezzat have stated, "The results of this investigation also indicate that the effects of rotor speed, the rate of change of rotor speed, and the duration for which any one speed is maintained are mere reflections of the changing bearing temperature relative to the nominally constant lubricant inlet temperature." A change in any of these variables, which did occur in the ninety-five experiments, intuitively notes a change in the heat transfer rate. For example, when the rate of change of rotor speed increased, the time needed for the bearing temperature to exceed the oil inlet temperature was decreased. This is likely a result of an increased rate of heat transfer to the bearing surface because of an elevated amount of heat generated in the lubricant. As the speed of the rotor was increased (just after start-up) so did the bearing surface temperature. Consequently, the orbit size decreased, as did the temperature difference between the inlet and bearing surface. Essentially, with each increase in speed the temperature difference between the inlet oil and the bearing surface decreased. The orbit continued to get smaller until the temperature difference was near zero; at this point oil whirl ceased. Oil whirl frequency ratios ranged from 0.485 to 0.495. These ratios were extracted from the oscilloscope photographs.

Under certain conditions, it was not possible for the experimenters to maintain the inlet oil temperature at a constant value. Because of low supply pressures and high oil

viscosities, the inlet oil temperature would rise, but not once did the rise exceed 10 degrees Celsius. Even with this slight change in conditions, the trend of the temperature-dependant oil whirl remained.

Through all 95 tests that were performed, different bearing clearances, lubricants, inlet pressures, speeds, rotor masses, oil inlet temperatures, and drive quill lengths were tried. Regardless of the combination of the variables, oil whirl presented itself if the inlet oil temperature were greater than that of the bearing surface. The converse was also seen. If the temperature of the oil was less than the temperature of the circumferential thermocouple readings, oil whirl was not present and could not be induced by intentionally disturbing the rotor.

Another set of experiments was conducted when the experimenters let the system reach a thermal equilibrium. The inlet oil was heated; thus, at start-up the rotor whirled. As the temperature difference became zero, oil whirl ceased. Under these conditions ($T_{bearing\ surface} > T_{oil\ inlet}$) oil whirl was not possible. Neither speeds greater than the

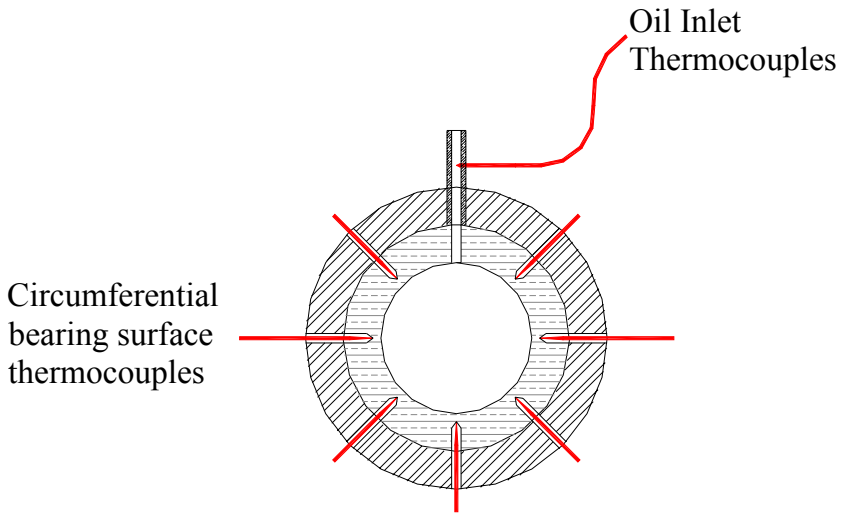

Figure 2.6 Thermocouple locations for the inlet oil and the bearing surface

theoretical predicted value (by linear stability analysis, 1200 rpm) nor external impact caused the rotating system to oil whirl. Instances of the inability to instigate whirl by impact is not new to the related experimental research, but the uncertainty remains in the relevance of the temperature relationship in having this effect. It should be noted that Maki and Ezzat never reported experimental agreement with a theoretical threshold curve when the temperature of the oil was not manipulated.

The authors stated that all of the results had good repeatability. Also, the maximum difference in the bearing surface temperature and the oil inlet temperature was 10 degrees Celsius for all tests. In the experiments performed, the presence of oil whirl in these experiments was dependent only on the temperature relation between the inlet oil and the bearing surface, as illustrated in figure 2.6. They further stated that the rotor mass, bearing clearance, lubricant properties, and rotational speed had no influence on the presence of oil whirl in any of the experiments.

The phenomena that occurred in the experiments that Maki and Ezzat performed have yet to be explained. Also, the amount of research that has been conducted pertaining to this particular subject is quite limited. The primary focus of present research is to gain further experimental insight on the phenomenon that Maki and Ezzat experienced.

In an earlier but related research, Pinkus[9] performed some experiments on oil whip. He took a variety of journal bearing configurations and subjected them to oil whip. He noticed that oil temperature, speed, load, amount of oil, and bearing cap tightness were all factors that had an influence on a journal bearing's stability. Pertaining to this thesis, Pinkus measured the oil inlet temperature and noted the effect it had on a systems

whip speed. He used temperatures of 25˚ C, 45˚ C, and 65˚ C. His results state that higher oil viscosities tended to raise the oil whip starting speed. It should be noted that he did not intentionally let the bearing system reach a thermal equilibrium at any time; he basically ramped up the speed until a half frequency vibration was present. It is also uncertain if he distinguished the difference between oil whirl and oil whip. However, his research does indicate that decreasing the oil temperature stabilized the system at a given speed. In a general sense, Maki and Ezzat also saw a cooler oil to be a stabilizing factor. As a side note, Pinkus noticed that a tight bearing cap often stabilized a bearing. It may be inferred that misalignment would be present in this case. As presented later, Craighead, , Dowson, Sharp, and Taylor[10] showed that misalignment can be used as a stabilizing tool.

Ma and Taylor conducted a series of experimental work on the thermal effects in journal bearings and published some of their results in a paper entitled "An Experimental Investigation of the Thermal Effects in Circular and Elliptical Plain Journal Bearings."[11] Their initial intention for this work was to gain credible data on the bearing surface temperature during various operating conditions. It had been previously stated by Dowson[12] that the temperature variation along the axial direction was very small. And Hopf and Schuler[13] reported that laminar flow caused a higher temperature than turbulent flow around the bearings circumference. Some of the studies that Ma and Taylor reported showed a temperature difference around the circumference of values greater than 20˚C. Naturally, as the speed and/or load increased, the bearing's properties changed. They experimentally confirmed the theoretical predictions, and one set of their results is displayed in figure 2.7. These results are for an axial grooved circular bearing,

but may have similar trends to that of a plain circular journal bearing. The temperature had only a slight differential between any two points in the axial direction. Under high loads and/or high speeds, there was a significant variance in

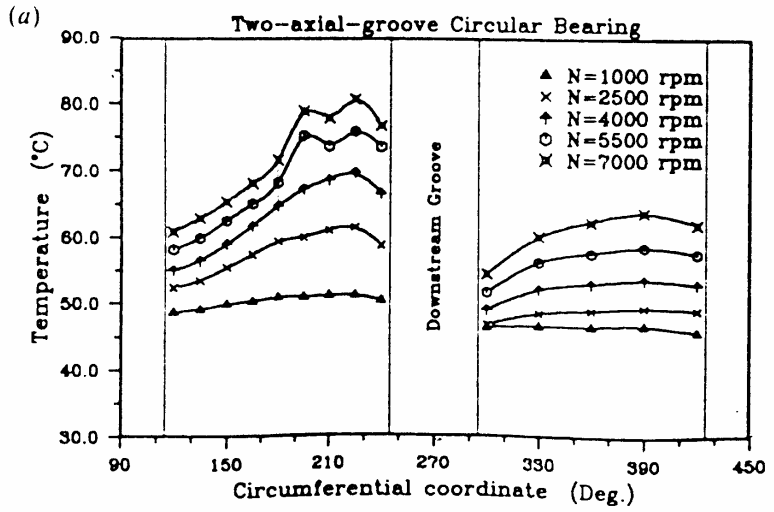

Figure 2.7 Circumferential temperature as a function of speed [Ma & Taylor].

the circumferential temperature. In a plain circular journal bearing, the cooling effect of the inlet port may not be as dramatic as that of the axial groove. However, the pattern of the circumferential temperature with respect to the rotational speed should be the same. If the temperature variation is large enough, it will have an effect on the viscosity and the clearance of the bearing system. Variable viscosity of the lubricant around the circumference of the journal bearing also has an effect on the variance of local stiffness and damping of the oil that could alter the stability of the system. Particularly, the stiffness and damping of the oil is directly responsible for the stability of the journal. Also, if the bearing were to become warped significantly due to the temperature variation around the circumference, this may have a stabilizing effect on the system. As stated by Tondl[14] in "Some Problems of Rotor Dynamics", experiments have proven that the whirl threshold of an elliptical bearing is slightly higher than that of an equivalent

cylindrical bearing. A perfect cylindrical bearing is an ideal case, and the existence of "out-of-roundness" can significantly change performance. Pertaining to this thesis, it is noted that the circumferential temperature is not always eligible to be considered constant. However, at low loads and low speeds, their results show that this assumption may be valid.

In "A review of thermal effects in hydrodynamic bearings Part II: Journal bearings," Khonsari[15] compiles many literature reports on thermally effects in journal bearings. A particular topic of interest that is discussed in this compilation is the work done by Nica. His work studies the change in clearance as the bearing temperatures change. The temperature of a journal bearing can change as little as a couple of degrees or may possibly change by more than 100 degrees, depending on the conditions. Especially, since the clearance of most journal bearings is extremely small, the slightest change in bearing temperature may have an adverse or desirable effect on the operation of the bearing system. In one case a very large thermal expansion of the journal and bearing may cause an undesirable surface contact during operation. Yet, small decreases in the clearance tend to raise the whirl instability threshold. Figuratively, the speed of the onset of oil whirl is increased as the clearance decreases. Khonsari also refers to work done by Dowson et al.[17]. Dowson experimentally determined that in most journal bearing cases the shaft surface temperature may be assumed as an isothermal element. Also, he has found through experiments that the journal surface temperature is usually within a few degrees of the bearing surface temperature. The relevance of the clearance change and shaft temperature become evident when studying oil whirl. Since the onset of oil whirl is inversely proportional to the clearance squared, slight changes in the

clearance have significant effects on oil whirl. In finding experimental results that deviate from idealistic theoretical predictions, this information becomes valuable in finding reliable data.

In an attempt to gain insight on situations that are not ideal, Craighead, Dowson, Sharp, and Taylor[11] did a theoretical study on the stability effects that misalignment, variable viscosity and non-laminar flow may have on a journal bearing system. Their results were published in an article entitled "The influence of thermal effects and shaft misalignment on the dynamic behavior of fluid film bearings." For each of these cases the stiffness coefficients, damping coefficients, and instability threshold were calculated and compared to the results of an ideal case. The input used in computing the threshold was a plain, cylindrical, short bearing with a L/D ratio equal to 0.5. In the case of variable viscosity, the stiffness and damping coefficients did not differ greatly from the isoviscous case. In turn, the instability threshold made a slight shift but had a very similar trend. Ultimately, variable viscosity caused a decrease in the instability threshold for Sommerfeld numbers greater than 0.5 and caused a stabilizing effect for Sommerfeld numbers less than 0.5 (figure 2.8(a)). Shaft misalignment had a greater effect and displayed in figure 2.8(b). By increasing the percentage of misalignment, the bearing system's threshold would significantly increase. This was basically consistent for the entire range of Sommerfeld numbers studied. Misalignment can also be thought of as an extra load on a certain portion of the bearing. Agreeably, as a bearing system's load is increased, the critical speed at which it begins to whirl is also increased. Also, the basic trend of the threshold of instability alters as the misalignment is increased. Laminar flow

of the lubricant around the circumference of the bearing is often assumed in the theoretical prediction of oil whirl. However, this may not be the case in an experimental

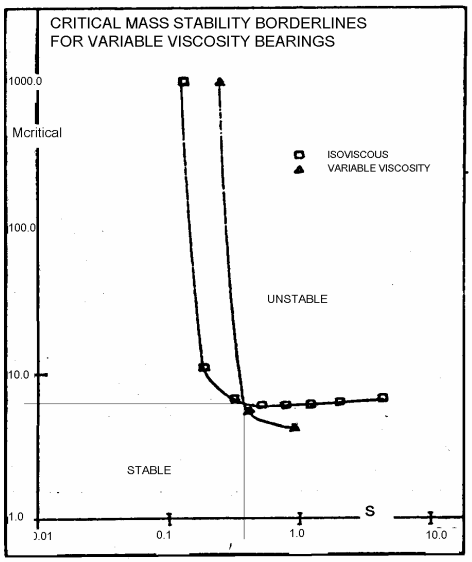

Figure 2.8(a) Effect of variable viscosity on the whirl threshold [Craighead et al.]

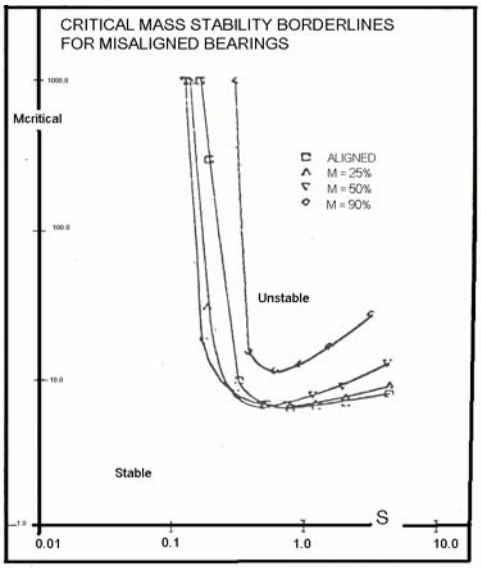

Figure 2.8(b) Effect of misalignment on the whirl threshold [Craighead et al.]

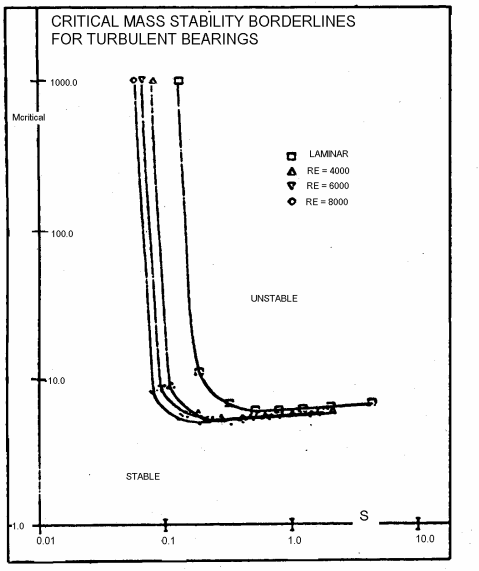

Figure 2.8(c) Effect of turbulence on the whirl threshold [Craighead et al.]

study or field application. The work of these researchers shows that turbulence lowers the threshold of instability compared to that predicted with laminar flow (figure 2.8(c)). As the Reynolds number increases (or turbulence increases), the threshold of instability declines. Thus, for an experimental system the journal would begin whirling at a lower speed than the speed predicted with laminar flowing lubricant. Note, the lines of the whirl threshold of instability remained in the same trend or pattern, regardless of the amount of turbulence present in the bearing.

In experimental practice it is known that oil whirl prediction is extremely delicate. Arriving at results that are comparable to the linearized theoretical prediction can sometimes be cumbersome. In helping with an understanding of why the experimental threshold may differ from the theoretical threshold, Khonsari and Chang[17] published theoretical work on a stability boundary that exists for a given journal bearing system. It

is revealed that a journal remains stable in the bearing while the journal's center remains inside the stability boundary. The stability boundary is of a circular form within the clearance circle and denotes the area in which the journal may be released (in theoretical

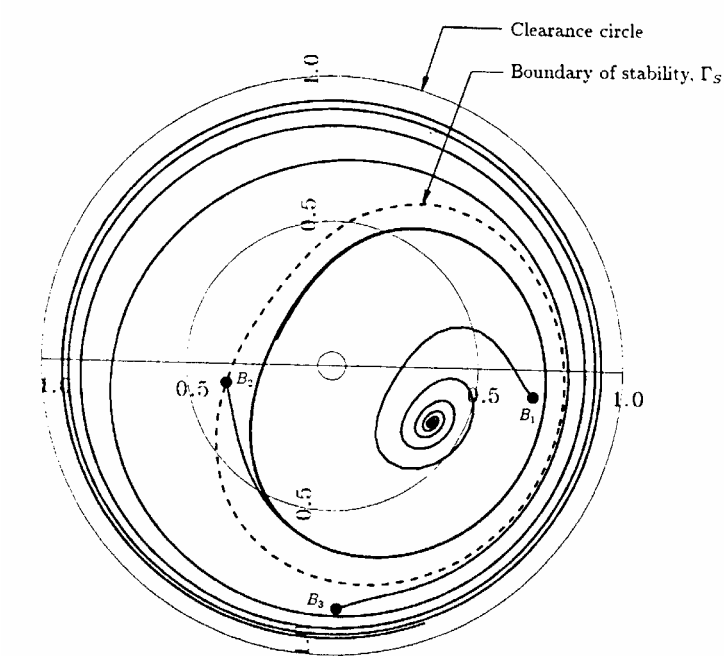

Figure 2.9 Illustration of the stability boundary with a journal bearing clearance circle. [Khonsari and Chang]

calculation process) to remain running stable. As the operating point on the stability graph gets closer to the instability threshold line, the stability boundary decreases in size. When the operating point coincides with the instability threshold line, the stability boundary becomes a very small region (essentially a point). Although the authors use the stability boundary as a criterion for the initial conditions of the journal, one may examine how the unbalanced vibration of a journal may relate to this phenomenon. If the journal bearing had an unbalance vibration, then it is likely that the threshold of the system would be reduced according to the stability boundary. The concept agrees with the

common experimental practice of "bumping" a rotor to make it begin whirling. This understanding can aid in deciphering the deviation of experimental results from the theoretical results.

3. Theoretical Methods

Oil whirl is a self-excited vibration that occurs in journal bearings. The motion of the journal bearing's lubricating fluid induces journal rotation around the bearing. Once certain conditions are met, the wedge of fluid loses its stationary position and begins revolve. Thus, the rotating fluid film forces the shaft to also rotate, or whirl, about the bearing's center. At the instant that this begins is known as the threshold for whirl instability. During oil whirl instability, the fluid forces generated by the pumping motion of rotation upset the force balance on the rotor and send it into this whirl.

An equation that helps describe hydrodynamic lubrication is known as Reynolds' equation. It was derived by Osborne Reynolds and is a general equation that analyzes any type of hydrodynamic lubrication. Hydrodynamic lubrication is defined as the occurrence of relative motion between two surfaces which causes fluid to form a lubricating wedge. A seal, slider bearing, journal bearing, and even a comb going through wet hair has hydrodynamic lubrication.

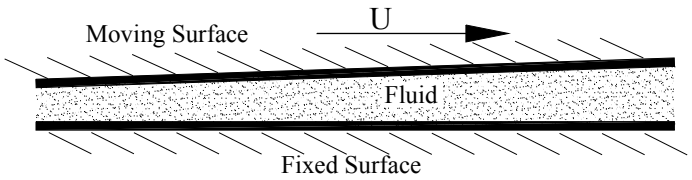

Figure 3.1 is the basic geometry of any hydrodynamic lubrication

A true understanding of these fundamentals is useful when trying to deal with whirl instability.

3.1 Hydrodynamic Analysis

To begin the analysis, a force balance on an arbitrary, infinitesimal fluid element is conducted. Using this element, Newton's 2nd law was applied. Combining this with the shear stress equation produced two equations for pressure as a function of velocity.

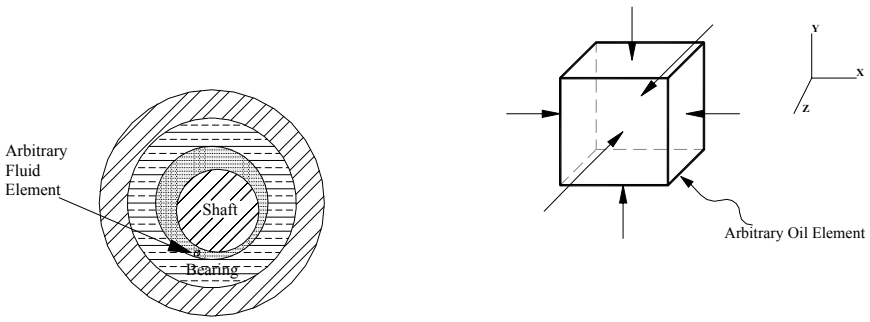

Figure 3.2 identifies the fluid element and the pressure acting on the element within the journal bearing

$$u = \frac{1}{\mu}\frac{\partial P}{\partial x}\frac{y(y-h)}{2} + U\frac{y}{h} \qquad (3.1)$$

$$w = \frac{1}{\mu}\frac{\partial P}{\partial z}\frac{y(y-h)}{2} + W\frac{y}{h} \qquad (3.2)$$

These two equations are for the axial and the circumferential directions. An equation of the same sort could not be produced for the y, or radial, direction because of the absence of shear along the y-faces. There is considered no relative motion between the adjacent y-faces. When Newton's 2cnd law is applied in this case, the result is that the change in pressure equals zero. Hence, pressure is not dependent on the y-direction.

Next, in order to combine all three dimensions, an equation relating all directions had to be formulated. Using the conservation of mass statement, the continuity equation was derived.

$$\text{continuity equation: } \frac{\partial u}{\partial x}+\frac{\partial v}{\partial y}+\frac{\partial w}{\partial z}=0 \qquad (3.3)$$

This equation relates the velocities in all three directions, and two equations exist that are functions of velocities. Therefore, plugging the two known velocity equations into the continuity equation and then integrating in a fashion to directly find the velocity in the radial direction obtained an equation relating all three velocities. This produced Reynolds general equation for a journal bearing[19].

$$\frac{\partial}{\partial x}(\frac{h3}{12\mu}\frac{\partial P}{\partial x})+\frac{\partial}{\partial z}(\frac{h3}{12\mu}\frac{\partial P}{\partial z})=-\frac{U}{2}\frac{\partial h}{\partial x}-\frac{W}{2}\frac{\partial h}{\partial z}+V \quad (3.4)$$

Some further simplifications can be made to suit my interests. In most cases a rotating shaft will not slide, along its axis, in and out of the bearing. Also, the radial velocity consists of two main components: time variation of film thickness and the vertical component of the tangential velocity. For the purposes of finding the whirl threshold, it can be assumed that the film thickness does not vary prior to whirl. Furthermore, in this study it is also assumed that the shaft does not become cocked within the bearing, i. e. misalignment. It is assumed that the shaft remains parallel to the bearing surface. Additionally, it can also be considered that the bearing is a short bearing. The infinitely short bearing approximation (ISA) refers that the rate of change of film pressure is much greater in the axial direction as opposed to that of the circumferential direction.[19] Taking all of the above assumptions into consideration, gives the final form of the Reynolds equation.

$$\frac{\partial}{\partial z}(\frac{h^3}{12\mu}\frac{\partial P}{\partial z}) = \frac{R\omega}{2}\frac{\partial h}{\partial x} + \frac{\partial h}{\partial t} \quad (3.5)$$

The Reynolds' equation was then integrated to find the local pressure at a particular point. This pressure is a function of the angular rotation speed, film thickness, axial location, and viscosity. It can be used to find the pressure at any point within the bearing. The pressure equation can be simplified for a shaft that has a steady state, stable condition. The film thickness does not vary with time and is a function of the clearance and the eccentricity.

$$h = C + \varepsilon\cos\theta \quad (3.6)$$

This produced the following local pressure[21]:

$$P = \frac{-3\mu\omega(z^2 - \frac{L^2}{4})\varepsilon\sin\theta}{C^2(1+\varepsilon\cos\theta)^3} \quad (3.7)$$

Since the pressure equations gives the local value of the pressure, integration of the pressure equation along the axis and about the circumference gives the force acting on the shaft (or -load on the bearing). Since fluid pressure acts normal to the surface, components of the pressure in a fixed coordinate system was needed to find resulting load. For ease of calculation, the coordinate system was associated with the line of centers of the bearing and the shaft. Two components of force were found and the combination of them resulted in the load on the bearing[21].

$$W_{total} = \frac{\mu\omega RL^3}{4C^2}\left(\frac{e}{\left(1-e^2\right)^2}\right)\sqrt{16e^2 + \pi^2\left(1-e^2\right)} \quad (3.8)$$

A common dimesionless parameter used in studying hydrodynamic lubrication is the Sommerfeld number. It is defined as the following for a short bearing

$$S = \frac{\mu \omega L R^3}{\pi W C^2} \qquad (3.9)$$

By substituting the Sommerfeld number equation into the bearing load equation, a relation between the Sommerfeld number and the bearing eccentricity is found. This becomes useful later in the instability threshold formulations.

$$S = \frac{4\mu\omega R^2 \left(1-e^2\right)^2}{\pi L^2 e\sqrt{16e^2 + \pi^2\left(1-e^2\right)}} = \frac{4R^2}{\pi L^2}\frac{\left(1-2e^2+e^4\right)}{e\sqrt{16e^2 + \pi^2\left(1-e^2\right)}} \qquad (3.10)$$

3.2 Theoretical Prediction of Whirl Instability

To begin the evaluation of whirl instability, the equations of motion must be considered. For this purpose, the rotor system was considered to be a flexible shaft with a lumped mass at the midpoint of the rotor. The rotor was supported on two equally spaced identical journal bearings. In finding the equations of motion three reference points were taken into consideration. They were the bearings' center, the journal's center and the rotor's center (which is located at the point of lumped mass). Observing the sum of the forces on the lumped mass, the first two equations of motion are found.

$$\begin{aligned} m\ddot{x}_r + k\left(x_r - x_j\right) &= 0 \\ m\ddot{y}_r + k\left(y_r - y_j\right) &= 0 \end{aligned} \qquad (3.11)$$

The notation of x_r and y_r are the postion of the rotor center and x_j and y_j are with respect to the journal center. The second two equations of motion are found when summing the forces on the fluid for a stable running condition.

$$\begin{aligned} 2f_x &= k\left(x_r - x_j\right) \\ 2f_y &= k\left(y_r - y_j\right) \end{aligned} \tag{3.12}$$

Also, note that the forces developed in the lubricating film are

$$\begin{aligned} f_x &= k_{xx}x_j + k_{xy}y_j + c_{xx}\ddot{x}_j + c_{xy}\ddot{y}_j \\ f_y &= k_{yx}x_j + k_{yy}y_j + c_{yx}\ddot{x}_j + c_{yy}\ddot{y}_j \end{aligned} \tag{3.13}$$

Next, a solution to the four equations of motion is assumed and to be of the following form.

$$\begin{aligned} x_r &= Ae^{\lambda t} & y_r &= Ce^{\lambda t} \\ x_j &= Be^{\lambda t} & y_j &= De^{\lambda t} \end{aligned} \tag{3.14}$$

(The variable λ is considered the eigen value.) Substituting equation 3.14 into 3.11 yields,

$$\begin{aligned} m\lambda^2 A + k\left(A - B\right) &= 0 \\ m\lambda^2 C + k\left(C - D\right) &= 0 \\ k\left(A - B\right) - 2\left(Bk_{xx} + Dk_{xy} + B\lambda c_{xx} + D\lambda c_{xy}\right) &= 0 \\ k\left(C - D\right) - 2\left(Bk_{yx} + Dk_{yy} + B\lambda c_{yx} + D\lambda c_{yy}\right) &= 0 \end{aligned} \tag{3.15}$$

The above system represents four equations and four unknown constants. Observing these equations in matrix form reveals that taking the determinant of the matrix and setting it equal to zero produces those values of A, B, C, and D (the four unknowns) that satisfy the equations of motion.

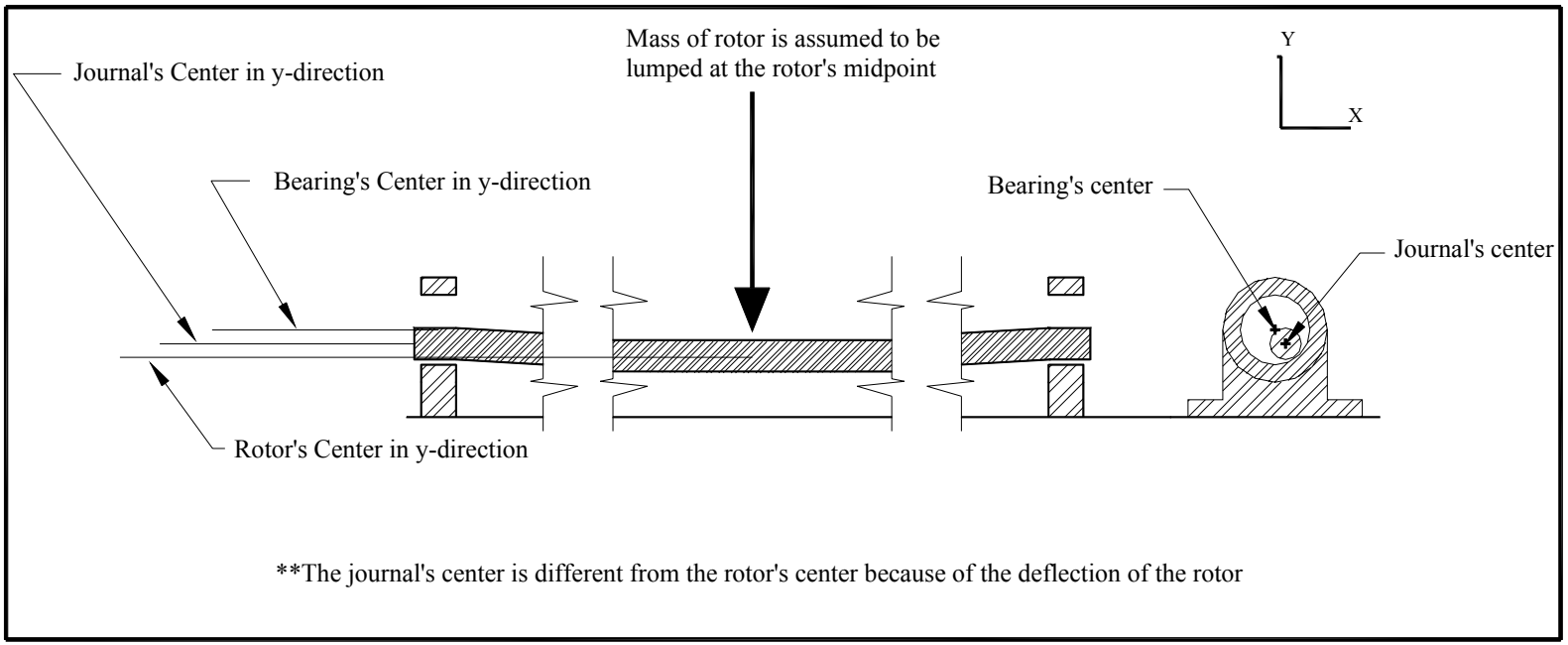

Figure 3.3 Basics for mathematical model

$$\begin{bmatrix} \left(m\lambda^2+k\right) & -\left(k\right) & 0 & 0 \\ 0 & 0 & \left(m\lambda^2+k\right) & -\left(k\right) \\ \left(k\right) & -\left(k+2k_{xx}+2\lambda c_{xx}\right) & 0 & -\left(2k_{xy}+2\lambda c_{xy}\right) \\ 0 & -\left(2k_{yx}+2\lambda c_{yx}\right) & \left(k\right) & -\left(k+2k_{yy}+2\lambda c_{yy}\right) \end{bmatrix} \begin{bmatrix} A \\ B \\ C \\ D \end{bmatrix} = 0 \qquad (3.16)$$

Taking the determinant of the matrix results in an equation that is referred to as the characteristic equation.

$$\det \begin{bmatrix} \left(m\lambda^2+k\right) & -\left(k\right) & 0 & 0 \\ 0 & 0 & \left(m\lambda^2+k\right) & -\left(k\right) \\ \left(k\right) & -\left(k+2k_{xx}+2\lambda c_{xx}\right) & 0 & -2\left(k_{xy}+2\lambda c_{xy}\right) \\ 0 & -\left(2k_{yx}+2\lambda c_{yx}\right) & \left(k\right) & -\left(k+2k_{yy}+2\lambda c_{yy}\right) \end{bmatrix} = 0 \qquad (3.17)$$

The following equation is the long-form of the characteristic equation.

$$\begin{aligned} &4\lambda^6 m^2\left(c_{yx}c_{xy}-c_{xx}c_{yy}\right)+ \\ &2\lambda^5 m^2\left(2k_{xy}c_{yx}+2k_{yx}c_{xy}-kc_{xx}-kc_{yy}-2c_{xx}k_{yy}-2k_{xx}c_{yy}\right)+ \\ &\lambda^4 m^2\left(4k_{yx}k_{xy}-4k_{xx}k_{yy}-2kk_{xx}-2kk_{yy}-k^2\right)+8\lambda^4 m\left(kc_{yx}c_{xy}-kc_{xx}c_{yy}\right)+ \\ &\lambda^3 m\left(8kk_{xy}c_{yx}+8kk_{yx}c_{xy}-2kc_{xx}-2kc_{yy}-8kc_{xx}k_{yy}-8kk_{xx}c_{yy}\right)+ \\ &\lambda^2 m\left(8kk_{yx}k_{xy}-8kk_{xx}k_{yy}-2k^2k_{xx}-2k^2k_{yy}\right)+4\lambda^2\left(k^2c_{yx}c_{xy}-k^2c_{xx}c_{yy}\right)+ \\ &4\lambda\left(k^2k_{xy}c_{yx}-k^2k_{yx}c_{xy}-k^2c_{xx}k_{yy}-k^2k_{xx}c_{yy}\right)+ \\ &4k^2\left(k_{yx}k_{xy}-k_{xx}k_{yy}\right)=0 \end{aligned} \qquad (3.18)$$

Making the equations dimensionless at this point will provide results of a general form. The dimensionless variables used in this problem are:

$$\bar{k}=k\frac{C}{W} \qquad \bar{c}=c\frac{C\omega}{W} \qquad \bar{m}=m\frac{C\omega^2}{W}$$

$$\bar{\lambda}=\lambda\frac{1}{\sqrt{\frac{W}{mC}}} \qquad \bar{\omega}=\omega\frac{1}{\sqrt{\frac{W}{mC}}} \qquad (3.19)$$

where “W” is the bearing load, “m” is the effective mass per bearing, “k” is the stiffness, “c” is the damping coefficient, “C” is the radial clearance, “ω” is the rotational speed (rad/s), and “λ” is the eigen value”. Substituting these dimensionless variables into the characteristic equation gives the following dimensionless form of the characteristic equation.

$$
\begin{aligned}
&16\frac{\bar{\lambda}^6}{\bar{\omega}^2}\left(\bar{c}_{yx}\bar{c}_{xy}-\bar{c}_{xx}\bar{c}_{yy}\right)+\\
&8\frac{\bar{\lambda}^5}{\bar{\omega}}\left(2\bar{k}_{xy}\bar{c}_{yx}+2\bar{k}_{yx}\bar{c}_{xy}-\bar{k}\bar{c}_{xx}-\bar{k}\bar{c}_{yy}-2\bar{c}_{xx}\bar{k}_{yy}-2\bar{k}_{xx}\bar{c}_{yy}\right)+\\
&4\bar{\lambda}^4\left(4\bar{k}_{yx}\bar{k}_{xy}-4\bar{k}_{xx}\bar{k}_{yy}-2\bar{k}\bar{k}_{xx}-2\bar{k}\bar{k}_{yy}-\bar{k}^2\right)+16\frac{\bar{\lambda}^4}{\bar{\omega}^2}\left(\bar{k}\bar{c}_{yx}\bar{c}_{xy}-\bar{k}\bar{c}_{xx}\bar{c}_{yy}\right)+\\
&4\frac{\bar{\lambda}^3\bar{k}}{\bar{\omega}}\left(4\bar{k}_{xy}\bar{c}_{yx}+4\bar{k}_{yx}\bar{c}_{xy}-\bar{c}_{xx}-\bar{c}_{yy}-4\bar{c}_{xx}\bar{k}_{yy}-4\bar{k}_{xx}\bar{c}_{yy}\right)+\\
&4\bar{\lambda}^2\bar{k}\left(4\bar{k}_{yx}\bar{k}_{xy}-4\bar{k}_{xx}\bar{k}_{yy}-\bar{k}\bar{k}_{xx}-\bar{k}\bar{k}_{yy}\right)+4\frac{\bar{\lambda}^2\bar{k}^2}{\bar{\omega}^2}\left(\bar{c}_{yx}\bar{c}_{xy}-\bar{c}_{xx}\bar{c}_{yy}\right)+\\
&4\frac{\bar{\lambda}\bar{k}^2}{\bar{\omega}}\left(\bar{k}_{xy}\bar{c}_{yx}-\bar{k}_{yx}\bar{c}_{xy}-\bar{c}_{xx}\bar{k}_{yy}-\bar{k}_{xx}\bar{c}_{yy}\right)+\\
&4\bar{k}^2\left(\bar{k}_{yx}\bar{k}_{xy}-\bar{k}_{xx}\bar{k}_{yy}\right)=0
\end{aligned}
\tag{3.20}
$$

Recall that the solution to the equations of motion was assumed in terms of the system’s eigenvalue. To find a solution to the equations of motion, λ must be found. The most general form of λ is of a complex form. It may be written as

$$\lambda = r + is\,, \tag{3.21}$$

where r is the real part of the eigen value and s is the imaginary part of the eigen value. Notice the form of the solution of the equations of motion.

$$x = Ae^{(r+is)t} = Ae^{rt}e^{ist} \tag{3.22}$$

If the real part of the solution is positive, then x goes to infinity, and if the real part is negative, then x goes to negative infinity. So for the rotor to be at a state that neither

declines nor inclines, *r* must be equal to zero. Thus, *r*=0 is a major stability threshold criteria and the eigen value takes the form

$$\lambda = is \tag{3.23}$$

By grouping terms in the dimensionless characteristic equation, an equation that is just a function of the eigen values remains. It is expressed as

$$-F_a s^6 + iF_b s^5 + F_c s^4 - iF_d s^3 - F_e s^2 + iF_f s + F_g = 0 \tag{3.24}$$

where,

$$\begin{aligned}
F_a &= \frac{16}{\bar{\omega}^2}\left(\overline{c_{yx}c_{xy}} - \overline{c_{xx}c_{yy}}\right) \\
F_b &= \frac{8}{\bar{\omega}}\left(2\overline{k_{xy}c_{yx}} + 2\overline{k_{yx}c_{xy}} - \overline{k}\,\overline{c_{xx}} - \overline{k}\,\overline{c_{yy}} - 2\overline{c_{xx}k_{yy}} - 2\overline{k_{xx}c_{yy}}\right) \\
F_{c1} &= 4\left(4\overline{k_{yx}k_{xy}} - 4\overline{k_{xx}k_{yy}} - 2\overline{k}\,\overline{k_{xx}} - 2\overline{k}\,\overline{k_{yy}} - \bar{k}^2\right) \\
F_{c2} &= \frac{16}{\bar{\omega}^2}\left(\overline{k}\,\overline{c_{yx}c_{xy}} - \overline{k}\,\overline{c_{xx}c_{yy}}\right) \\
F_d &= \frac{4}{\bar{\omega}}\left(4\overline{k_{xy}c_{yx}} + 4\overline{k_{yx}c_{xy}} - 4\overline{k_{xx}c_{yy}} - 4\overline{k_{yy}c_{xx}} - \overline{k}\,\overline{c_{xx}} - \overline{k}\,\overline{c_{yy}}\right) \\
F_{e1} &= 4\bar{k}\left(4\overline{k_{yx}k_{xy}} - 4\overline{k_{xx}k_{yy}} - \overline{k}\,\overline{k_{xx}} - \overline{k}\,\overline{k_{yy}}\right) \\
F_{e2} &= \frac{4\bar{k}^2}{\bar{\omega}^2}\left(\overline{c_{yx}c_{xy}} - \overline{c_{xx}c_{yy}}\right) \\
F_f &= \frac{4\bar{k}^2}{\bar{\omega}}\left(\overline{k_{xy}c_{yx}} - \overline{k_{yx}c_{xy}} - \overline{k_{yy}c_{xx}} - \overline{k_{xx}c_{yy}}\right) \\
F_g &= 4\bar{k}^2\left(\overline{k_{yx}k_{xy}} - \overline{k_{xx}k_{yy}}\right)
\end{aligned} \tag{3.25}$$

If the grouped characteristic equation must equal zero, then the imaginary part must equal zero and the real part must equal zero. Thus, two equations can be made.

$$\begin{aligned}
&-F_a s^6 + F_c s^4 - F_e s^2 + F_g = 0 \\
&iF_b s^5 - iF_d s^3 + iF_f s = 0
\end{aligned} \tag{3.26}$$

By making the assumption that $S = s^2$, a quadratic equation evolves and the roots of this equation can be found to be solutions of the imaginary part of the characteristic equation.

$$S = F_d \pm \frac{\sqrt{\left(-F_d\right)^2 - 4F_bF_f}}{2F_b} \tag{3.27}$$

Since the two solutions of S must satisfy the imaginary part of the characteristic equation, substitute (3.27) into the real part of the characteristic equation and solve for the dimensionless speed. However, the dimensionless speed does not appear in the equations directly. Therefore, the characteristic equation is rewritten with the constants G_n in the real part. The following two equations and two unknowns (dimensionless speed and S) will emerge.

$$-\frac{G_a}{\overline{\omega}^2}s^6 + i\frac{G_b}{\overline{\omega}}s^5 + \left(G_{c1} + \frac{G_{c2}}{\overline{\omega}^2}\right)s^4 - i\frac{G_d}{\overline{\omega}}s^3 - \left(G_{e1} + \frac{G_{e2}}{\overline{\omega}^2}\right)s^2 + i\frac{G_f}{\overline{\omega}}s + G_g = 0 \tag{3.28}$$

$$i\frac{G_b}{\overline{\omega}}s^5 + -i\frac{G_d}{\overline{\omega}}s^3 + i\frac{G_f}{\overline{\omega}}s = 0 \tag{3.29}$$

$$-\frac{G_a}{\overline{\omega}^2}s^6 + \left(G_{c1} + \frac{G_{c2}}{\overline{\omega}^2}\right)s^4 - \left(G_{e1} + \frac{G_{e2}}{\overline{\omega}^2}\right)s^2 + G_g = 0 \tag{3.30}$$

$$S = G_d \pm \frac{\sqrt{\left(-G_d\right)^2 - 4G_bG_f}}{2G_b} \tag{3.31}$$

where,

$$G_a = 16\left(\overline{c_{yx}}\,\overline{c_{xy}} - \overline{c_{xx}}\,\overline{c_{yy}}\right)$$

$$G_b = 8\left(2\overline{k_{xy}}\,\overline{c_{yx}} + 2\overline{k_{yx}}\,\overline{c_{xy}} - \overline{k}\,\overline{c_{xx}} - \overline{k}\,\overline{c_{yy}} - 2\overline{c_{xx}}\,\overline{k_{yy}} - 2\overline{k_{xx}}\,\overline{c_{yy}}\right)$$

$$G_{c1} = 4\left(4\overline{k_{yx}}\,\overline{k_{xy}} - 4\overline{k_{xx}}\,\overline{k_{yy}} - 2\overline{k}\,\overline{k_{xx}} - 2\overline{k}\,\overline{k_{yy}} - \overline{k}^2\right)$$

$$G_{c2} = 16\left(\overline{k}\,\overline{c_{yx}}\,\overline{c_{xy}} - \overline{k}\,\overline{c_{xx}}\,\overline{c_{yy}}\right)$$

$$G_d = 4\left(4\overline{k_{xy}}\,\overline{c_{yx}} + 4\overline{k_{yx}}\,\overline{c_{xy}} - 4\overline{k_{xx}}\,\overline{c_{yy}} - 4\overline{k_{yy}}\,\overline{c_{xx}} - \overline{k}\,\overline{c_{xx}} - \overline{k}\,\overline{c_{yy}}\right)$$

$$
\begin{aligned}
G_{e1} &= 4\bar{k}\left(4\overline{k_{yx}}\,\overline{k_{xy}} - 4\overline{k_{xx}}\,\overline{k_{yy}} - \bar{k}\,\overline{k_{xx}} - \bar{k}\,\overline{k_{yy}}\right) \\
G_{e2} &= 4\bar{k}^2\left(\overline{c_{yx}}\,\overline{c_{xy}} - \overline{c_{xx}}\,\overline{c_{yy}}\right) \\
G_f &= 4\bar{k}^2\left(\overline{k_{xy}}\,\overline{c_{yx}} - \overline{k_{yx}}\,\overline{c_{xy}} - \overline{k_{yy}}\,\overline{c_{xx}} - \overline{k_{xx}}\,\overline{c_{yy}}\right) \\
G_g &= 4\bar{k}^2\left(\overline{k_{yx}}\,\overline{k_{xy}} - \overline{k_{xx}}\,\overline{k_{yy}}\right)
\end{aligned}
\qquad (3.32)
$$

The evaluation results in two numbers for the dimensionless speed. One of the solutions is usually near zero, while the other gives a logical value. Only the latter is valid. This value is the whirl threshold speed.

$$
\bar{\omega} = \sqrt{\frac{G_a S^3 - G_{c2} S^2 - G_{e2} S}{G_{c1} S^2 - G_{e1} S^2 - G_g}} \qquad (3.33)
$$

The whirl threshold is ultimately a function of the dynamic stiffness and damping coefficients, and the coefficients are pure functions of the eccentricity. Since equation 3.10 shows that eccentricity is a function of the Sommerfeld number (or the bearing parameters), a relation between the whirl threshold and the bearing parameters can be formulated. Evaluating this relation for a range of the Sommerfeld number results in the following plot. For a particular system under given conditions, an evaluation of the Sommerfeld number and the dimensionless speed will produce a point on this graph. If that point lies above the whirl threshold line, the journal bearing system is whirling. Conversely, if the point lies below the line, the bearing system is stable with respect to oil whirl. And if the point were to lie on the whirl threshold line, the bearing system would be considered marginally stable (on the brink of whirling). In practice it is nearly impossible to make a journal bearing system operate exactly on such a point.

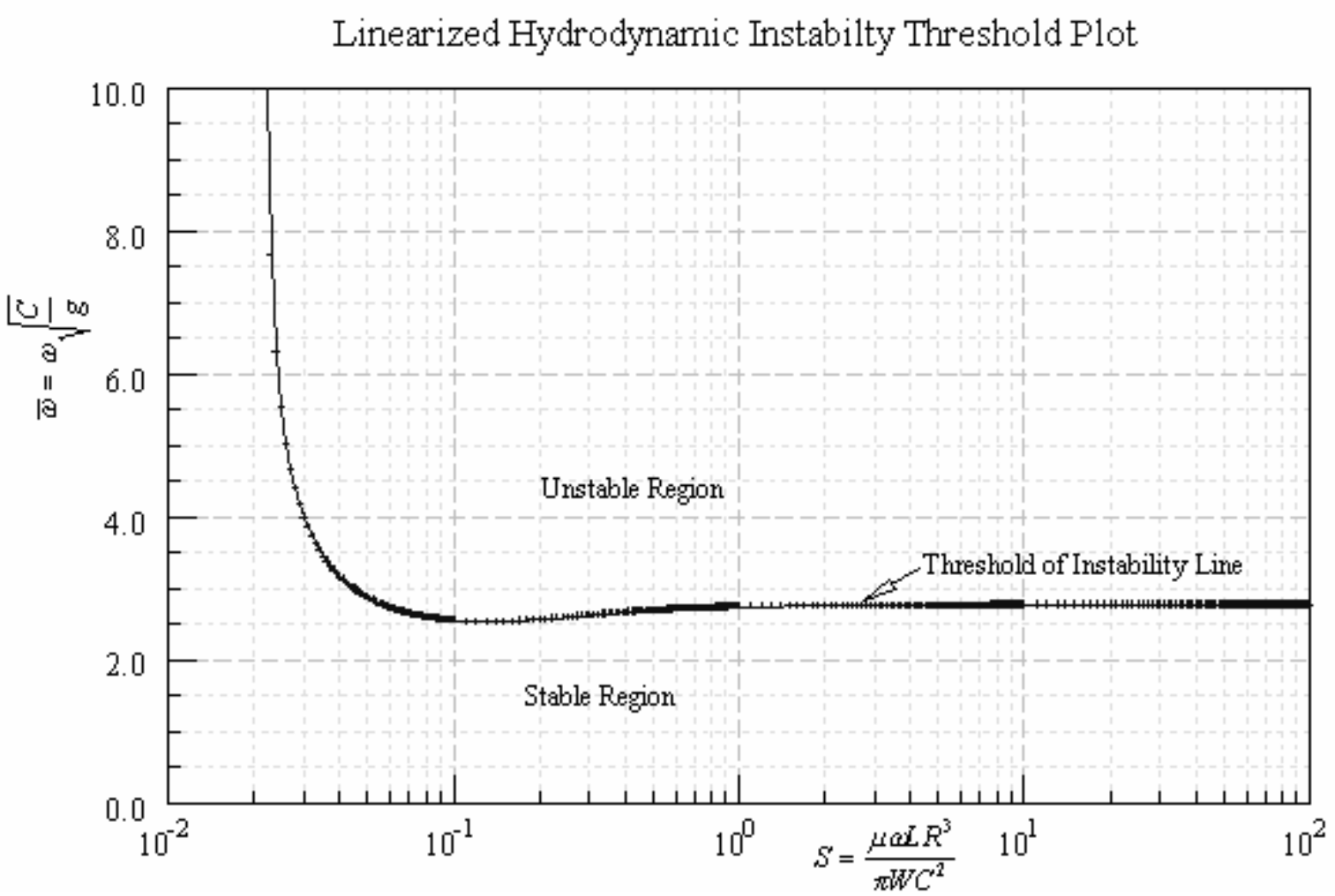

Figure 3.4 Threshold of whirl instability predicted by linear theory

4. Description of the Experimental System

The apparatus constructed to produce and test oil whirl is basic in design. A one-half horsepower, universal electric motor drives a one-inch diameter shaft supported by two identical plain journal bearings. The two journal bearings are mounted within a housing and are moveable on the base plate. The bearing housings have securing locations that provide equal loading on each bearing. In other words, each bearing has the same amount of overhang. The shaft is coupled to the motor's drive shaft with a stainless steel flexible coupling that has a spring-like mid-section. Its flexibility allows for movement in the lateral as well as the axial direction during operation. Along with the journal bearing housings, the motor is mounted on a 1 1/2 inch thick steel plate. Specifically, the bearing assembly was designed to ensure adaptability for future experiments as well as reliability for the present experiments. Thus, the entire bearing

Table 4.1: Rotor Kit Specifications

DIAMTERAL CLEARANCE	0.004 inch
ROTOR WEIGHT	5.34 lb, 8.50 lb, 12.02 lb
SHAFT DIAMETER	1.000 inch
JOURNAL DIAMETER	1.000 inch
INLET PRESSURE	4.5 psi
LUBRICANT	ISO 32
ROTATIONAL SPEED	0 - 10,000 rpm
DATA ACQUISITION SYSTEM	Bently Nevada's 108 DAI
DATA ACQUISITION SOFTWARE	ADRE

assembly consisted of a solid steel housing with interchangeable bearing inserts that have the desired bearing surface, geometrical configuration and clearance. Bearing inserts were made simple in design with cylindrical bores and various clearances. The basic cylindrical shape enables the experimenters to perform theoretical predictions on the

bearing system. The insert that was used had a radial clearances, between bearings and journals, of 0.002 inch . Brass was the material used for the bearing insert. Some general data on the conditions of the rotor kit are given in Table 4.1 and information on the speed control and drive system may be viewed in Table 4.2.

The base plate began as a cold rolled, A36 steel plate. A flat, parallel surface is needed along the top, bottom and sides so that the system may be aligned. However, internal stresses, produced during manufacturing, were released during machining and made it impossible to form these desirable surfaces. To remedy this, the plate was stress

Table 4.2: Electronic Specifications

MOTOR	DAYTON AC-DC Series motor
POWER TO MOTOR	0-65 VDC
MOTOR POWER	1/2 hp
MAXIMUM ROTATIONAL SPEED	10000 rpm
ELECTRONIC MOTOR DRIVE	Minerak XL3200A
POWER INPUT TO DRIVE	115 VAC 60 Hz
DRIVE TYPE	open-chasis DC drive
DRIVE REGULATION	0.5% of running speed
ACCELERATION TIME RANGE	1-12 seconds
ELECTRONIC SPEED CONTROLLER	Minerak DLC600
POWER INPUT TO CONTROLLER	115 VAC 60 Hz
FEEDBACK SOURCE	12 VDC NPN-type proximity detector
STANDARD GATE TIME	1 second
SPEED REGULATION	0.05% of running speed

relieved and then ground flat and parallel. The stress relief was accomplished by increasing its base plate's temperature to approximately 1200 degrees Fahrenheit and controllably cooled to room temperature over a period of 12 hours.

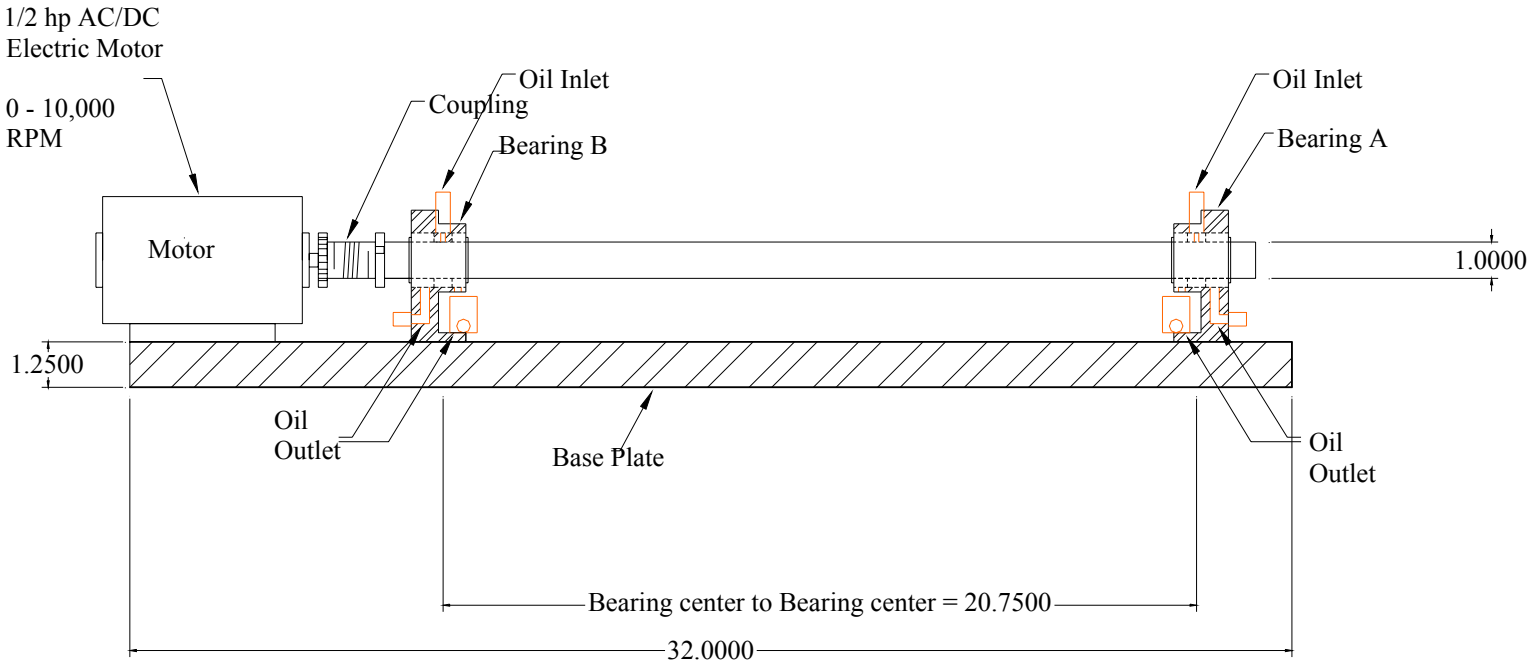

Figure 4.1 Illustration of the experimental test rig

Flatness and parallelism of surfaces on the top and bottom of the plate is necessary for precise alignment in the *z*-direction (figure 4.2). The height of the motor's shaft center, bearing A's center and bearing B's center must be extremely close to the same value. Since the clearance on the diameter between the journal and the bearing is 0.004 inch, or 0.002 inch in terms of the radius, any small difference in these heights could cause an undesired preload on the bearing. This preload would become unaccounted in calculations and could cause a much higher whirl threshold. After the grinding process, the machinist found that any point on the surface of the plate does not vary (increase or decrease) more than 0.001 inch with any other point.

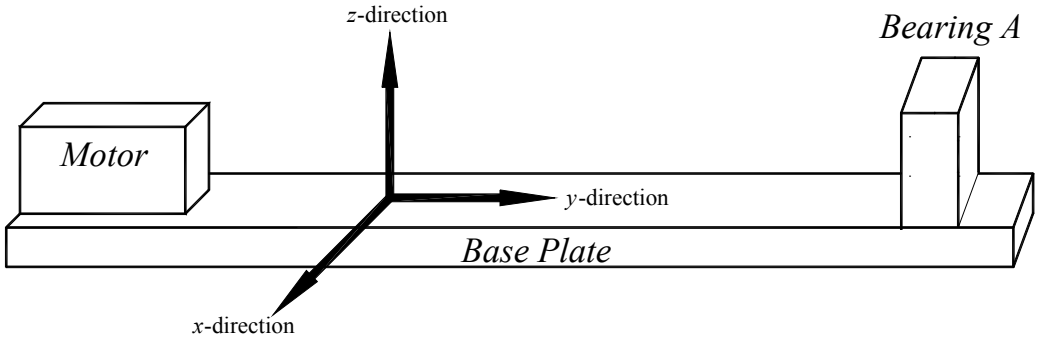

Figure 4.2 Directional coordinates adopted for the system

The long sides of the base plate were used in aligning the bearing housings and motor in the x-direction. Thus, the long sides were also ground flat and parallel after the stress relieving process. Since the short sides, or ends, are not used during the alignment process, they were just machined parallel to each other. Once the base plate was returned to the LSU machine shop, the base plate was again checked to be flat and parallel. In order to maintain alignment in the *x*-direction (figure 4.2) between the journal bearings a few measures were taken. A key way was cut down the length of the base plate in the axial direction to provide a linear alignment of the bearing housing in the *x*-direction.

The width of the key way was milled to be just 0.001 inch wider than that of the key stock to provide a hand-fit placement of the housings without sacrificing the desired alignment. The base plate was also drilled and tapped for securing locations for the journal bearing housings. The holes were drilled every 2 inches on the plate along the entire length of the shaft.

The alignment of the bearings was taken into consideration when manufacturing the bearing assemblies. In general for the bearing housings to be aligned with one another, the bores must have the same centerline and their surfaces must be parallel when mounted on the base plate. In other words, they cannot be "cocked" with respect to one another. In solving these problems, the two bearing housings were initially bolted together as one unit (figure 4.3). Beginning with two solid blocks of steel, each piece is made so that all of its joining faces form ninety-degree angles and non-meeting faces are parallel. Note, the mating surface of bearing housing A and that of bearing housing B were also ground flat. They were then bolted together and another pass with the milling machine was made on all sides to ensure identical blocks.

Particularly, the bottom of the housing, that which contacts the base plate, must be machined flat and then reground in order to have a surface to work off of. Next, the bores of the housing were machined. This ensures that the bores are not only parallel to each other, but also that the bores are parallel to the bottom. While bolted together the key way is machined in the bottom in the y-direction. All of the excess material is milled off of the bearing housing, and the two pieces were unbolted. In general, the entire procedure assures the experimenter that the two bearing housings are dimensionally equal

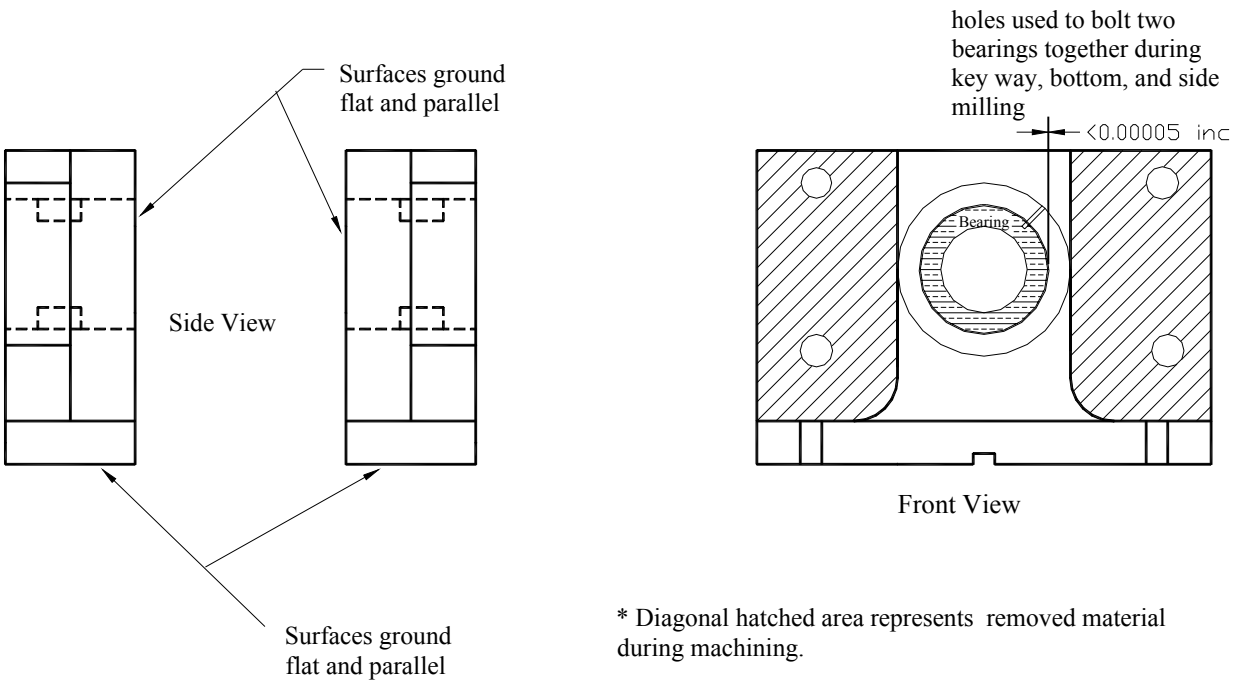

Figure 4.3: Bearing housing as it is made from two blocks of steel

in the *x*, and *z*-directions. Also, the housings can be considered "not cocked" with respect to one another because the keyway and the bores were milled while the two pieces were bolted together. Two identical journal bearing housings have been manufactured, and within practical means the journal bearing housings are aligned when mounted on the base plate.

The bearing housings, like the base plate, were made of A36 steel. These components were not heat treated for stress relief, but were checked for distortion after the machining was performed. No measurable distortion was found. The bearing housing bore was milled to a diameter of 1.513 inches. After the bearings were unbolted, thermocouples holes, oil inlet holes, oil exit holes, and proximity sensor holes were drilled into the bearing housings. Also, misalignment in the bearing inserts was not neglected. The tolerance between the bearing housing inside diameter and the bearing

insert outside diameter was made to be less than 0.001 inch and greater than 0.0005 inch (figure 4.4). In addition, an axial alignment groove was cut on the outside diameter of the inserts and secured with two set- screws from the bearing housing. This was taken to be sufficient measures in bearing alignment consideration.

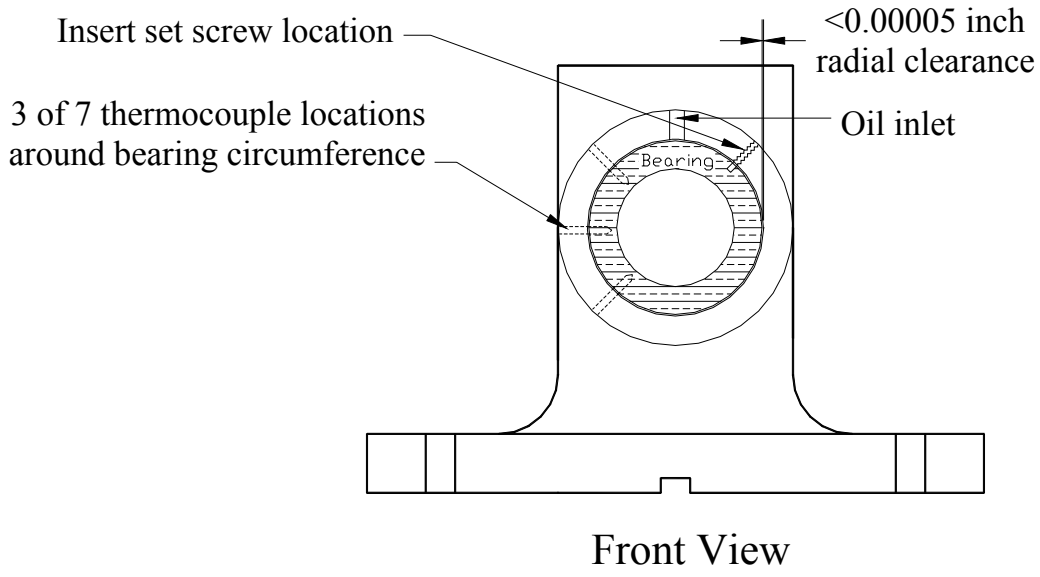

Figure 4.4 Clearance between the bearing and the bearing housing

Since journal bearings have small clearances, relative to maintaining a well-aligned system, it seemed imperative to install and couple the drive motor with the same care as that taken with the bearings. A flexible coupling allows for small percentage of misalignment between the motor's shaft and the rotor's shaft. The alignment of the motor to the bearing housings was the most difficult part of the alignment. The motor must not only be positioned in the correct *x* and *z*-locations, but also, the angular alignment in the *x* and *z*-directions are crucial. In the alignment of the bearing housings angular alignment was resolved by machining the housings from an ultimately, single block. For the height-alignment of the motor, it was placed on a 1/2 inch ground plate and then shimmed. The amount and location of shimming was found through the use of a

dial indicator and a special insert in the bearing housing (figure 4.5). By reading the dial indicator off of the outside diameter of the insert, the correct height of the motor can be found. At the same time the angular position of the motor must be observed. Angular and centerline alignments are interdependent.

The alignment on both bearings must be performed at the same time since adjusting one bearing's alignment is liable to alter the other. The angular alignment is accomplished by reading a dial indicator off of the face of the insert. Any variance in the indicator reading (on the face) as it is rotated around the circumference notes a tilting of the motor in that respective direction. A similar procedure is done to align the shaft's centerline; however, the dial indicator is read off of the outside diameter of the bearing alignment tool. By alternating back and forth with these two readings around the entire circumference, both the *x*- direction and *z*-direction centering and angular alignments are attained. Reading the dial indicators while adjusting the motor position through "hand force" can be quite cumbersome. To aid in the precise positioning of the motor, another alignment procedure was developed. Four (4) fine-threaded, jack-bolts were positioned on the sides of the motor (two on each side: see figure 4.5). This allows delicate movement of the motor.

4.1 Instrumentation

The main data of interest are: temperature of the inlet oil, temperature of bearing surface, the current rotational speed, and the vibration amplitude. All of the temperature measurements were found by using type *J* thermocouples. The oil temperature was measured by placing the thermocouple in the stream of the oil just before the oil entered the bearing (figure 4.6). The tip of the thermocouple was always in contact with the

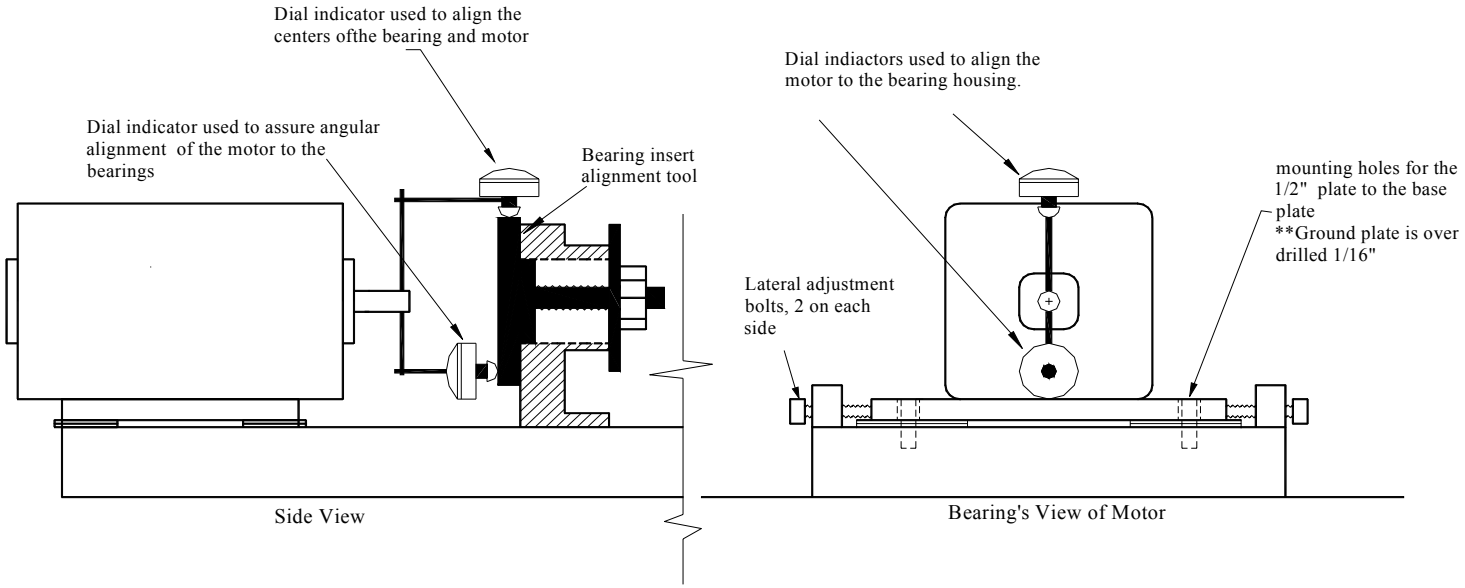

Figure 4.5 Basic diagram of the motor alignment tools and their functions

lubricant; no air was present in the oil line. In finding the bearing surface temperature, thermocouples were placed 0.050 inch from the inner diameter of the surface (figure 4.7). This was believed to be a close approximation of the surface temperature. There were seven total thermocouples installed in this manner. Spanning 315 degrees of the

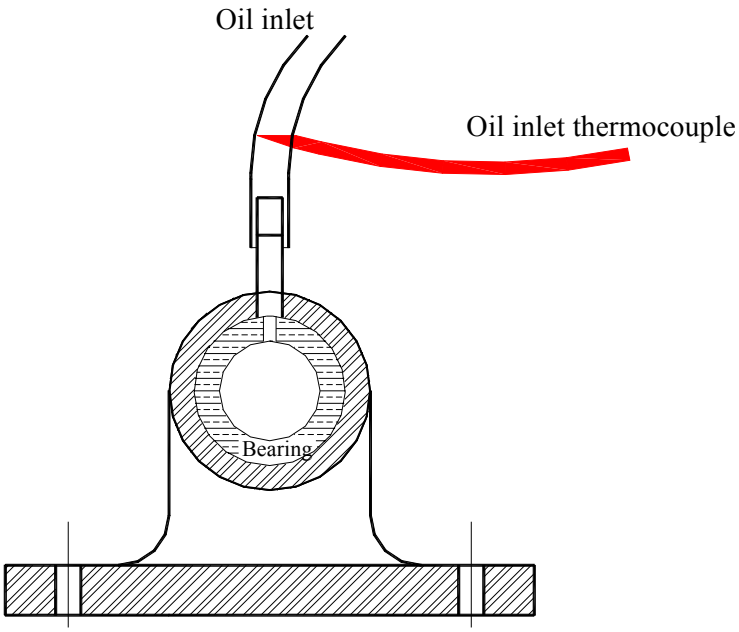

Figure 4.6 Location of the inlet oil temperature measurement

circumference, each thermocouple was 45 degrees away from its neighboring thermocouple. The thermocouple leads were then fed into an electronic temperature display.

The rotational speed was also continuously monitored with the aid of proximitors and proximity probes. The proximity probes can detect a change in distance from its tip

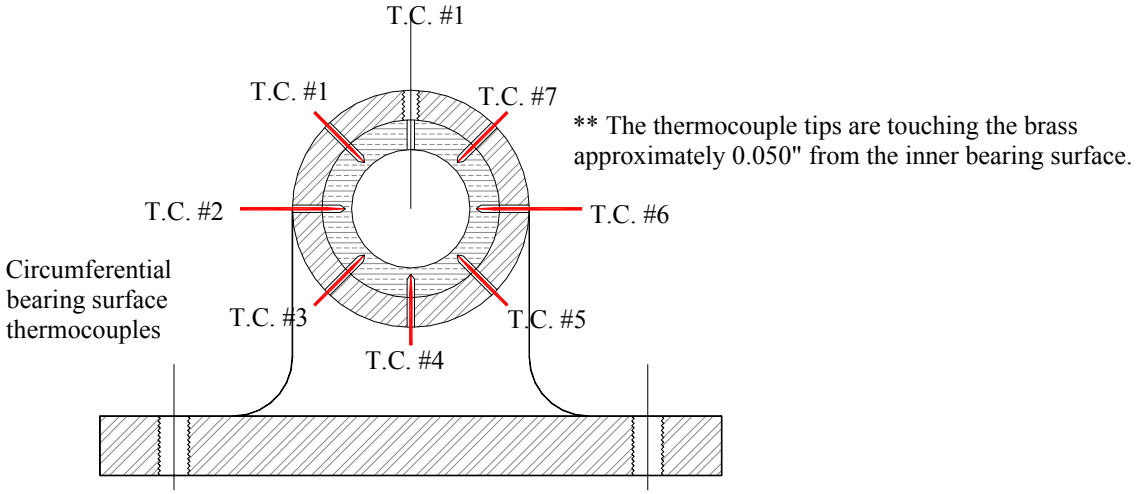

Figure 4.7 Circumferential position of the bearing temperature sensors

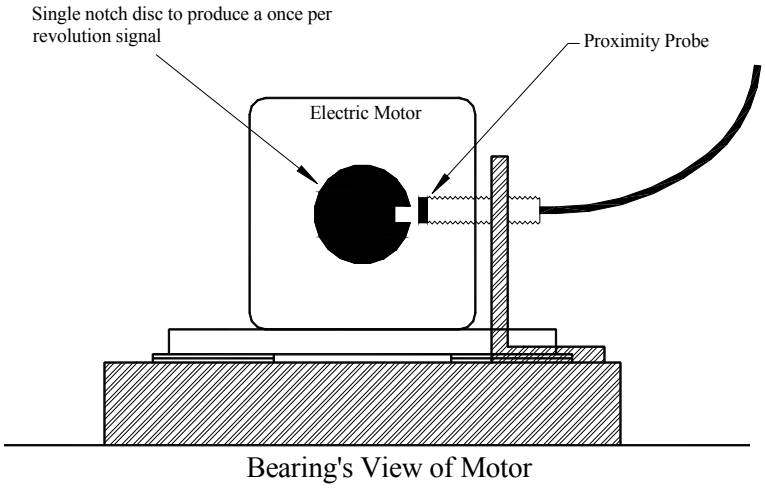

Figure 4.8 Proximity probe that marks the rotational speed (a once per revolution signal)

to the metallic object it is positioned near. To detect the rotational speed, a small notch is cut in a disc located near the coupling. A spike in the voltage reading sent to the proximitor will be seen once for every revolution. This coupled with a timer produces the rotational speed of the shaft. The proximity probes and proximitors were also used to detect the vibration amplitude of the journal. Two proximity probes, 90 degrees apart, were positioned near the journal. The voltage sent by the proximity probe to the proximitor is linearly dependent on the gap distance between its tip and the steel shaft. The linear relationship is 200 milli-volts per thousandth of an inch gap distance. If the probe is 0.040 inch from the shaft, then the voltage read by the proximitor is 8 volts. Now, the measurement of the vibration amplitude is a dynamic event. It only accounts

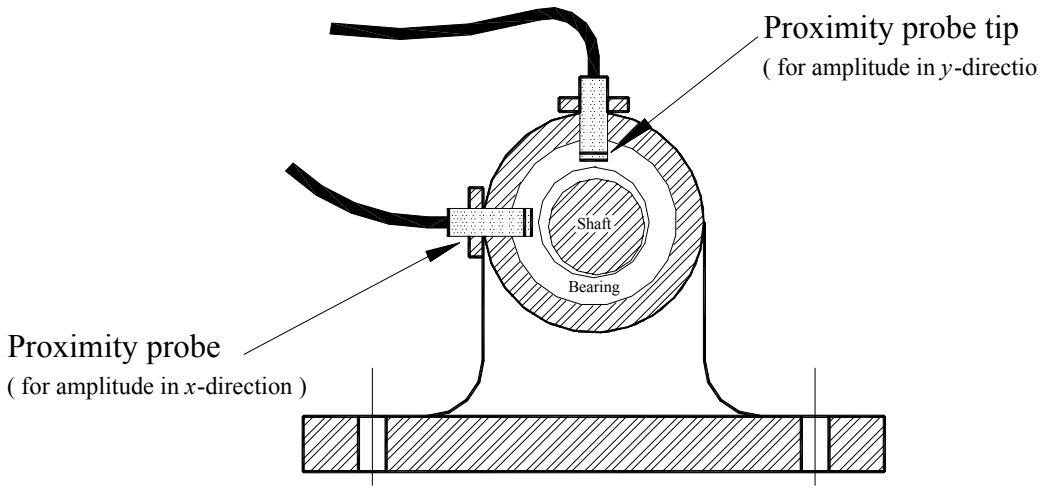

Figure 4.9 Proximity probes used to measure the vibration amplitude

for a change in voltage (which correlates to a change in shaft position); thus, the peak-to-peak amplitude is read. Since the probes are 90 degrees apart, one probe gives the *x*-direction of amplitude, and the other could provide the *y*-direction. By combining the two, a polar plot can illustrate the shaft's center whirl pattern.

The proximitors indicate the rotational speed and amplitude of vibration by sending a voltage signal to the Bently Nevada 108 DAI. This is a data acquisition unit the can store this information. After collection, the data can then be downloaded to the computer and organized through the Bently Nevada software, ADRE. It is from this software that the various plots in this thesis are configured.

5. Experimental Procedure

For all experiments performed, a testing procedure was implemented in order to obtain consistent results and maintain repeatability. Thermal equilibrium, bearing temperature, lubricant supply temperature, rotational speed, rate of increase of the rotational speed, vibration amplitude, and vibration frequencies were some of the items that were monitored. Bently Nevada's 108 DAI recorded the data for the speed of rotation, frequencies of vibration, and amplitude of vibration as discussed in chapter 3. The temperature data was displayed of Bently Nevada's 3300 data acquisition system. These figures were then manually recorded.

Three different experiments were run during the research period. The first type investigated the threshold of instability under thermal equilibrium conditions. The second studied the conditions of the system when whirl instability was present at the start-up of the rotor. A third type of experiment that was performed investigated the effect of lubricant supply temperature while the system was operating just below the threshold of instability.

5.1 Determination of Instability under Steady-State Conditions

The experimental procedure for finding the threshold of instability under thermal equilibrium conditions is as follows. First, the oil supply was turned on and remained on without the motor in operation for a reasonable amount of time, typically 10-15 minutes, to ensure an adequate supply of oil was present in the bearing. After this period of time, the motor was started at a slow speed, typically 800 - 1500 rpm. The motor ran at this speed until the bearing reached the thermal equilibrium for these given conditions. This usually took 30 minutes and was monitored by examining circumferential temperature

data. The rotational speed was then increased and again the system was allowed to reach thermal equilibrium. This repetitive procedure was continued. As a result of increasing the speed, eventually, the journal began whirling within the bearing. Notably, it became critical to make small adjustments of rotational speed, as the journal bearing system got closer to its threshold. Small disturbances can cause a stable journal to become unstable; hence, any jolt from the motor induces a vibration down the shaft and can send the journal into an oil whirl. The speed at which whirl began - and was sustained - marked the recorded experimental whirl threshold. These experiments were performed several times in order to gain confidence in the performance of the testing system.

5.2 Data Captured for Instances of Initial Whirl

Additionally, the action of whirl instability at the start-up of the rotor was the second type of experiment that was performed. First, the oil was supplied to the bearing. It remained on without motor operation for a reasonable amount of time, typically 10-15 minutes, to ensure that an adequate supply of oil was present in the bearing. Then, the motor was ramped up to a specified speed. Typically, the speeds were increased to values between 1000 and 3000 rpm. The data acquisition system was set to record prior to motor start-up.

5.3 Increase of Lubricant Temperature below Threshold of Instability

The third type of experiment that was performed included the increase of the supply oil temperature at a speed just below the threshold of instability. The procedure of the first experiments was followed up to a point that was just below the instability threshold. A particular rotor speed was established and thermal equilibrium was reached. (The actual speed changed according to the given experiment.) Then, the upper reservoir

containing the supply oil increased the temperature of the lubricant to 60 C. The journal bearing system was monitored for occurrence of hydrodynamic instability.

A general outline of the lubrication system can be seen in Figure 5.1. The lubricant comes down a common main line and then branches into two, equal length lines, which distribute the oil to each bearing. The supply line is 3/8" ID clear vinyl tubing that has lengths as depicted in Figure 5.1.

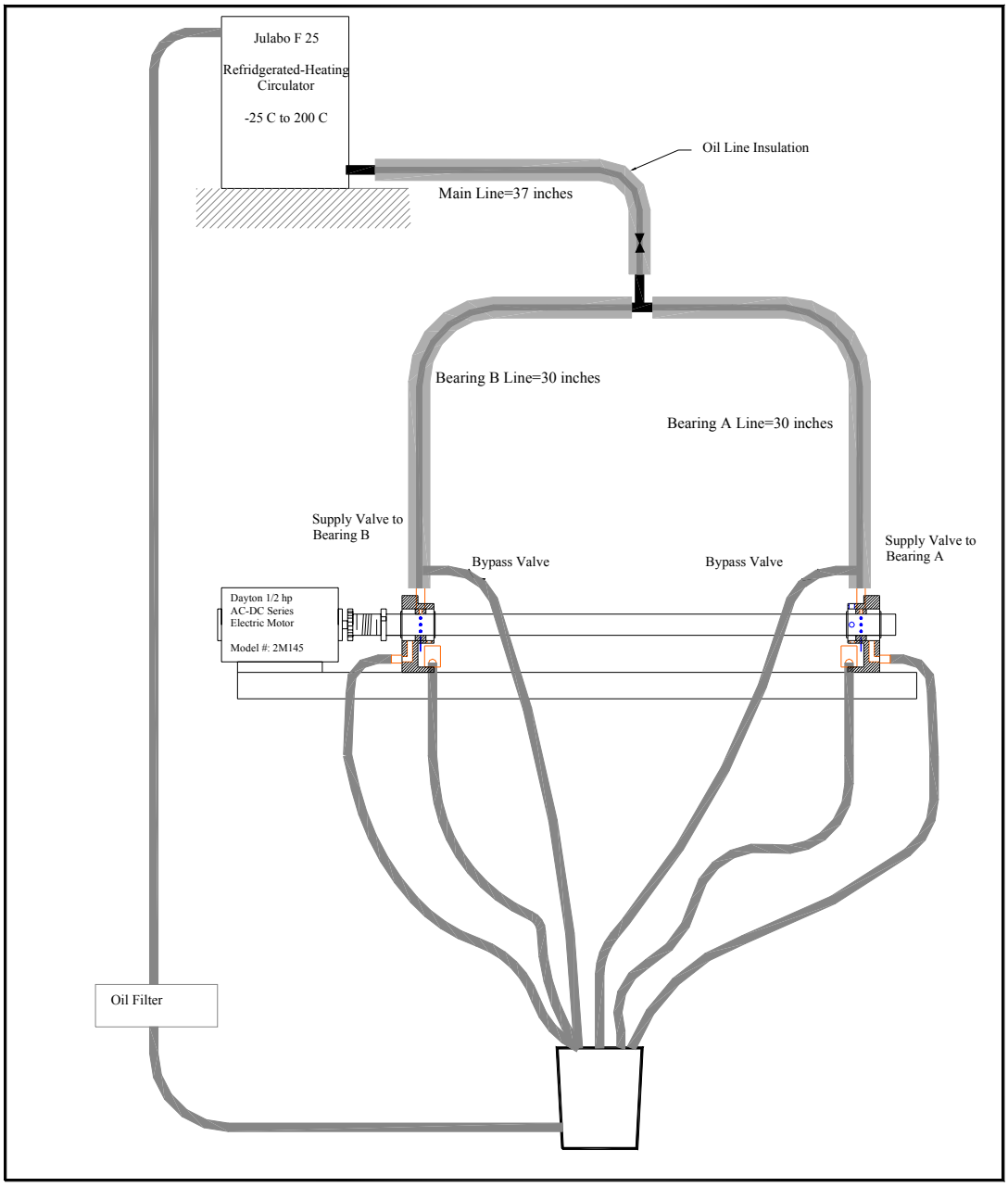

Figure 5.1 is a general diagram of the oil supply to the bearings

6. Experimental Results

Over 45 experiments were run throughout the testing period with three different rotors. The results of rotors #1, #3 and #4 are discussed below. Rotor #2 was not studied intensively; thus, the results were not analyzed. The results of rotors #1, #3, and #4 showed significant repeatable data and have been compiled to describe the behavior of whirl instability in this rotor bearing system. Table 6.1 gives some common properties of the different rotor systems.

	Rotor #1	Rotor #3	Rotor #4	*Units*
Stiffness via Myosotis Method	2380	7707	10954	*Lb_f/in^2*
Dimensionless Stiffness	2.88	3.69	3.66	*Unitless k*(C/W)*
Weight of Rotor	3.3	8.34	12.02	*Lbf*
First Natural Frequency	527.89	597.55	593.40	*rad/s*
Theoretical Threshold of Whirl Instability	7600	8050	7950	*Rpm*
Experimental Threshold of Whirl Instability	4000, 4800, 5600 ** See section 6.1*	5600, 7500 ** See section 6.3*	8350	*Rpm*

Table 6.1: Properties of journal bearing systems

The plots used in this chapter are referred to as waterfall, orbit, spectrum and bode plots. The waterfall plot is a three-dimensional plot where the x-axis is the frequency of vibration, the y-axis is the time (or rotational speed since rpm increases with respect to time), and the z-axis is the amplitude of vibration. The rotational speed can be matched to the vibration frequency. This shows the "1X" frequency of vibration. The vibration produced by whirl instability occurs at a frequency that is less than ½ of the rotational frequency. It can be seen in the graphs by observing any amplitude near the frequency that is ½ of the rotational frequency.

The orbit plots are a combination of the total displacements in the x and y directions of the journal at a particular instant. Figure 4.9 shows the eddy-current proximity probes that measure the relative motion in the two directions. Together they produce the motion of the center of the journal. This is not a plot of the journal's postion within the bearing since the proximity probes can only detect the relative displacement of the journal. Also, under stable conditions the orbit plot produces one "keyphaser" dot for each orbit. However, a journal operating in oil whirl will produce two "keyphaser" dots for each orbit. Figure 6.4(b) shows a stable journal that has an orbit due to unbalance. Figure 6.4(d) illustrates that the journal is experiencing oil whirl as illustrated by the high amplitude and two "keyphaser" dots on each orbit.

The "keyphaser" dot is that point at which the third proximity probe, as seen in Figure 4.8, detects the notch in the disc. Since there is only one notch on the circumference, the data acquisition unit can record the speed of rotation. Under whirl stability the excitability of the rotor is due to unbalance. Thus, the shaft rotates about the center of the bearing at a frequency equal to the frequency of rotation. However, under whirl instability the shaft orbits within the bearing at a frequency that is approximately ½ of the rotational frequency. Therefore, in one orbit of the shaft's center, the rotor would have rotated twice. Two "keyphaser" dots appear on the orbit of the shafts center during whirl instability.

The spectrum plot is a two dimensional plot of the frequency of vibration versus the amplitude of vibration at a particular instant. It is used in Figure 6.13 to show rotor #4 entering whirl instability. The bode plot was also used to illustrate the presence of whirl at start-up. The bode plot is also a two dimensional plot of the total amplitude of

vibration versus rotational speed. This was useful to show that the rotor was ramped up to a particular speed and was allowed to run at that speed for a period of time. If whirl ceased, it could be seen as a drop in amplitude. Figure 6.5 is such an example.

6.1 Experimental Threshold of Rotor #1

The first experiments conducted were to investigate the experimental threshold of rotor #1. Theoretically, the speed at which the system should begin to whirl is 7600 rpm; however, the experimental speed at the onset of instability was significantly lower. There were three different sets of results defining the experimental threshold. Each set was performed approximately five months apart. The results obtained were repeatable and conclusive at the time of the respective experimentation, but there were significant differences between the three sets. The controllable parameters of the system were checked and set to matching conditions for all periods of experimentation.

The presence of oil whirl with rotor #1 was highly sensitive to the conditions of the system. In March of 2002 the established experimental threshold for rotor #1 was approximately 4000 rpm. The physical characteristics of the system are as stated in Chapter 3. Some notable conditions for the particular set of tests are: the bearings are fed lubricant via gravity, which has a supply pressure of approximately 1.5 psi at the bearing inlet, and the bearings are fed lubricant at a temperature equivalent to the temperature of the room. These results were repeatable and clear during this time. However, tests were not run with rotor #1 again until September of 2002. By this time the Julabo F25, described in chapter 4, had been installed. The Julabo F25 is a refrigerating/heating circulator for the lubricant. For these tests the lubricant temperature was set to 25˚C and the pressure was near 4.5 psi. The experimental threshold of the rotor was found to be

approximately 4800 rpm. Again, these results were repeatable and conclusive during this period. After this testing period, rotor #1 had not been run until February 2003. Again, a different experimental threshold was found to occur at 5600 rpm. These results were also repeatable; however, there were some instances where the transition from a stable rotor to a whirling rotor was not "smooth." That is, the rotor system would cycle between stable conditions and that of whirl. In most cases, the rotor would eventually settle into a state of whirl; however, there were some instances that a definitive speed could not be established at which the system would maintain whirl.

During the three periods in which the experimental threshold speeds were found, the cause of the difference in the results was investigated. Among other things, the motor alignment was checked (sometimes adjusted), the lubricant was changed, journal surfaces were inspected, and bearing surfaces were inspected. At times the lubricant quality did have an impact on the behavior of a whirling rotor. Older oil had a stabilizing effect and caused the instability threshold to increase. Motor alignment seemed to play a major role with rotor #1. Since this rotor operated at a low eccentricity (typically at 0.05), any small adjustment of the motor is fed to the flexible coupling. However, the flexible coupling does not seem to be compliant for this lightly loaded case. To avoid motor influence on the rotor, angular and lateral motor alignment within 0.0005" may be necessary. Alignment to this degree was not easy to achieve. In most cases the alignment of the motor's shaft was within 0.0015" of the rotor in both the angular and lateral directions. As shown in Figure 6.1 and Figure 6.2, the experimental threshold speed of rotor #1 in September 2002 is approximately 4800 rpm. Experimental thresholds near 4800

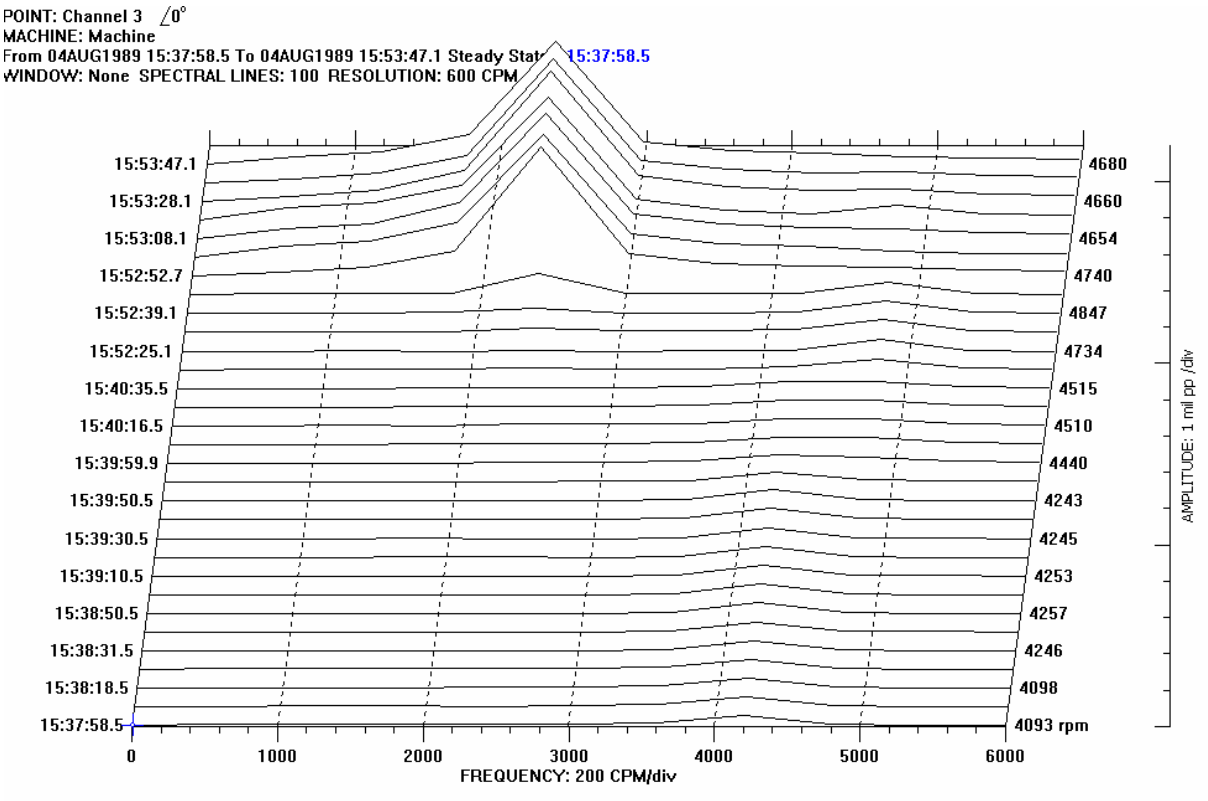

Figure 6. 1: The waterfall plot of the experimental threshold of instability of rotor #1 (September 2002).

rpm were repeatedly found during the testing in September. Judging from Figures 6.1 and 6.2, the transition of the rotor into whirl instability is clear. The introduction of vibration occurring at half the frequency of the rotation is sudden and maintained; thus, an experimental threshold speed for the given conditions can be identified. In Figure 6.2(b) a small disturbance is present and two "keyphaser" dots per orbit are beginning to appear. In Figure 6.2(c) fully developed whirl instability is present.

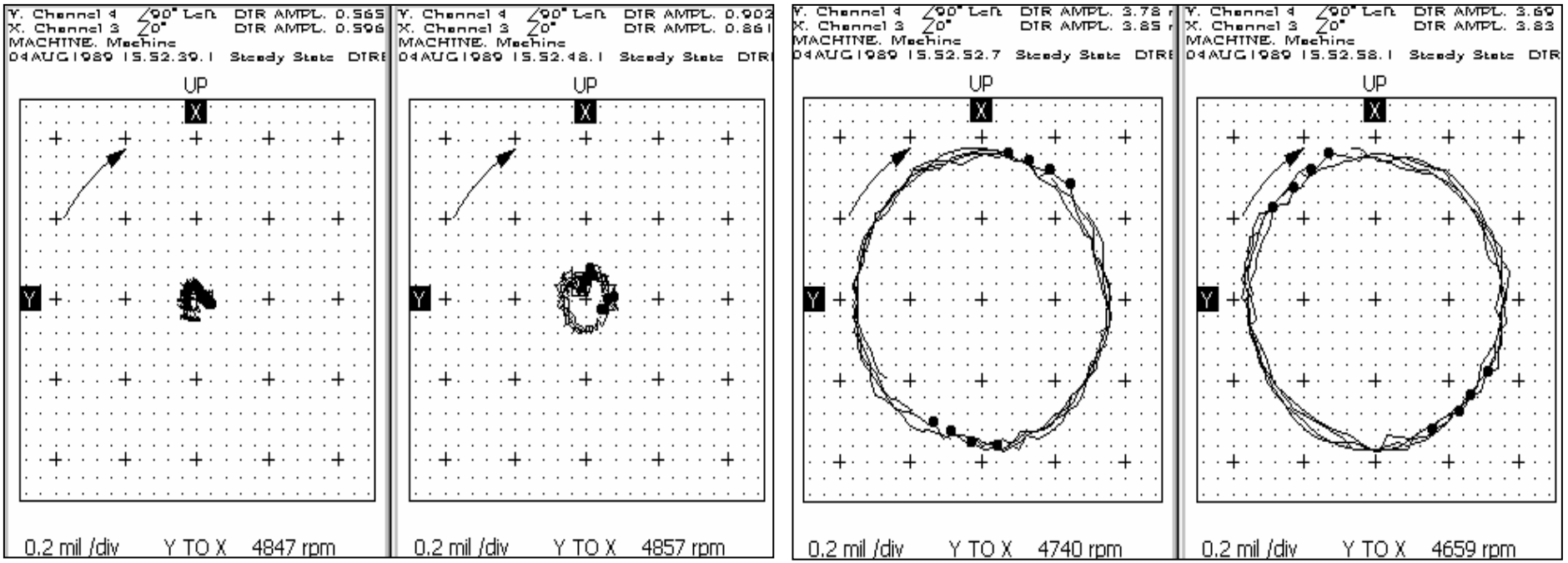

(a) **(b)** **(c)** **(d)**

Figure 6.2 (a)-(d): The orbits illustrate the transition of rotor #1 to oil whirl instability. (September 2002).

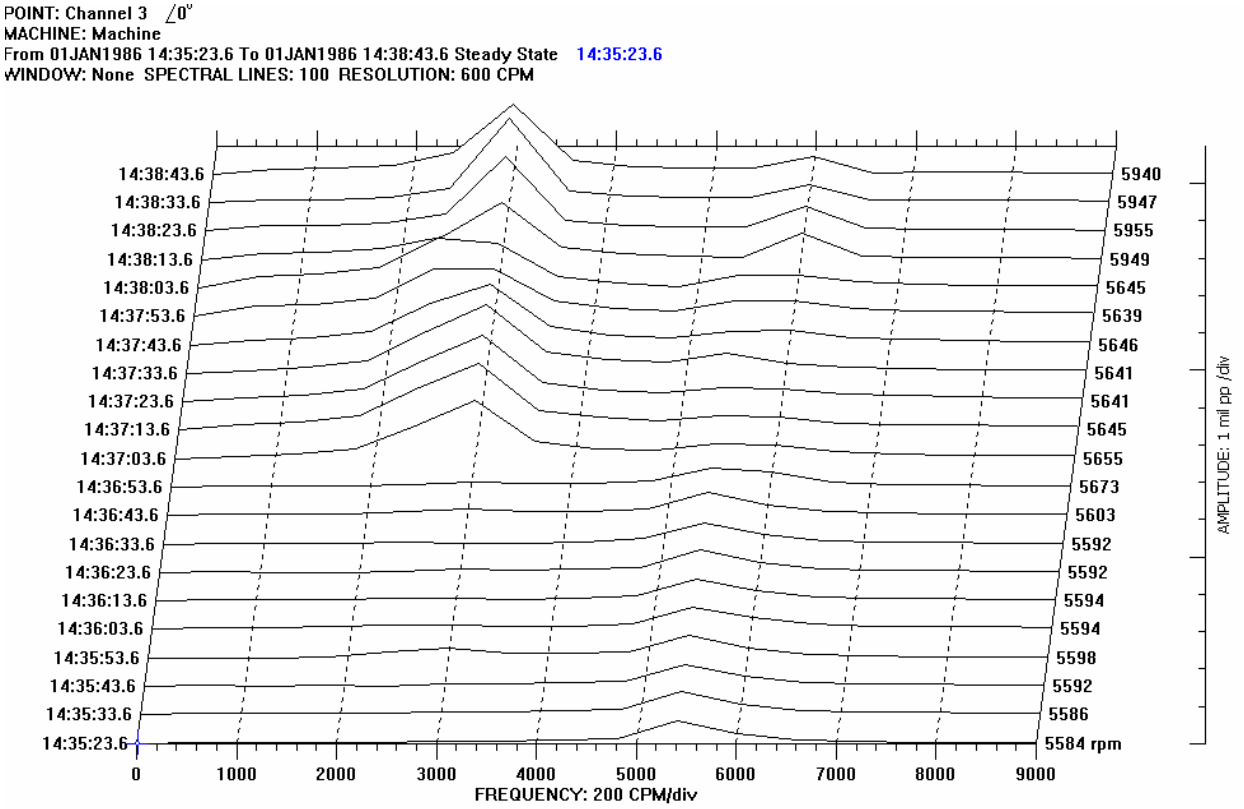

Figure 6.3: The waterfall plot of the experimental threshold of instability of rotor #1 (February 2003).

Figure 6.3 and Figure 6.4 shows the experimental threshold for rotor #1 in February of 2003 to be near 5650 rpm. The threshold speed differs significantly from the results established in March 2002 and September 2002. Whirl instability is present in Figure 6.4(c) and (d), but the amplitude is much smaller than previously encountered. The amplitude of vibration did not grow to the order of the bearing clearance. The magnitudes of vibration are approximately 0.002-0.0025 inch, while the bearing's diametric clearance is 0.004 inch. It is also seen in Figure 6.3 that this low-amplitude oil whirl persists for a significant period of time.

Having three sets of results for one set of conscious conditions illustrates that the set of conscious conditions is not inclusive of the variance in the system conditions.

After experimentation and analysis, a few areas have been noted for further investigation. The ability to have a consistent motor alignment, presence of excessive rigidity in the coupling, and any small changes in lubricant properties is expected to contribute to the variances with a rotor system operating at such a small eccentricity. Rotors that operated at low eccentricity can be thought of as lightly loaded or low inertia systems. Thus, exceptionally small variations or changes in operating conditions will influence this idealized prediction.

6.2 Instance of Oil Whirl at Start-up in Rotor #1

In addition to establishing a threshold for rotor #1, another item was studied. It was noticed that at the start-up of rotor #1, there were times when the rotor would experience oil whirl. Thus, experiments were performed to record the occurrence of oil whirl at the beginning of a test run. In some instances the oil whirl was present only for a fraction of a second before stabilizing. At other times the oil whirl would remain present from the start and continue beyond the time needed for the system to reach thermal equilibrium. In the latter case, the rotation of the rotor would have to be stopped or a momentary external load, applied by the index finger, would have to be applied to the rotor in order to stabilize the system. Also, there were experiments performed with rotor #1 that did not show any whirl instability frequencies. The occurrence of initial oil whirl was only present with rotor #1 and did not show up in any of the higher eccentricity rotors studied.

The bode plot in Figure 6.5 illustrates the total amplitude of vibration after start-up. The motor speed was initially set to approximately 1500 rpm, which can be seen as the dark, thick portion of the plotted line. After a short period of time, the rotor

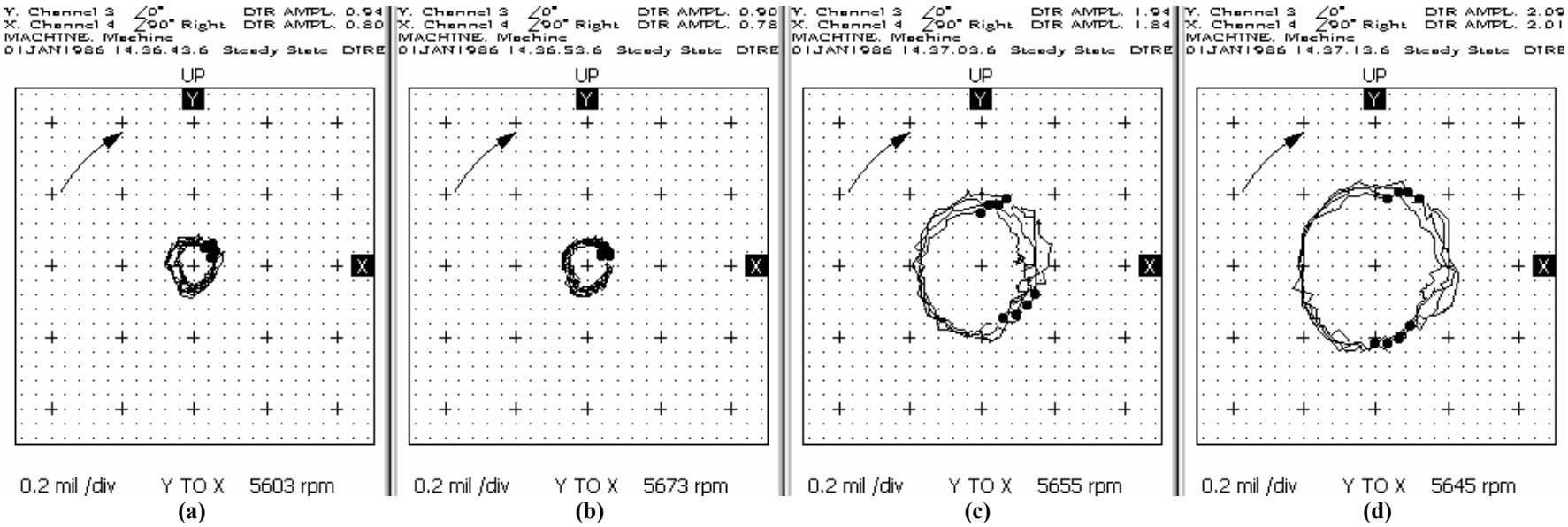

Figure 6.4: The orbits illustrate the transition of rotor #1 to oil whirl instability. (February 2003).

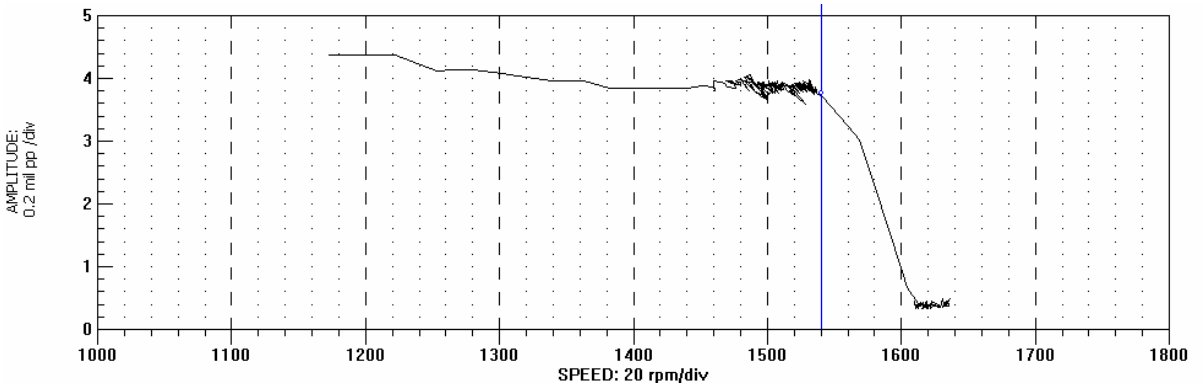

Figure 6.5: The bode plot shows the initial high amplitude at start-up.

stabilized. (As the whirl subsided, the speed of the rotor increased due to the lowered torque of a non-whirling rotor. Recall that the speed control system for this experiment is a closed loop system governed by a potentiometer.) The trend of initial whirl stabilizing after a few minutes of operation occurred in several experiments. The plot in figure 6.6 is from a different set of data; however, the same effect is recorded. After operating at 2000 rpm for 2 minutes, instability subsided and rotor #1 stabilized from whirl instability.

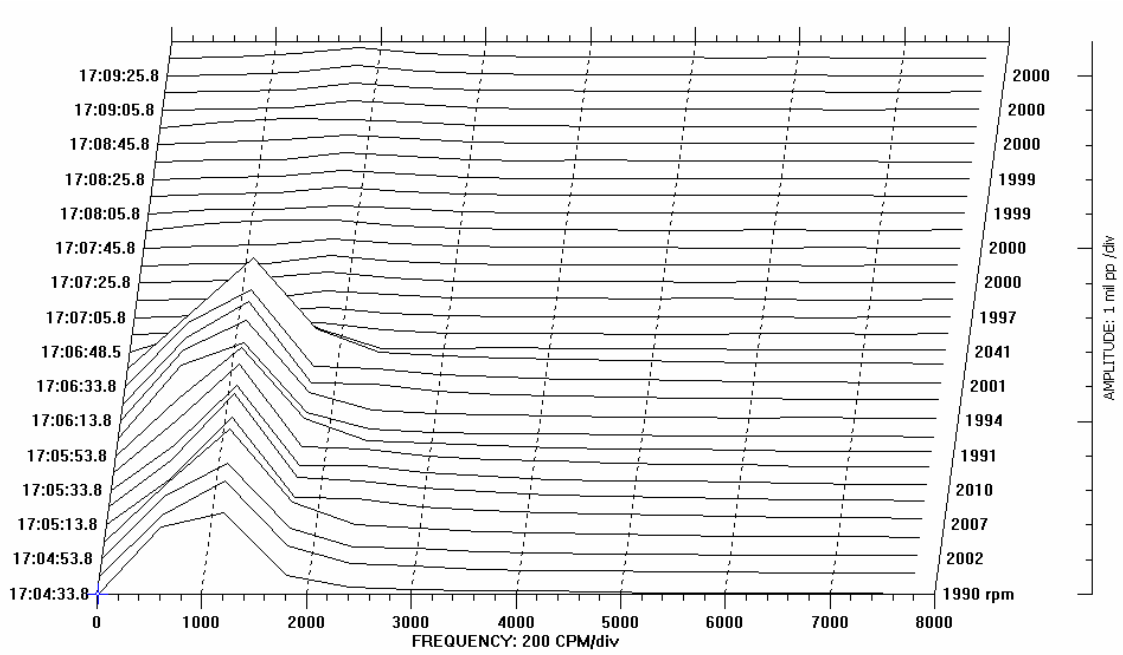

Figure 6.6: The waterfall plot illustrates the initial occurrence of oil whirl

Initial whirl instability being present and remaining developed was the other situation encountered. An experiment was run under the conditions similar to the previous experiments; however, the speed was initially increased to a greater speed, 2100 rpm. This oil whirl lasted for nearly thirty minutes, which is approximately 10 minutes beyond the thermal equilibrium stage. The experiment had to be stopped in order to stabilize the instability. Some sample orbits can be seen in Figure 6.7. There was a steady presence of whirl instability throughout this experiment.

Figure 6.8 illustrates another quick increase in speed (~3100 rpm). The high amplitude seen above is contributed to the existence of oil whirl. In this case the whirl began at the start-up and did not cease within the 45 minutes of operation. According to temperature readings on the bearing circumference, thermal equilibrium had been reached within 15-20 minutes of the start. In this case the rotor was stabilized by momentarily loading the shaft.

Figure 6.9 is the orbit plots corresponding to figure 6.8 and it shows the increase in speed from 1331 rpm to 3081 rpm. Notice that the amplitude of vibration is relatively constant regardless of its rotational speed. This is a common trait of whirl instability. It is noted that the experimentally determined instability threshold for this time period was near 4800 rpm; thus, the running speed for the experiment in figure 6.9 is well bellow the threshold.

Although the results described here were repeated in several experiments, the occurrence of initial whirl was not predictable. For all “initial whirl” experiments there was no noticed or recorded relationship between the presence of oil whirl and the relative temperatures of the lubricant and the bearing. However, Maki and Ezzat

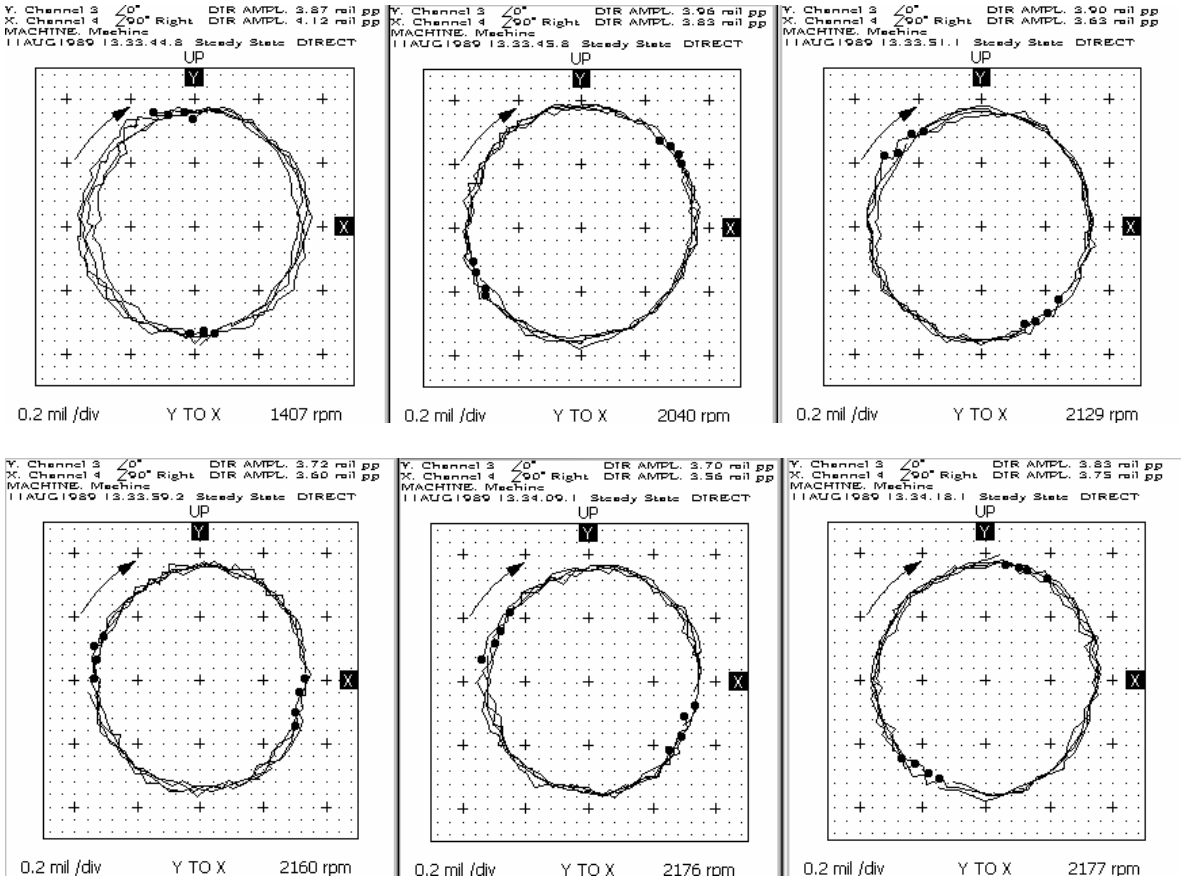

Figure 6.7: The orbit plots of initial oil whirl that does not cease.

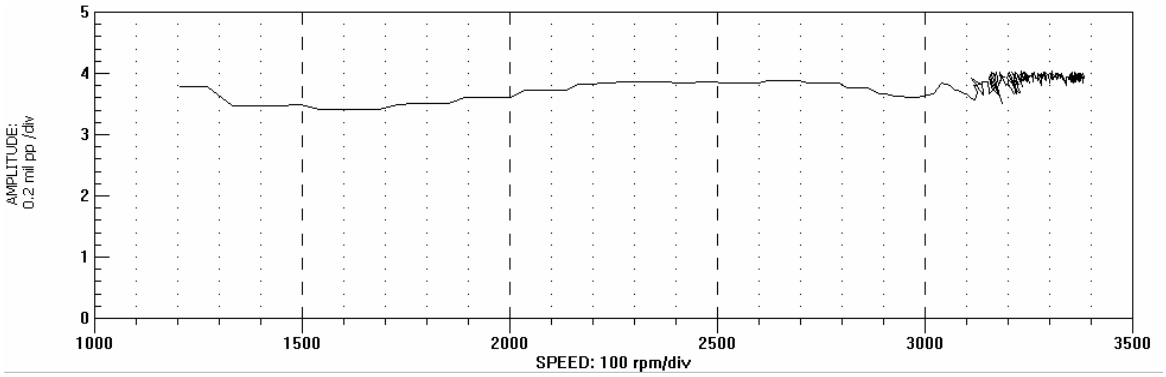

Figure 6.8: The bode plot illustrating a non-stabilizing, oil whirl start-up.

performed over 95 experiments that showed a distinct relationship between the temperature of the lubricant and the bearing temperature. They also began with whirl at start-up and found that the system stabilized once the lubricant temperature 2 inches before the inlet became less than the average of the circumferential bearing temperature (~0.05 inch from the bearing surface). The test rig at LSU is instrumented in this same manner. However, the physical dimensions, bearing type, and method of recording temperature were slightly different than their experimental set-up. It is important that similar results of initial whirl were recorded. In these experiments the relation of the temperature was not established, but the whirl at startup for a rotor operating near an exceptionally low eccentricity ratio was found.

6.3 Experimental Threshold of Rotor #4

Rotor #4 was the largest rotor used during this experimentation and typically operated with an eccentricity ratio of 0.17 at 8000 rpm. The experimental threshold was

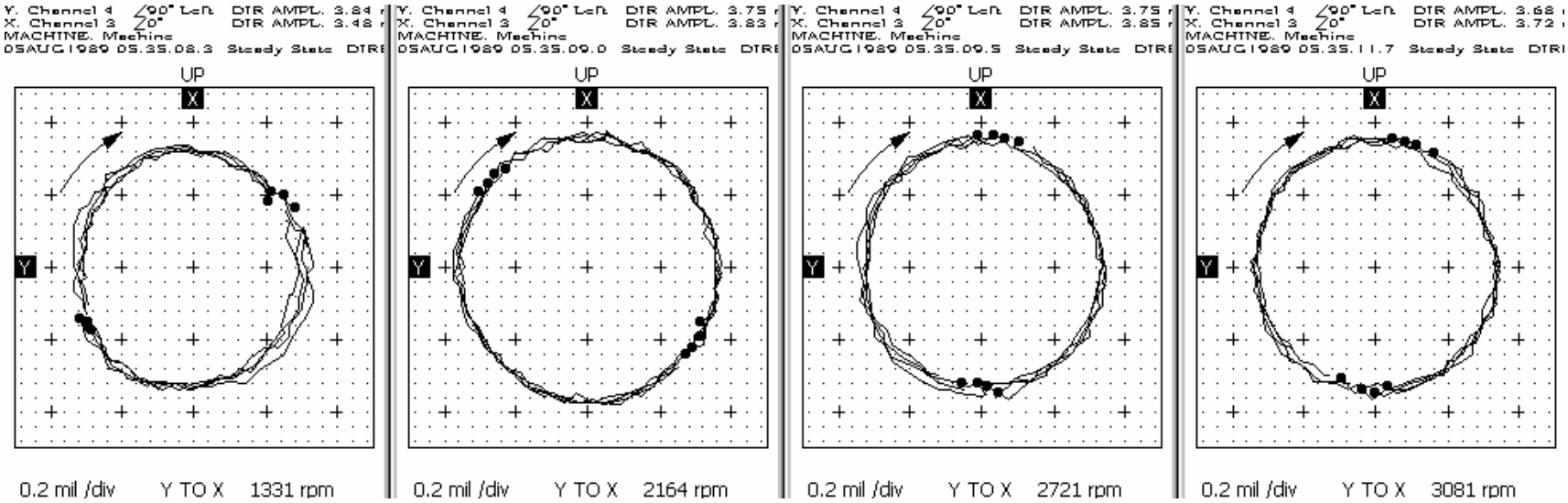

Figure 6.9: The matching orbit plots of figure 8.

found according to the procedure presented in chapter 5. The system was allowed to reach thermal equilibrium prior to any changes in conditions. The results were clear and repeatable. The waterfall plot in Figure 6.10 shows a sample of these results. The rotational frequency varies from 8000 to 8388 cycles per minute. The presence of "half-frequency" vibration is established very quickly and dominates the total vibration amplitude. From Figure 6.10 the experimental threshold speed can be estimated to be near 8336 rpm. The speed at which rotor #4 began to whirl was repeatable and definitive in all experiments run. For comparative purposes it is established at 8350 rpm. The orbit

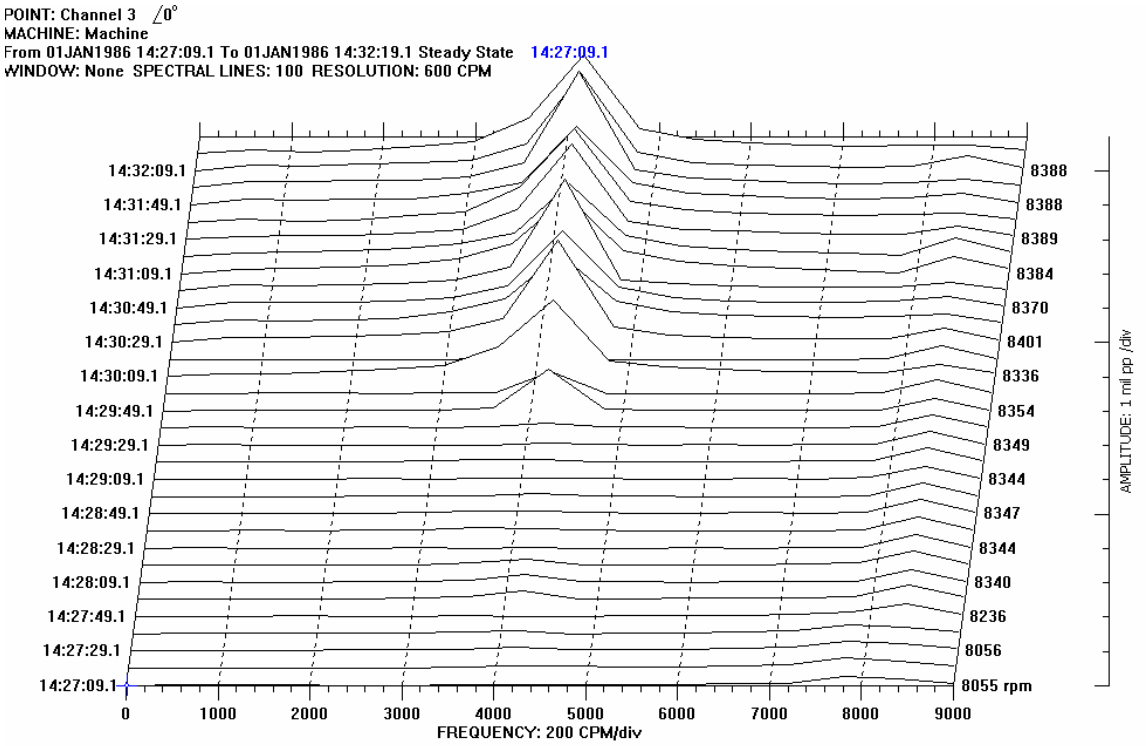

Figure 6.10: The waterfall plot of the experimental threshold of rotor #4

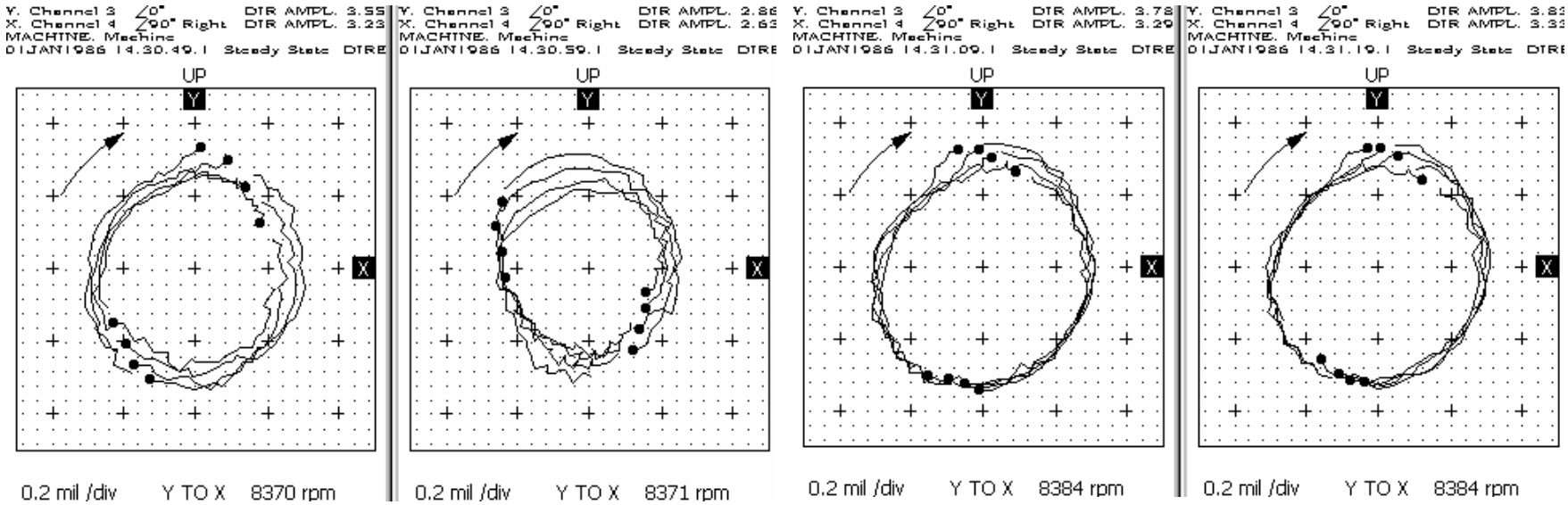

Figure 6.11: The orbit of rotor #4 just beyond the threshold of instability

plots in figure 6.11 show the orbit of rotor #4 just beyond the threshold of instability. The plot of the journal orbit can be considered free of unbalance forces because of the uniform circular motion of the orbit. Any significant unbalance would cause the orbit to have a dip or loop. The amplitude, which is on the order of the bearing clearance, is indicative that the journal has a rotating minimum film thickness that remains constant, relative to the bearing clearance.

6.4 Onset of Oil Whirl in Rotor #4 as the Supply Temperature Increases

The focus of these experiments was to observe the effect of temperature on a system near its instability threshold. The rotor's speed was increased to values just below the previously determined experimental threshold. The rotor system was then allowed to reach a thermal equilibrium condition. After arriving at this point, the temperature of the oil was increased and the conditions were recorded.

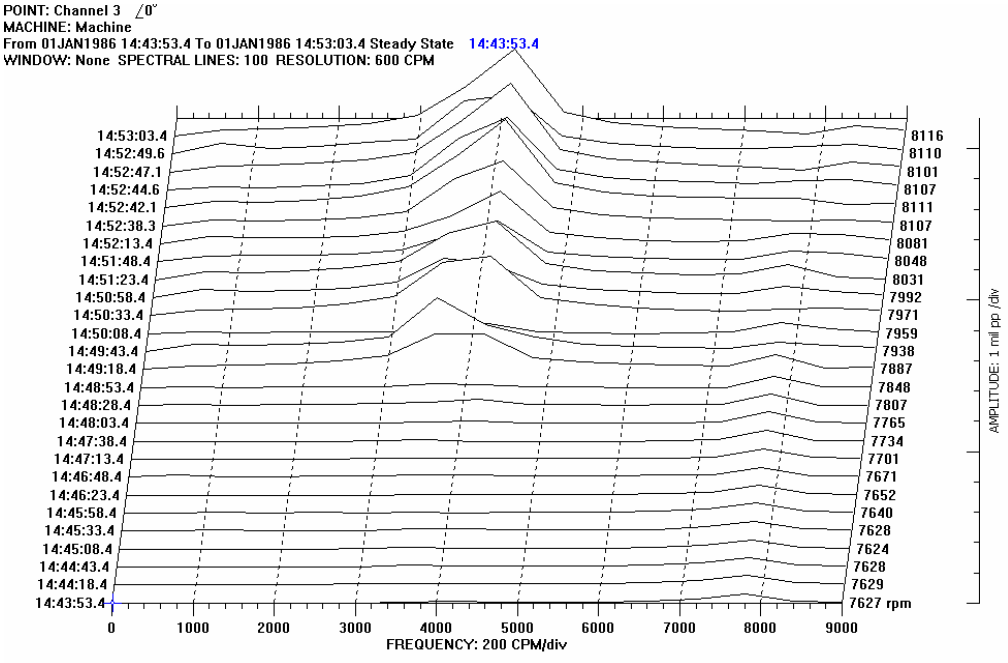

Figure 6.12: The waterfall plot of rotor #4 as it approaches the threshold via increase in oil temperature

The data captured for figure 6.12 was that recorded at the lowest occurring speed of oil whirl. The rotor was brought to thermal equilibrium at 7500 rpm, which is nearly 850 rpm lower than the experimentally determined threshold. Then the upper reservoir temperature supplying the lubricant was increased from 25° C to 60° C. As the hot lubricant began to feed the bearing, the speed slightly increased due to the reduction in the friction within the bearing. (Recall that the speed is controlled by a closed loop system governed by a potentiometer.) However, oil whirl set in at 7800 rpm. This is nearly 550 rpm lower than that produced with supply lubricant at room temperature. Similar results were produced for thermal steady state conditions at speeds of 8100 rpm, 8000 rpm and 7600 rpm. In these cases the rotor began to whirl when the speeds were 8200 rpm, 8150 rpm, and 8000 rpm, respectively.

By observing the spectrum diagrams in figure 6.13(a)–(p), there is a variance in the amplitude at the frequency of ½ the rotational frequency. As illustrated in Figures 6.13(e)-(h), the half frequency amplitude grows and then diminishes. However, after a few moments the rotor sustains oil whirl as seen in Figures 6.13(n)-(p). This effect was seen each time in the temperature manipulation experiments with rotor #4. The effect of going into and out of whirl is believed to occur because the system is going through the instability threshold very slowly. The rate at which the viscosity decreases is small; thus, the Sommerfeld number decreases slowly. The decrease in the Sommerfeld number is the action that brings the stable journal into whirl instability.

These experiments illustrate the presence of a dip in the instability threshold. By increasing the temperature of the lubricant, the system began to whirl at speeds that were lower than those obtained with supply lubricant near the temperature of the room. It was

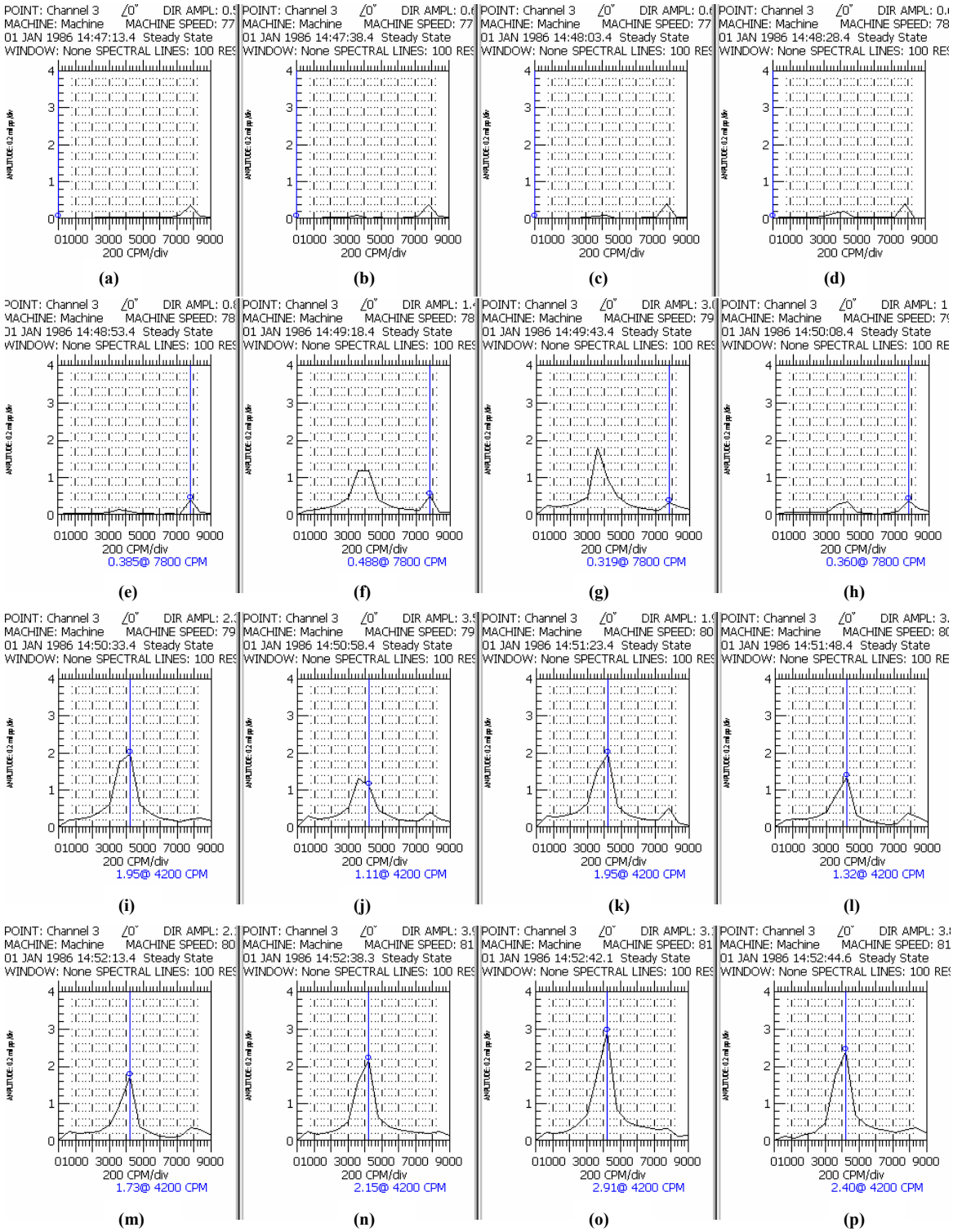

Figure 6.13 (a)–(p): The sequential spectrum plots of rotor #4 during oil supply temperature increase.

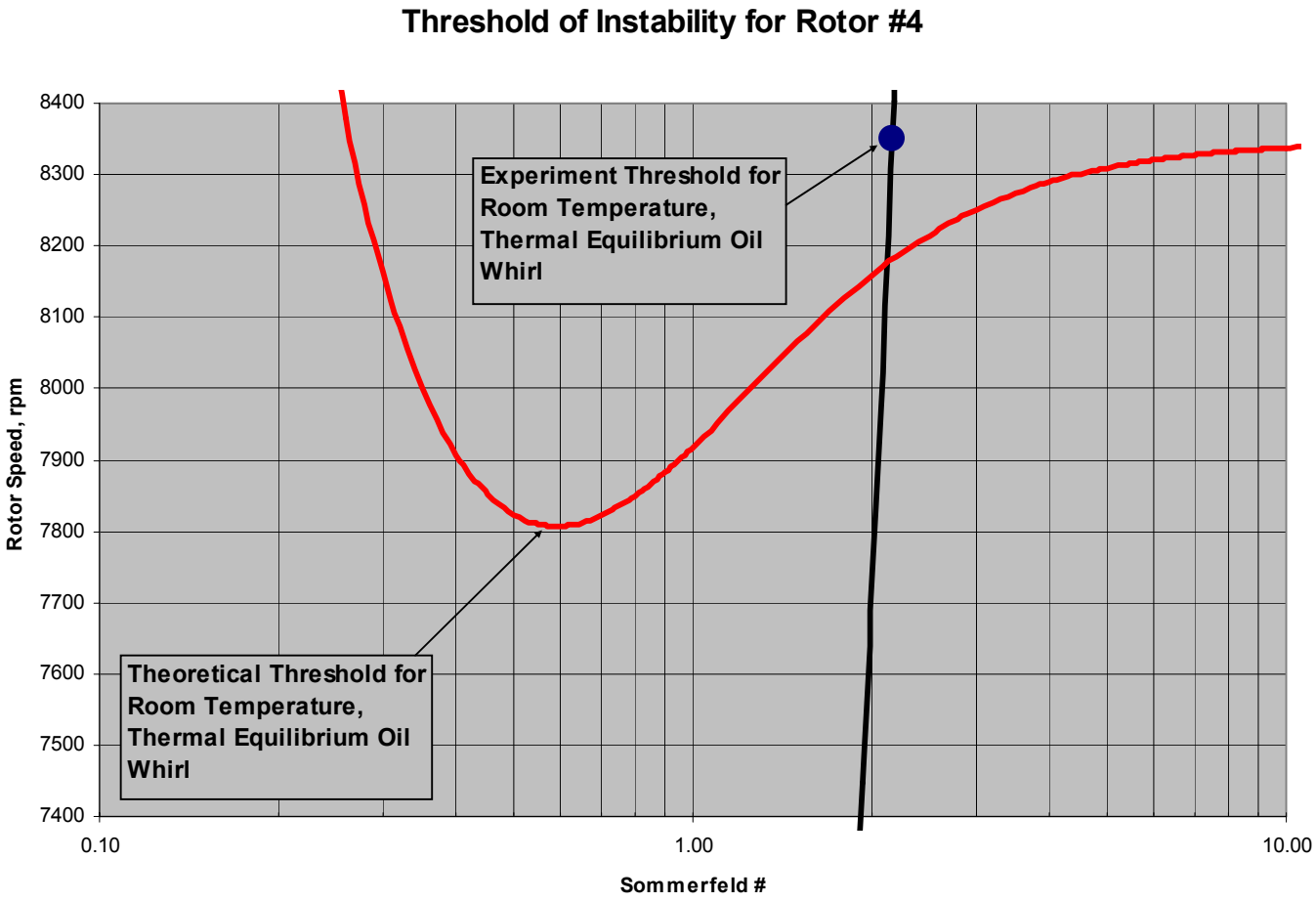

Figure 6.14 Theoretical threshold of instability illustrating "dip"

not possible to record the exact temperatures of the lubricant entering the bearing; thus, specific locations on the stability map could not be identified. However, the fact remains that the system did cross the instability threshold at a point lower than that previously found. Since the instability threshold is effectively a function of rotational speed and bearing clearance, deduction of the presence of such a dip in the instability threshold is possible. An illustration of the "dip" in the instability threshold prediction may be seen in Figure 6.14.

6.5 Experimental History of Rotor #3

Rotor #3 was designed prior to rotor #4. The intent of this rotor was to investigate a rotor that operated at a slightly higher eccentricity. At 8000 rpm this rotor theoretically operated at an eccentricity of 0.07. The first experiments were run to establish the experimental threshold of rotor #3. Recall that after fabrication, the rotor was balanced within 0.0010 ounce. Initial data showed the system was, at times, reluctant to whirl (see section 6.4.0). However, records do show that oil whirl was present at 7500 rpm and sustained beyond 7700 rpm. Before any further testing could be done with rotor #3, the rotor was damaged. It was dropped from nearly 36" and impacted the floor. The rotor was thoroughly inspected and no visual signs of damage were present; thus, rotor #3 was used further in experiments. The effect of the drop was not discovered until a number of experiments were performed.

A reference of the system's experimental threshold prior to the damage cannot be accurately determined from the tests run before this incident. However, it can be stated that oil whirl was not present in the system prior to 7500 rpm. Figure 6.15 shows the.

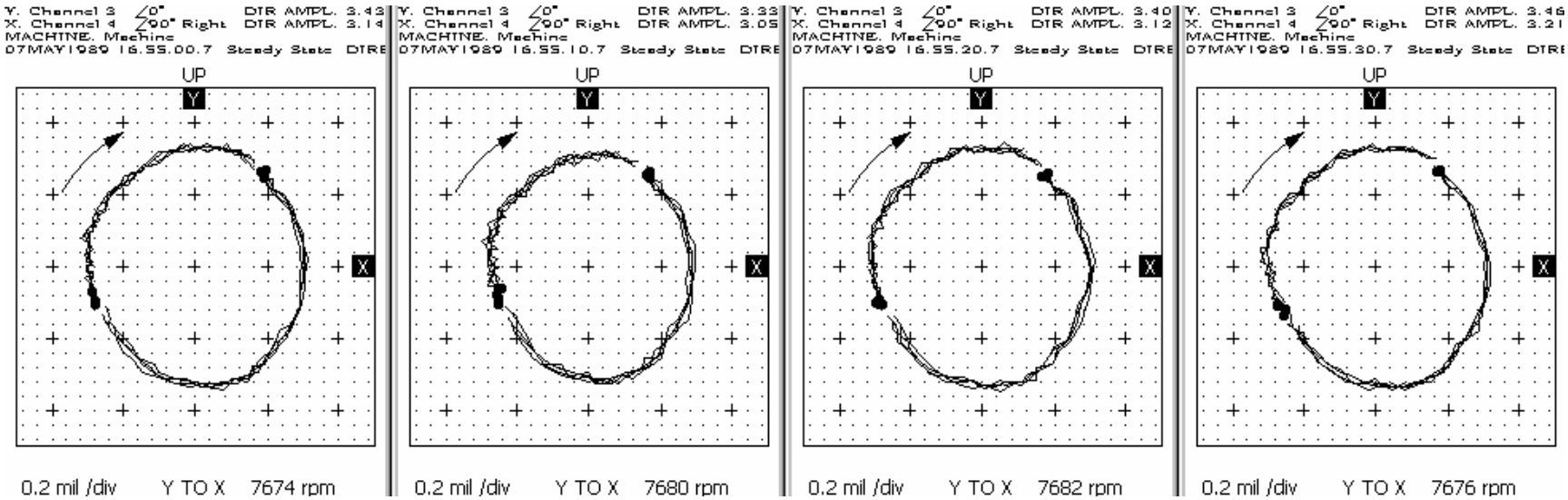

Figure 6.15: Orbits of rotor #3 prior to the damage.

undamaged rotor operating in a whirling condition. The speed 7500 rpm is thought of as a reference value for future comparison. The speed at which rotor #3 became unstable after the incident was significantly lower than this reference

6.6 The Effect of Rotor Damage to the Whirl Stability of Rotor #3

Despite uncertainty on the effect the incident had on the whirl instability of the system, tests were continued with rotor #3. Prior to dropping rotor #3, the orbit of the rotor mimicked that of Figure 6.15. The orbit in figure 6.15 is circular and seems free from any disturbances. However, after the rotor was damaged an "unbalance loop" appeared in the orbit plots. It can be seen partially in figure 6.16 and clearly in figure 6.18.

Figures 6.16 and 6.17 show the onset of oil whirl just after the rotor had been damaged. These results clearly show that the experimental threshold of instability is near 5600 rpm. These results were repeatable and definitive. In figure 6.17 there is no amplitude at the "half frequency" mark until oil whirl is established. This makes the determination of the experimental threshold very clear.

The result of this unexpected incident supports the logic of the stability region discussed in Chapter 2 illustrated in Figure 2.9 [16]. Ultimately, this incident illustrates that after an unbalance entered the system, the experimental threshold of instability decreased. However, since no quantification of the unbalance was recorded, complete data prior to the damage was not obtained, and this is an isolated case. A complete comparison to this theory is not possible. However, this experiment encourages further investigation of this subject. It should be of particular interest to damage analysis of industrial rotors and its effect on whirl instability.

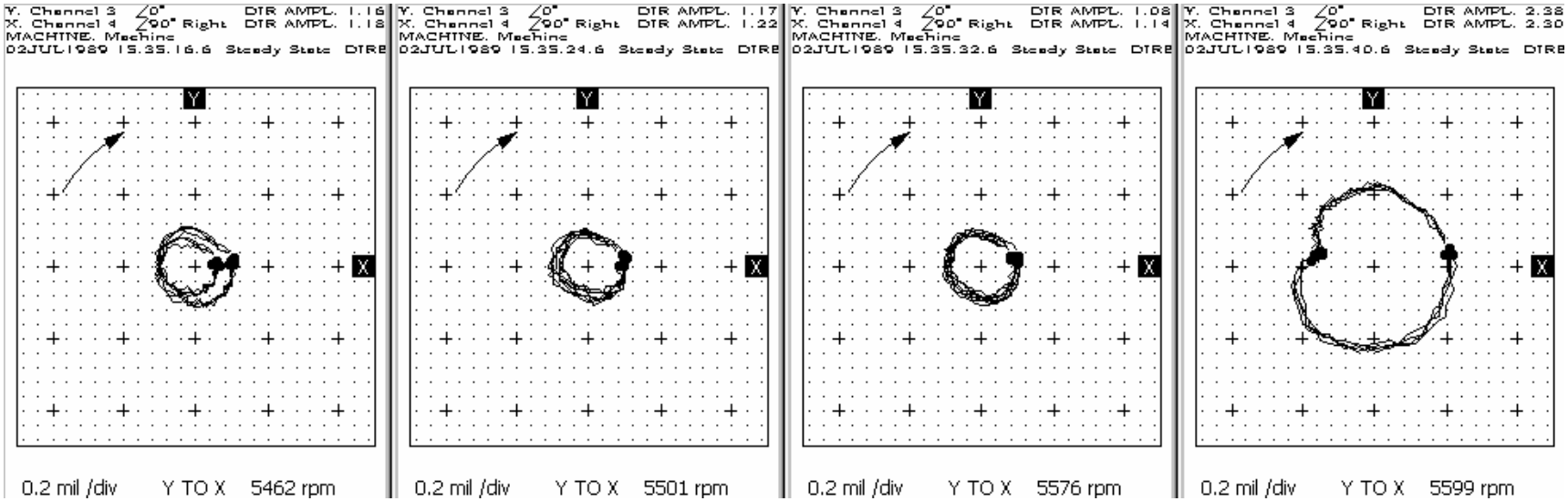

Figure 6.16: The orbit of rotor #3 just after the damage occurred

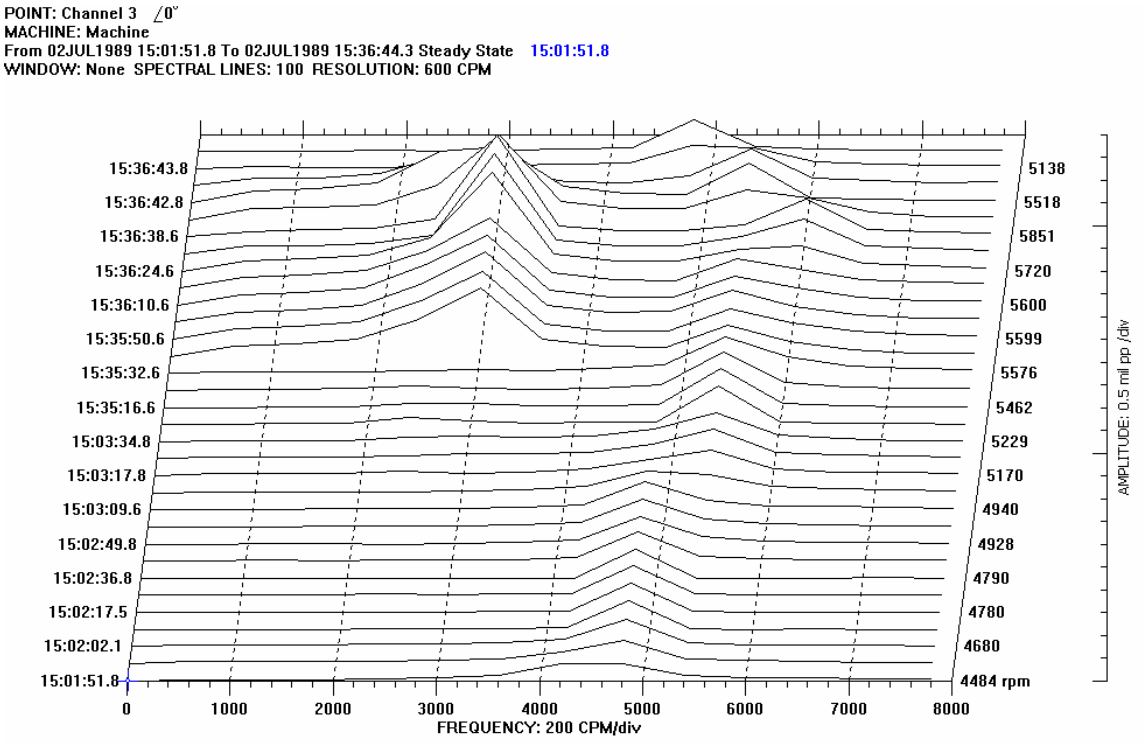

Figure 6.17: The waterfall plot of rotor #3 after the damage occurred.

The latest whirl orbits for rotor #3 are displayed in Figure 6.18 and show this feature. While the rotor was balanced to within 0.0035 ounces, there still existed a sign of unbalance in the whirl orbit. This "unbalance loop" has been present in all of the orbits produced by rotor #3 since the damage occurred.

Once rotor #3 had been re-balanced, the results were somewhat surprising. Figures 6.19 and 6.20 show the results of rotor #3 after it had been re-balanced and the oil was changed. As one can see in the figure 6.20, there is still an unbalance in the rotor. In figure 6.19 the transition from a stable condition to oil whirl is not smooth. It is rather difficult to define an instability threshold speed. There are relatively low

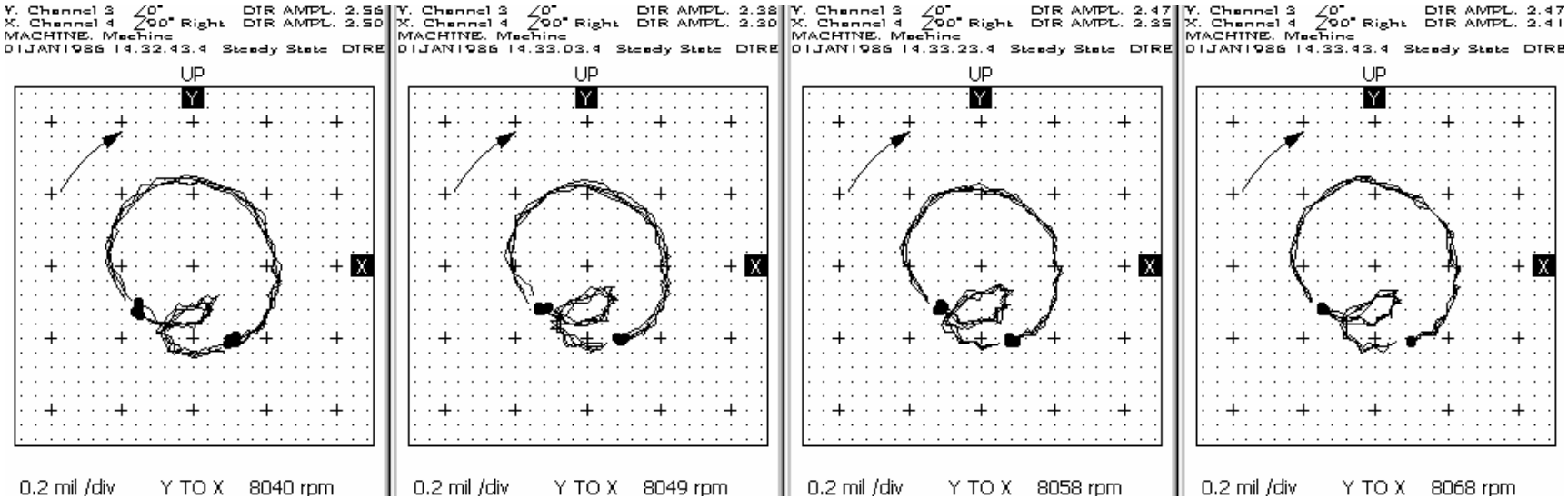

Figure 6.18: Orbits of rotor #3 after damage and rebalancing

amplitude instances at the “half frequency” mark. This illustrates that the excitation is present; however, there is a restriction on the rotor that prevents orbits from developing to its full range. The orbits full range should be equal to a magnitude near the value of the bearing clearance.

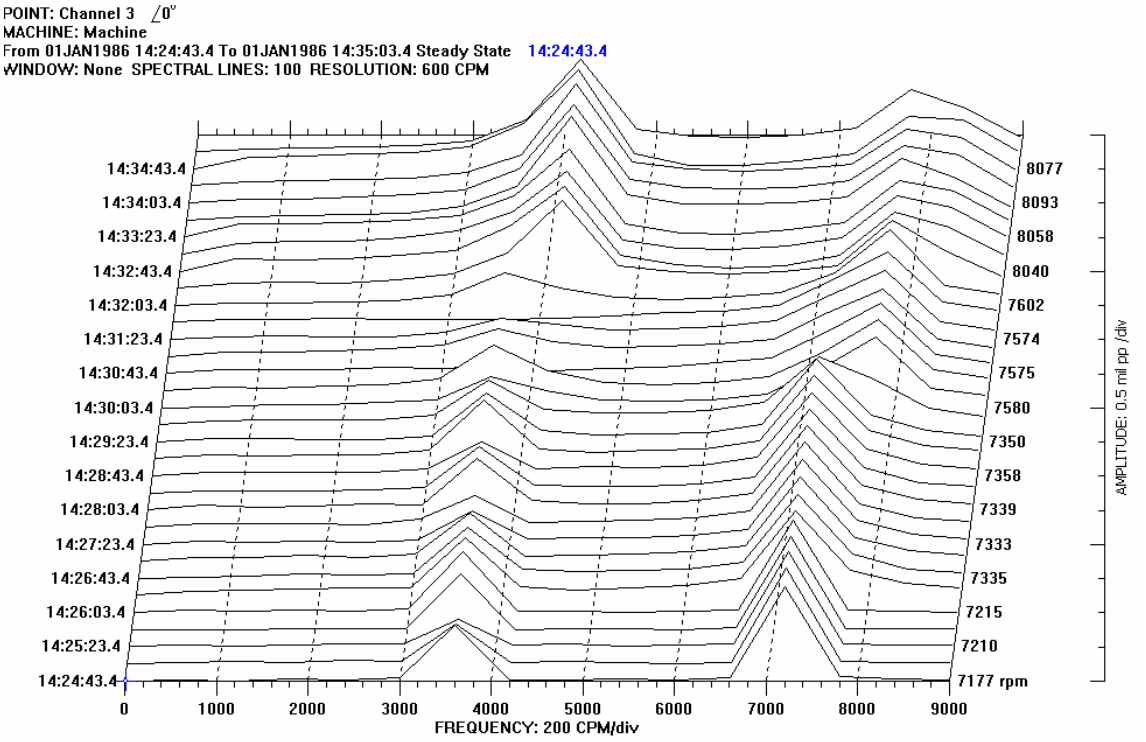

Figure 6.19: The waterfall plot of rotor #3 after re-balancing.

6.7 The Reluctance to Sustain Oil Whirl in all Rotors Investigated

There were instances that the system showed reluctance to remain in oil whirl or develop a full orbit. This was occasionally observed to occur with all rotors that were studied. Figure 6.21 shows four changes of stability within two seconds. In Figures 6.21(a)-(b) and Figures 6.21(e)-(f), the journal is going from an unstable region to a stable region. In Figures 6.21(c)-(d) and Figures 6.21(g)-(h), the journal is becoming

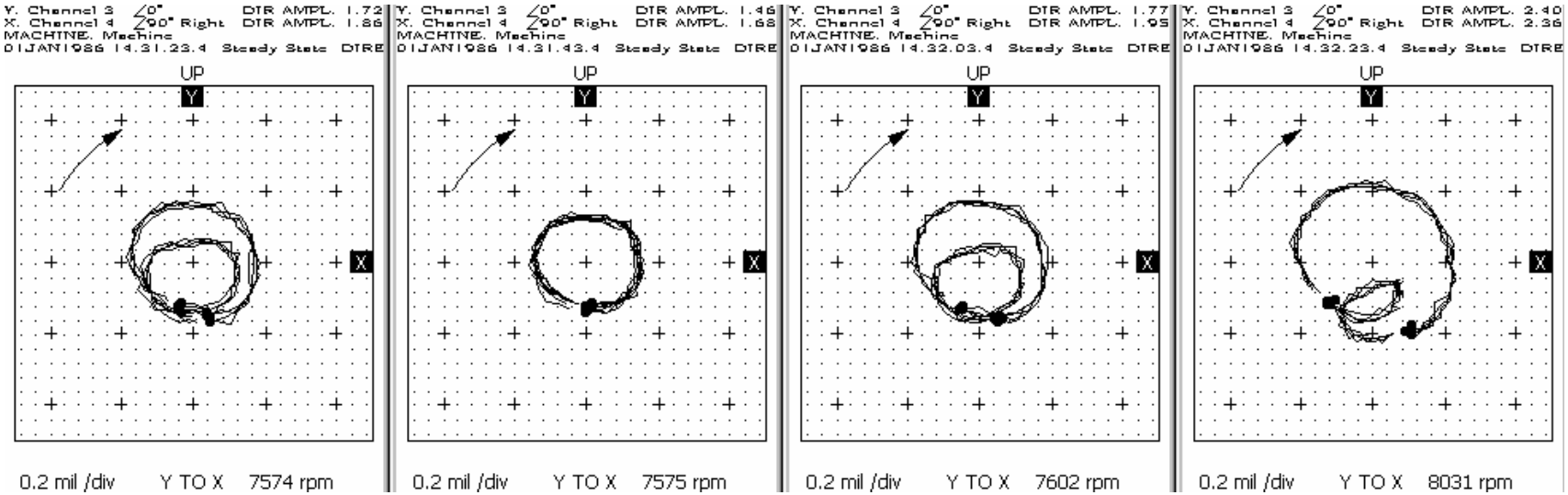

Figure 6.20: Orbit of rotor #3 after re-balancing

unstable. This figure is a group of successive data captures illustrating rotor #3 going into and out of whirl. It should be noted that Figure 6.21(a)-(h) all occurred within 2 seconds. Although the cyclic action of entering and exiting instability could be common if the rotor was near its threshold, other peculiarities are associated, such as those seen in Figure 6.19 and 6.20. There is a frequency that is one-half of the rotational frequency present throughout the range of speeds in Figure 6.19 (900 rpm). It is evident that the system is not near a threshold region for such a large range of rotational speed. In another case, Figure 6.22 displays the resistance of rotor #1 to whirl. It is evident that there is amplitude at half the rotational frequency; however, the magnitude of the amplitude of whirl should be near the value of the bearing clearance. Instead, it is present initially and gradually reduces.

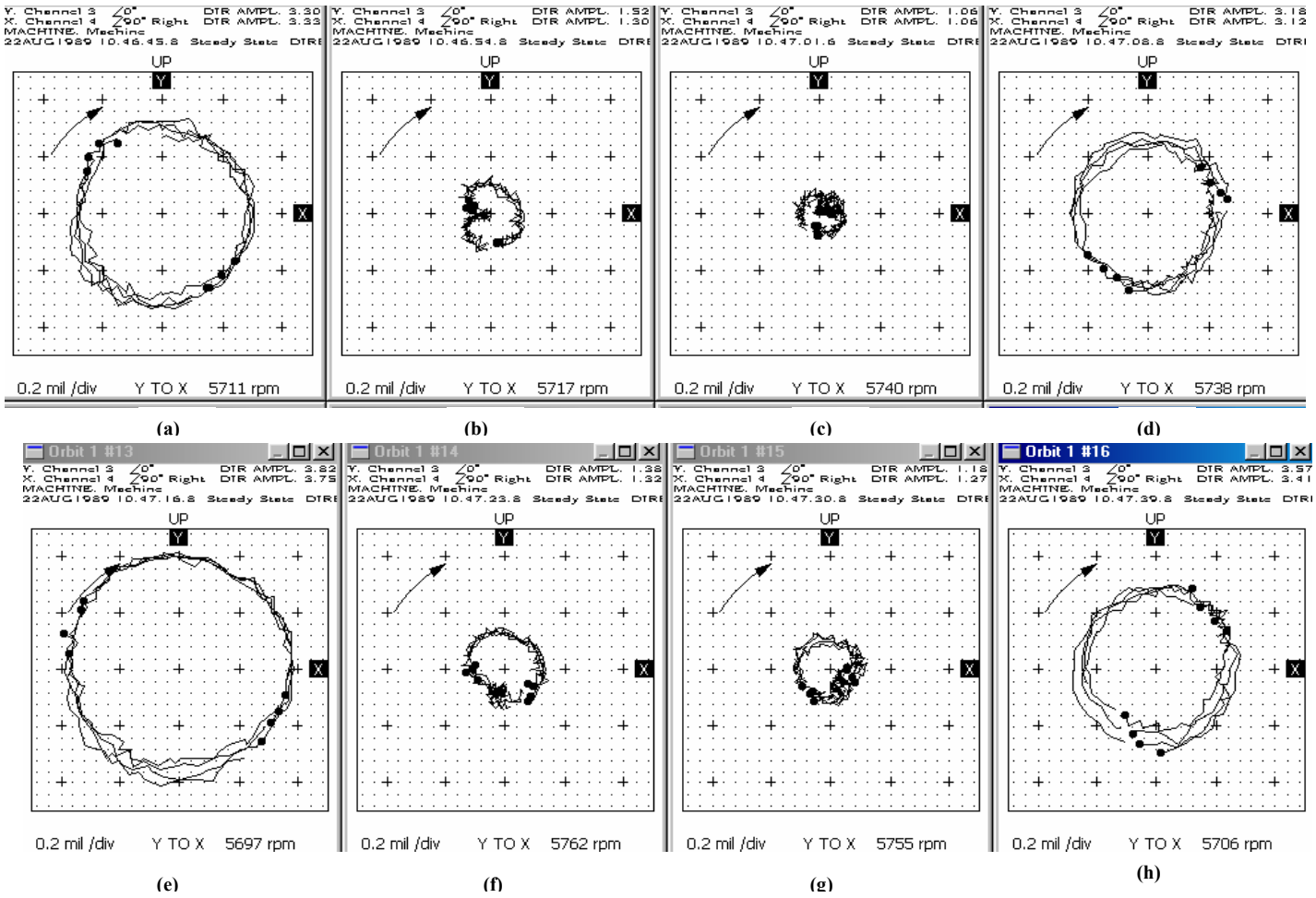

Figure 6.21(a)-(h): Orbits of rotor #3 not maintaining whirl

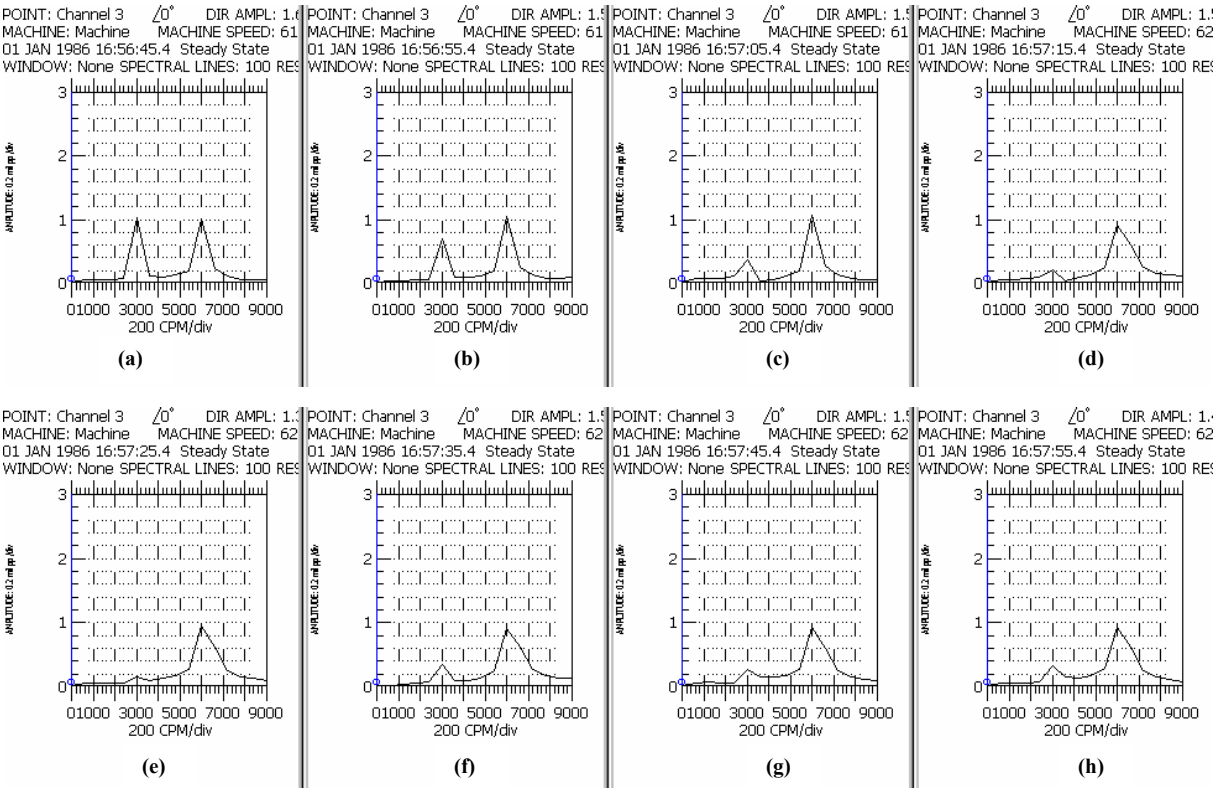

Figure 6.22(a)-(h): The spectrum plots for rotor #1 showing reluctance to whirl

7. Conclusions

The aim of this thesis was to gain some insight on experimental hydrodynamic journal bearing instability. Theoretical and experimental research has been ongoing on this subject since its discovery in 1924; however, a complete, conclusive description of the behavior of this phenomenon has yet to be established. Experimental research by Maki and Ezzat[1], Pinkus[9] , and Newkirk and Lewis[3] have resulted in interpretations that differ with respect to each other as well as the current theoretical predictions. Thus, a secondary purpose of the study was to investigate what features might be useful in future research to reach conclusions on a phenomenon that has been researched extensively without clear and concise results.

The results of Maki and Ezzat have shown that oil whirl was present at start-up for many cases of an extremely low eccentricity. They found that there was a relationship between the circumferential bearing temperature, the supply lubricant temperature, and the presence of oil whirl at the start-up of a rotor-bearing system. The relation between temperature and oil whirl is obviously intriguing; however, the fact that oil whirl is present under conditions that have not been defined by current theory should also be given attention. In the current study, while the conditions of initial whirl did not trend as those produced by Maki and Ezzat, the presence of whirl at start-up for an exceptionally low eccentricity system was found. Given the prior relevant research, the findings of the current study and those reported by Maki and Ezzat suggest that the available contemporary theoretical prediction methods do not completely address all of the required parameters to accurately predict oil whirl specifically for low eccentricity systems. Experimentally, more care must be taken in instrumentation and mechanical

system set-up to accurately and fully account for the performance of exceptionally low eccentricity systems. Theoretically, many researchers have contributed to understanding the general phenomenon of oil whirl, and prior to the current investigation, the only study to address initial whirl was Maki and Ezzat. The combination of findings reported by Maki and Ezzat, and the observations, experiences, and findings of this current study, suggest that practical and theoretical understandings may be enhanced through carefully designed and highly focused experiments.

The results of the current study reveal that there were significant variations in the instability threshold due to unnoticeable changes in the rotor #1 bearing system. Thus, it seems evident that the hydrodynamic stability of low eccentricity journal bearing systems was highly sensitive with this testing rig. In the series of experiments for this study uncontrollable and undetectable changes in conditions had an effect on the threshold of instability of the system. Of these conditions, extremely accurate motor alignment, the influence of the coupling on the rotor, and minute changes in lubrication quality seemed to produce the greatest variability on systems performance. While such conditions are not yet easily controlled, the consistency of observations across experiments in this study suggests that future efforts to effectively address these might contribute to achieving more conclusive findings. For example, the laboratory conditions used in the Maki and Ezzat study included a coupling that had a lesser influence on the performance of the rotor than was available for use in the current study. Therefore, some system modifications may be necessary to effectively study such exceptionally low eccentricity operations. While such studies continue to be challenging, they are worthwhile to pursue.

The performance of rotor #4 in the experiments performed was comparable to theoretical predictions. The experimental threshold was within 5% of the linear theoretical prediction of instability. Also, the presence of a dip in the instability threshold was empirically verified. By increasing the temperature of the lubricant, the system began to whirl at speeds that were lower than those obtained with supply lubricant near the temperature of the room. The system crossed the instability threshold and did so at a point on the stability map lower than that previously found. Since the instability threshold is effectively a function of rotational speed and bearing clearance, deduction of the presence of such a dip in the instability threshold is possible. Given the review of the literature, this series of experiments provides the first known empirical evidence of the "dip' in the instability prediction map shown in Figure 7.1.

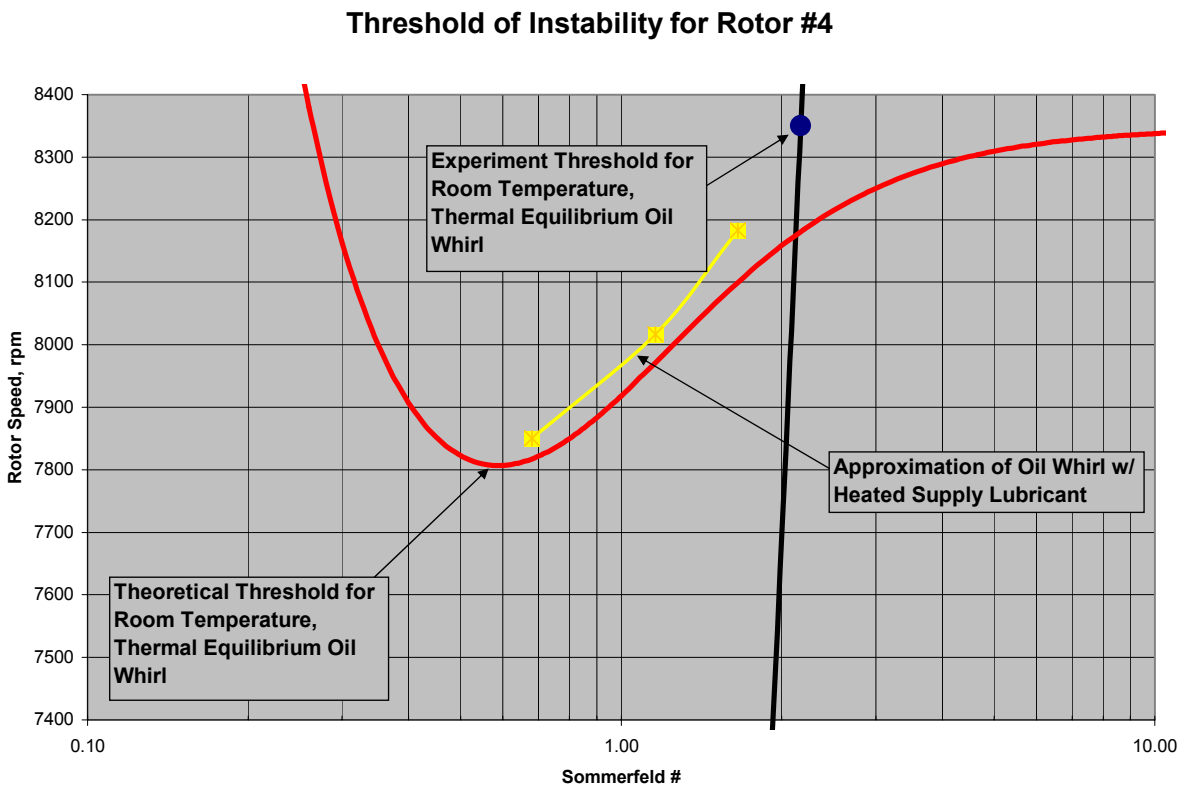

Figure 7.1: Threshold of instability of rotor #4.

Khonsari and Chang[16] reported theoretical prediction that the onset of oil whirl is dependent upon a stability boundary and, as mentioned in Chapter 2, became serendipitously important in examining the results of experiments with rotor #3. As mentioned previously, the unexpected damage to this rotor resulted in an unanticipated opportunity to examine data collected prior to and after the occurrence of rotor damage. While these data were not consistent or conclusive, they are noteworthy and suggest that future research in support of Khonsari and Chang's findings would be a worthwhile endeavor.

Another important outcome of the current study relates to determining the experimental threshold of instability. Throughout the experiments for all rotors, a peculiarity was often noticed at the onset of whirl. In some instances the rotor would not develop into a fully formed orbit, or the rotor would cycle between stable and unstable conditions. Not achieving a fully formed orbit may be present due to restrictions in the system that damp the exciting force of oil whirl instability. As discussed in Chapter 6, some experiments showed a reluctance to enter into oil whirl instability. For example, in those experiments, the frequency of oil whirl was observed, but the characteristic amplitude of vibration did not develop to a magnitude of the order of the bearing clearance. For the instances of the rotor cycling between stable and instable conditions, this seemed to be due to the system operating near the threshold of instability. As the system moved beyond the region of the threshold, the cyclic action would cease. While these cases may be a function of the system variances, it should be important to note for future experimental determination of threshold of instability.

While there has been considerable research investigating the phenomenon of oil whirl, much of it has focused on a broad range of system conditions, rather than examining iteratively specific stages in which oil whirl might be observed. In addition these studies have not achieved complete agreement in terms of explaining oil whirl. As a result of a review of the literature, the Maki and Ezzat study was the only investigation targeting the particular phenomenon of initial oil whirl. This study suggests that research targeting a narrower focus might afford enhanced understanding through control over a small set of conditions and the opportunity to better manage results. In an attempt to further this line of inquiry a decision was made to focus this study strictly on initial oil whirl and the influence of lubricant supply temperature on the stability of the system.

In reflection, several important findings were obtained that contribute to the existing research literature. First, results of this study confirm the presence of oil whirl upon the system start-up, but studies to replicate these findings are necessary. Therefore, the pursuit of additional studies in this area might replicate these findings and provide important information for understanding the nature of oil whirl, theoretically and practically. Second, the differences between laboratory conditions for this study and those reported by Maki and Ezzat, combined with experimentation observation of the current study, suggest that solutions for controlling system conditions might be difficult, but they are necessary. Third, this study produced empirical evidence supporting the theoretical "dip" in the instability threshold map. This finding is significant and provides a notable contribution to the professional literature. Lastly, as sometimes happens in research, unfortunate incidences (e.g., equipment damage) occur, but serendipitously might provide valuable insight. In this study, the consequences yielded data that, while

not conclusive, is encouraging for researchers who wish to pursue Khonsari and Chang's prediction of stability boundaries.

References

1. Maki, E. R., and Ezzt, H. A., "Thermally Induced Whirl of a Rigid Rotor on Hydrodynamic Journal Bearings," *Trans ASME*, Vol 102, No. 1, (January, 1980): 8-14.

2. Newkirk, B. L., and Lewis, J. F.,"Shaft Whipping due to Oil Action in Journal Bearings*," General Electric Review*, (August 1925): 559-568.

3. Newkirk, B. L., and Lewis, J. F., "Oil Film Whirl-An Investigation of Disturbances Due to Oil Flms in Journal Bearings." *Trans. ASME*, Vol 78, (1956): 21-27.

4. Bently Nevada Corporation, "The Difference between Whirl and Whip." *Orbit Magazine*, First Quarter Edition, (1998): 9.

5. Hagg, A. C.. "Oil Whip.". Westinghouse Research Laboratories.

6. Holmes, R.,"The Vibration of a Rigid Shaft on Short Sleeve Bearings." *Journal of Mechanical Engineering Science* (1960): 337-341.

7. Hagg, A. C. and Warner, P. C. "Oil-Whip of Flexible Rotors," *Trans. ASME*, Vol. 75, No. 7, (1953): 1339-1344.

8. Hahn, E. J. "The Excitability of Flexible Rotors in Short Sleeve Bearings," Journal of Lubrication Technology, *Trans. ASME*, Ser. F, Vol. 97, (January 1975): 105-115.

9. Pinkus, O., "Experimental Investigation of Resonant Whip." *Trans. ASME* (1957): 975-983.

10. Craighead, I.A., Dowson, D. Sharp, R.S., and Taylor, C.M., "The Influence of Thermal Effects and Shaft Misalignment on the Dynamic Behaviour of Fluid Film Bearings." *Proc. Inst. Mech. Engrs.*, (1980): 47-55.

11. Ma, M.-T. amd Taylor, C. M., "An Experimental Investigation of Thermal Effects in Circular and Elliptical Plain Journal Bearings." *Tribology International*, Vol. 29, No. 1, (1996): 19-26.

12. Dowson, D., Hudson, J., Hunter, B., and March, C. "An Experimental Investigation of the Thermal Equilibrium of Steadily Loaded Journal Bearings." *Proc. Inst. Mech. Engr*., Vol 101, 3B, (1966-67).

13. Hopf, G. and Schuler, D., "Investigations on Large Turbine Bearings Working under Transitional Conditions between Laminar and Turbulent Flow." *ASME Trans., J. Trib.*, Vol. 111, (1989): 628.

14. Tondl, A., *Some Problems of Rotor Dynamics*, Chapmann & Hall, 1965.

15. Khonsari, M. M. "A Review of Thermal Effects in Hydrodynamic Bearings, Part II: Journal Bearings", *ASLE Trans*., Vol. 30, (1987):26-33.

16. Khonsari, M. and Chang, Y. "Stability Boundary of Non-Linear Orbits Within Clearance Circle of Journal Bearings," *ASME Journal of Vibration and Acoustics*, V. 115, (1993): 303-307.

17. Den Hartog, J.P., *Strength of Materials*, Dover Publications, 1949.

18. Khonsari, M. M. and Booser, E. R., *Applied Tribology Bearing Design and Lubrication*, John Wiley & Sons, 2001.

19. Chang, Y. J. *The Effect of Supply Temperature and Shaft Flexibility on the Shaft of Journal Bearings*. master's thesis, University of Pittsburgh, 1990.

20. Khonsari, M.M. Jang, J. Y., and Fillon, M., "On the Generalization of Thermodynamic Analyses for Journal Bearings." *Journal of Tribology Vol. 118* (1996): 571-579.

21. Kakoty, S. K., and Majumdar, B.C., "Effect of Fluid Film Inertia on Stability of Flexibly Supported Oil Journal Bearings: A Non-Linear Analysis." *Tribology Transactions, Vol. 45* (2002): 253-257.

22. Lund, J. W., "Stability and Damped Critical Speeds of a Flexible Rotor in Fluid-Film Bearings." *Journal of Engineering for Industry* (1974): 509-517.

23. Milne-Thomson, L. M. 1960. *Theoretical Hydrodynamics*. Fourth edition. Original edition, 1938. London: MacMillan.

24. Fuller, Dudley, D., *Theory and Practice of Lubrication for Engineers*. John Wiley & Sons,
New York, 1956.

25. Den Hartog, J. P., *Mechanical Vibrations.* McGraw-Hill, New York, 1956.

Appendix

Appendix A: Explanation of Whirl Instability Vibration Frequency

A useful, intuitive relation can also be explained. The whirling frequency has been known to equal approximately one half of the rotational frequency. To understand this, I applied the conservation of mass to a controlled volume of fluid as the shaft is whirling. For the simple case of two parallel plates, one can observe the lubricant velocity as it varies from the moving plate to the stationary plate. In a infinitely small section is taken of the bearing and journal, then this assumption has some validity. A constant velocity gradient is found to be present in this situation. Hence, the velocity of the fluid varies from the linear speed of the rotating journal to the linear speed of the stationary bushing, zero. Thus the average velocity of the fluid is one-half of the tangential velocity of the shaft. Equating the volume flow rate of fluid in and out of the control volume shown below, gives such a relation. Not only is fluid being pumped into the pressure wedge at the maximum film thickness and out of the pressure wedge at minimum film thickness, but fluid must take up the space created by the whirling shaft. Referring to the figure below, the shaft is moving up at this instance. Thus, the upward must be filled with oil motion creates a void underneath the shaft. This void is part of the control volume and Remember, this is an ideal case of parallel surfaces, and once curvature is considered, the velocity gradient is no longer constant. Resulting, the velocity gradient sharply decreases as the distance from the moving surface increases. Practically, the average velocity of the lubricant will never be greater than one half of the rotational speed and, in most application, will be found to equal a value slightly less than one half of the rotational speed.

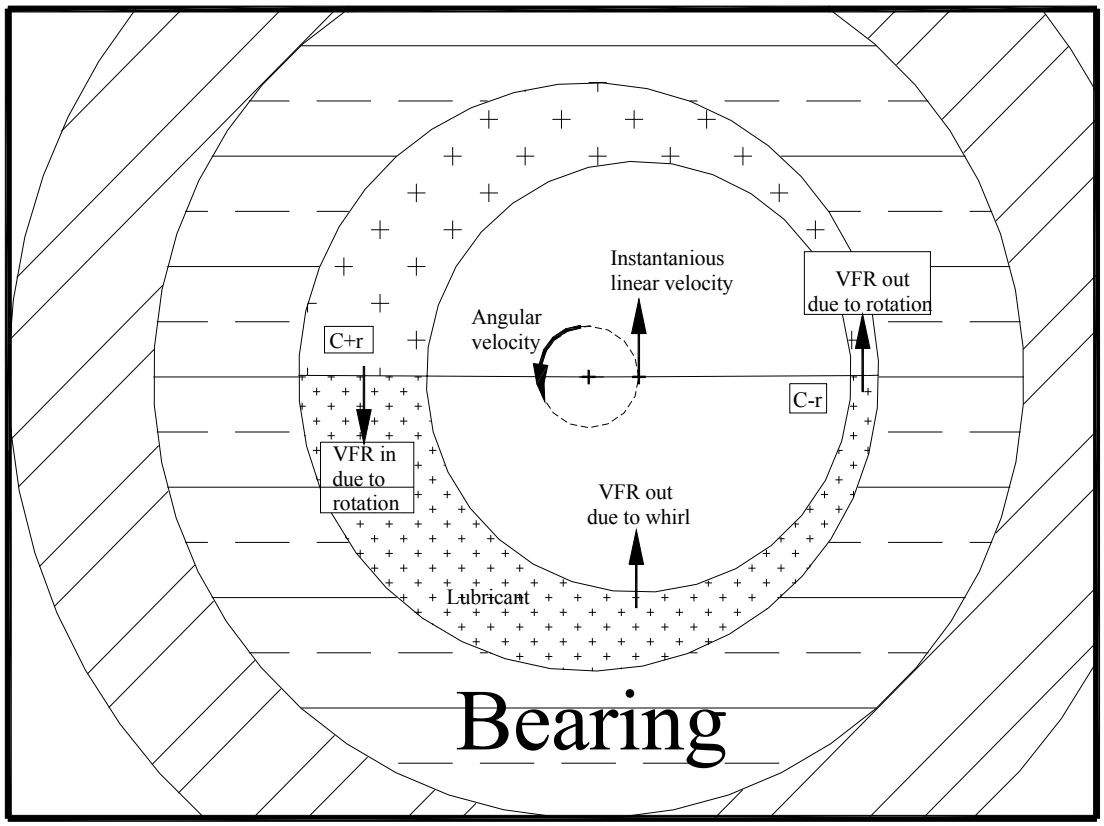

Figure A.1: Control volume of lubrication film

Appendix B: Maple Program to Calculated the Instability Threshold of a Flexible Rotor Bearing System.

```
> restart;
```
Enter in all of the system's parameters.
```
> k:=3.66;
```

> `L:=.5;` bearing length
> `d:=1;` journal diameter
> `R:=d/2;` journal radius
> `C:=0.002;` radial clearance
> `W:=1.58;` bearing load

The eccentricity ratio is a function of the sommerfeld number and can be found
```
> for S from .02 by .001 to .1 do epsilon:=fsolve((S=(L/d)^(-2)*(1-
epsilonn^2)^2/Pi/epsilonn*(Pi^2*(1-epsilonn^2)+16*epsilonn^2)^(-
.5)),epsilonn,0.0001..1);
```

The following are calculations of the stiffness and damping constants for a given eccentricity ratio.
```
> kxx:=evalf(4*(2*Pi^2+(16-Pi^2)*epsilon^2)/(Pi^2+(16-
Pi^2)*epsilon^2)^1.5);
> kyy:=evalf(4*(Pi^2+(32+Pi^2)*epsilon^2+2*(16-Pi^2)*epsilon^4)/((1-
epsilon^2)*(Pi^2+(16-Pi^2)*epsilon^2)^1.5));
> cxx:=evalf(2*Pi*(1-epsilon^2)^.5*(Pi^2+2*(Pi^2-
8)*epsilon^2)/(epsilon*(Pi^2+(16-Pi^2)*epsilon^2)^1.5));
> cyy:=evalf(2*Pi*(Pi^2+2*(24-
Pi^2)*epsilon^2+Pi^2*epsilon^4)/(epsilon*(1-epsilon^2)^.5*(Pi^2+(16-
Pi^2)*epsilon^2)^1.5));
> kxy:=evalf (-Pi*(-Pi^2+2*Pi^2*epsilon^2+(16-
Pi^2)*epsilon^4)/(epsilon*(1-epsilon^2)^.5*(Pi^2+(16-
Pi^2)*epsilon^2)^1.5));
> kyx:=evalf(-Pi*(Pi^2+(32+Pi^2)*epsilon^2+2*(16-
Pi^2)*epsilon^4)/(epsilon*(1-epsilon^2)^.5*(Pi^2+(16-
Pi^2)*epsilon^2)^1.5));
> cxy:=evalf(-8*(Pi^2+2*(Pi^2-8)*epsilon^2)/(Pi^2+(16-
Pi^2)*epsilon^2)^1.5);
> cyx:=cxy;
>
```
The following "f" constants are merely pieces of the characteristic equation. They are broken down this way to aid in the calculation of the instability threshold.
```
> f1:=16*(cxy*cyx-cxx*cyy);
> f2:=8*(2*kxy*cyx+2*kyx*cxy-2*kxx*cyy-2*kyy*cxx-k*cxx-k*cyy);
> f31:=4*(4*kxy*kyx-4*kxx*kyy-k^2-2*k*kxx-2*k*kyy);
> f32:=16*k*(cxy*cyx-cxx*cyy);
> f4:=4*k*(4*(kxy*cyx+kyx*cxy-kxx*cyy-kyy*cxx)-k*(cxx+cyy));
> f51:=4*k*(4*kxy*kyx-4*kxx*kyy-k*kxx-k*kyy);
> f52:=4*k^2*(cxy*cyx-cxx*cyy);
> f6:=4*k^2*(kxy*cyx+kyx*cxy-kxx*cyy-kyy*cxx);
> f7:=4*k^2*(kxy*kyx-kxx*kyy);
```

The two "M" constants are just more pieces enroute to finding the instability threshold.
```
> M1:=(f4+(f4^2-4*f2*f6)^.5)/2/f2;
> M2:=(f4-(f4^2-4*f2*f6)^.5)/2/f2;
```

Here, I calculated the instability threshold. It is necessary to calculate it twice because M has two roots M1 and M2. One of them is 0 and the other is the speed at which the system is on the verge of instability.

```
> critical_mass1:=((f1*M1^3-f32*M1^2+f52*M1)/(f31*M1^2-f51*M1+f7))^.5;
> critical_mass2:=((f1*M2^3-f32*M2^2+f52*M2)/(f31*M2^2-f51*M2+f7))^.5;
> print (critical_mass1*(386.4/C)^0.5*60/2/3.1415); end do:
```

RUN 2

```
> for S from .1 by .01 to 1 do epsilon:=fsolve((S=(L/d)^(-2)*(1-
epsilonn^2)^2/Pi/epsilonn*(Pi^2*(1-epsilonn^2)+16*epsilonn^2)^(-
.5)),epsilonn,0.0001..1);
```

The following are calculations of the stiffness and damping constants for a given eccentricity ratio.

```
> kxx:=evalf(4*(2*Pi^2+(16-Pi^2)*epsilon^2)/(Pi^2+(16-
Pi^2)*epsilon^2)^1.5);
> kyy:=evalf(4*(Pi^2+(32+Pi^2)*epsilon^2+2*(16-Pi^2)*epsilon^4)/((1-
epsilon^2)*(Pi^2+(16-Pi^2)*epsilon^2)^1.5));
> cxx:=evalf(2*Pi*(1-epsilon^2)^.5*(Pi^2+2*(Pi^2-
8)*epsilon^2)/(epsilon*(Pi^2+(16-Pi^2)*epsilon^2)^1.5));
> cyy:=evalf(2*Pi*(Pi^2+2*(24-
Pi^2)*epsilon^2+Pi^2*epsilon^4)/(epsilon*(1-epsilon^2)^.5*(Pi^2+(16-
Pi^2)*epsilon^2)^1.5));
> kxy:=evalf (-Pi*(-Pi^2+2*Pi^2*epsilon^2+(16-
Pi^2)*epsilon^4)/(epsilon*(1-epsilon^2)^.5*(Pi^2+(16-
Pi^2)*epsilon^2)^1.5));
> kyx:=evalf(-Pi*(Pi^2+(32+Pi^2)*epsilon^2+2*(16-
Pi^2)*epsilon^4)/(epsilon*(1-epsilon^2)^.5*(Pi^2+(16-
Pi^2)*epsilon^2)^1.5));
> cxy:=evalf (-8*(Pi^2+2*(Pi^2-8)*epsilon^2)/(Pi^2+(16-
Pi^2)*epsilon^2)^1.5);
> cyx:=cxy;
>
```

The following "f" constants are merely pieces of the characteristic equation. They are broken down this way to aid in the calculation of the instability threshold.

```
> f1:=16*(cxy*cyx-cxx*cyy);
> f2:=8*(2*kxy*cyx+2*kyx*cxy-2*kxx*cyy-2*kyy*cxx-k*cxx-k*cyy);
> f31:=4*(4*kxy*kyx-4*kxx*kyy-k^2-2*k*kxx-2*k*kyy);
> f32:=16*k*(cxy*cyx-cxx*cyy);
> f4:=4*k*(4*(kxy*cyx+kyx*cxy-kxx*cyy-kyy*cxx)-k*(cxx+cyy));
> f51:=4*k*(4*kxy*kyx-4*kxx*kyy-k*kxx-k*kyy);
> f52:=4*k^2*(cxy*cyx-cxx*cyy);
> f6:=4*k^2*(kxy*cyx+kyx*cxy-kxx*cyy-kyy*cxx);
> f7:=4*k^2*(kxy*kyx-kxx*kyy);
```

The two "M" constants are just more pieces enroute to finding the instability threshold.

```
> M1:=(f4+(f4^2-4*f2*f6)^.5)/2/f2;
> M2:=(f4-(f4^2-4*f2*f6)^.5)/2/f2;
```

Here, I calculated the instability threshold. It is necessary to calculate it twice because M has two roots M1 and M2. One of them is 0 and the other is the speed at which the system is on the verge of instability.

```
> critical_mass1:=((f1*M1^3-f32*M1^2+f52*M1)/(f31*M1^2-f51*M1+f7))^.5;
> critical_mass2:=((f1*M2^3-f32*M2^2+f52*M2)/(f31*M2^2-f51*M2+f7))^.5;
> print (critical_mass1*(386.4/C)^0.5*60/2/3.1415); end do:
```

RUN 3

```
> for S from 1 by .1 to 10 do epsilon:=fsolve((S=(L/d)^(-2)*(1-
epsilonn^2)^2/Pi/epsilonn*(Pi^2*(1-epsilonn^2)+16*epsilonn^2)^(-
.5)),epsilonn,0.0001..1);
```

The following are calculations of the stiffness and damping constants for a given eccentricity ratio.

```
> kxx:=evalf(4*(2*Pi^2+(16-Pi^2)*epsilon^2)/(Pi^2+(16-
Pi^2)*epsilon^2)^1.5);
> kyy:=evalf(4*(Pi^2+(32+Pi^2)*epsilon^2+2*(16-Pi^2)*epsilon^4)/((1-
epsilon^2)*(Pi^2+(16-Pi^2)*epsilon^2)^1.5));
> cxx:=evalf(2*Pi*(1-epsilon^2)^.5*(Pi^2+2*(Pi^2-
8)*epsilon^2)/(epsilon*(Pi^2+(16-Pi^2)*epsilon^2)^1.5));
> cyy:=evalf(2*Pi*(Pi^2+2*(24-
Pi^2)*epsilon^2+Pi^2*epsilon^4)/(epsilon*(1-epsilon^2)^.5*(Pi^2+(16-
Pi^2)*epsilon^2)^1.5));
> kxy:=evalf (-Pi*(-Pi^2+2*Pi^2*epsilon^2+(16-
Pi^2)*epsilon^4)/(epsilon*(1-epsilon^2)^.5*(Pi^2+(16-
Pi^2)*epsilon^2)^1.5));
> kyx:=evalf(-Pi*(Pi^2+(32+Pi^2)*epsilon^2+2*(16-
Pi^2)*epsilon^4)/(epsilon*(1-epsilon^2)^.5*(Pi^2+(16-
Pi^2)*epsilon^2)^1.5));
> cxy:=evalf (-8*(Pi^2+2*(Pi^2-8)*epsilon^2)/(Pi^2+(16-
Pi^2)*epsilon^2)^1.5);
> cyx:=cxy;
>
```

The following "f" constants are merely pieces of the characteristic equation. They are broken down this way to aid in the calculation of the instability threshold.

```
> f1:=16*(cxy*cyx-cxx*cyy);
> f2:=8*(2*kxy*cyx+2*kyx*cxy-2*kxx*cyy-2*kyy*cxx-k*cxx-k*cyy);
> f31:=4*(4*kxy*kyx-4*kxx*kyy-k^2-2*k*kxx-2*k*kyy);
> f32:=16*k*(cxy*cyx-cxx*cyy);
> f4:=4*k*(4*(kxy*cyx+kyx*cxy-kxx*cyy-kyy*cxx)-k*(cxx+cyy));
> f51:=4*k*(4*kxy*kyx-4*kxx*kyy-k*kxx-k*kyy);
> f52:=4*k^2*(cxy*cyx-cxx*cyy);
> f6:=4*k^2*(kxy*cyx+kyx*cxy-kxx*cyy-kyy*cxx);
> f7:=4*k^2*(kxy*kyx-kxx*kyy);
```

The two "M" constants are just more pieces enroute to finding the instability threshold.

```
> M1:=(f4+(f4^2-4*f2*f6)^.5)/2/f2;
> M2:=(f4-(f4^2-4*f2*f6)^.5)/2/f2;
```

Here, I calculated the instability threshold. It is necessary to calculate it twice because M has two roots M1 and M2. One of them is 0 and the other is the speed at which the system is on the verge of instability.

```
> critical_mass1:=((f1*M1^3-f32*M1^2+f52*M1)/(f31*M1^2-f51*M1+f7))^.5;
> critical_mass2:=((f1*M2^3-f32*M2^2+f52*M2)/(f31*M2^2-f51*M2+f7))^.5;
> print (critical_mass1*(386.4/C)^0.5*60/2/3.1415); end do:
```

RUN 4

```
> for S from 10 by 1 to 100 do epsilon:=fsolve((S=(L/d)^(-2)*(1-
epsilonn^2)^2/Pi/epsilonn*(Pi^2*(1-epsilonn^2)+16*epsilonn^2)^(-
.5)),epsilonn,0.0001..1);
```

The following are calculations of the stiffness and damping constants for a given eccentricity ratio.

```
> kxx:=evalf(4*(2*Pi^2+(16-Pi^2)*epsilon^2)/(Pi^2+(16-
Pi^2)*epsilon^2)^1.5);
```

```
> kyy:=evalf(4*(Pi^2+(32+Pi^2)*epsilon^2+2*(16-Pi^2)*epsilon^4)/((1-
epsilon^2)*(Pi^2+(16-Pi^2)*epsilon^2)^1.5));
> cxx:=evalf(2*Pi*(1-epsilon^2)^.5*(Pi^2+2*(Pi^2-
8)*epsilon^2)/(epsilon*(Pi^2+(16-Pi^2)*epsilon^2)^1.5));
> cyy:=evalf(2*Pi*(Pi^2+2*(24-
Pi^2)*epsilon^2+Pi^2*epsilon^4)/(epsilon*(1-epsilon^2)^.5*(Pi^2+(16-
Pi^2)*epsilon^2)^1.5));
> kxy:=evalf (-Pi*(-Pi^2+2*Pi^2*epsilon^2+(16-
Pi^2)*epsilon^4)/(epsilon*(1-epsilon^2)^.5*(Pi^2+(16-
Pi^2)*epsilon^2)^1.5));
> kyx:=evalf(-Pi*(Pi^2+(32+Pi^2)*epsilon^2+2*(16-
Pi^2)*epsilon^4)/(epsilon*(1-epsilon^2)^.5*(Pi^2+(16-
Pi^2)*epsilon^2)^1.5));
> cxy:=evalf(-8*(Pi^2+2*(Pi^2-8)*epsilon^2)/(Pi^2+(16-
Pi^2)*epsilon^2)^1.5);
> cyx:=cxy;
>
```

The following "f" constants are merely pieces of the characteristic equation. They are broken down this way to aid in the calculation of the instability threshold.

```
> f1:=16*(cxy*cyx-cxx*cyy);
> f2:=8*(2*kxy*cyx+2*kyx*cxy-2*kxx*cyy-2*kyy*cxx-k*cxx-k*cyy);
> f31:=4*(4*kxy*kyx-4*kxx*kyy-k^2-2*k*kxx-2*k*kyy);
> f32:=16*k*(cxy*cyx-cxx*cyy);
> f4:=4*k*(4*(kxy*cyx+kyx*cxy-kxx*cyy-kyy*cxx)-k*(cxx+cyy));
> f51:=4*k*(4*kxy*kyx-4*kxx*kyy-k*kxx-k*kyy);
> f52:=4*k^2*(cxy*cyx-cxx*cyy);
> f6:=4*k^2*(kxy*cyx+kyx*cxy-kxx*cyy-kyy*cxx);
> f7:=4*k^2*(kxy*kyx-kxx*kyy);
```

The two "M" constants are just more pieces enroute to finding the instability threshold.

```
> M1:=(f4+(f4^2-4*f2*f6)^.5)/2/f2;
> M2:=(f4-(f4^2-4*f2*f6)^.5)/2/f2;
```

Here, I calculated the instability threshold. It is necessary to calculate it twice because M has two roots M1 and M2. One of them is 0 and the other is the speed at which the system is on the verge of instability.

```
> critical_mass1:=((f1*M1^3-f32*M1^2+f52*M1)/(f31*M1^2-f51*M1+f7))^.5;
> critical_mass2:=((f1*M2^3-f32*M2^2+f52*M2)/(f31*M2^2-f51*M2+f7))^.5;
> print (critical_mass1*(386.4/C)^0.5*60/2/3.1415); end do:
```

Vita

Mr. Darryl Chauvin was born on December 20, 1976, in New Orleans, Louisiana. He earned his bachelor's degree in mechanical engineering technology from Nicholls State University in Thibodaux, Louisiana. He joined Louisiana State University in January 2000 to pursue a master's degree in mechanical engineering. His areas of interest are tribology, machine design, fluid dynamics, and vibrations. He successfully defended his thesis on April 4, 2003 and will receive the degree of Master of Science in Mechanical Engineering in May 2003.